ASSESSMENT OF PERFORMANCE AND EFFICIENCY OF MEMBRANE DISTILLATION FOR TREATMENT OF IMPAIRED WATER AND BRINE WITH HIGH SCALING POTENTIAL

by

John Arthur Bush

A thesis submitted to the Faculty and the Board of Trustees of the Colorado School of Mines in partial fulfillment of the requirements for the degree of Doctor of Philosophy (Civil and Environmental Engineering).

Golden, Colorado

Date _____

Signed: _____

John A. Bush

Signed: _____

Dr. Tzahi Y. Cath

Thesis Advisor

Golden, Colorado

Date _____

Signed: _____

Dr. Terri Hogue

Professor and Department Head

Department of Civil and Environmental Engineering

ABSTRACT

Water recovery is limited in pressure-driven membrane processes such as reverse osmosis (RO) and nanofiltration (NF) due to increase in scaling risk and osmotic pressure of the feed water with concentration. Membrane distillation (MD) is an emerging thermally-driven membrane desalination processes that utilizes a difference in vapor pressure across a microporous, hydrophobic membrane as the driving force. Thus, it is not limited by differences in the osmotic pressure between the feed and permeate and is tolerant of much higher salinity than RO. Nevertheless, MD still suffers from problems associated with membrane fouling, which is one of the major challenges that hinder its commercialization.

The overall objective of this dissertation is to elucidate scaling and fouling behavior in MD by various inorganic contaminants relevant to inland brackish desalination, which typically must achieve high water recovery to minimize brine disposal costs. Water flux, thermal efficiency, and rejection were experimentally measured in laboratory experiments using real and synthetic solutions supersaturated with respect to soluble salts, sparingly soluble salts, and silica. Various mitigation and cleaning strategies were tested, and the long-term effects of scaling on MD performance were evaluated by performing repeated experiments on previously-fouled membranes using new solutions.

Impacts and control of silica scaling was emphasized because it is ubiquitous in natural water supplies and is of particular concern in brackish desalination. Cleaning of MD membranes scaled by silica was impractical, but several mitigation strategies were effective at preventing silica scale, including modification of feed pH and optimization of feed temperature. Silica scaling propensity in MD was increased by the presence of calcium and magnesium, but the effects were reduced with increased carbonate alkalinity. Desalination of hypersaline brines with high mineral scaling potential were also investigated using water obtained from the Great Salt Lake (GSL). NaCl scaling occurred rapidly at its saturation limit, resulting in immediate loss of performance, and gradual decline in performance was also observed due to both mineral scaling and organic fouling. However, sustainable operation was achieved by operation at low feed temperatures combined with periodically reversing the direction of water flux.

TABLE OF CONTENTS

LIST OF FIGURES

LIST OF TABLES

ACKNOWLEDGEMENTS

I would like to thank the National Science Foundation under agreement CBET-1236846 and the US Department of Energy under the GTO Award # GTP62800 and Award # A16-0135 for providing major funding for this research, as well as the Edna Bailey Sussman Foundation for additional financial support. I am also grateful to the GE, 3M, and DOW corporations for generously providing the membranes used to conduct the research, and to Compass Minerals and Ormat Technologies for providing water samples.

I would also like to thank the many people whom I have had the distinct pleasure of working with during my graduate studies at CSM who provided valuable support and assistance. First and foremost, I would like to thank my advisor, Dr. Tzahi Cath, for reaching out to me and providing me with the opportunity to pursue research in a field that I am passionate about and that I believe may help provide solutions to some of the most important challenges facing the modern world. His commitment to academic excellence and insistence that his students produce the best work possible have taught me invaluable lessons on how to become a more focused and effective researcher. I would also like to thank Dr. Johan Vanneste, who was an exceptional mentor to me and always willing to explore the interesting questions, and who provided valuable guidance in solving the difficult problems. Special thanks are given to Mike Veres and Tani Cath for their technical expertise and for providing excellent assistance in the development and automation of the experimental systems used in my research. I am also grateful to Estefani Bustos and Kate Spangler for their knowledge and assistance in sample testing and analysis.

I would also like to thank the many members of Dr. Cath's diverse and talented research group for their eagerness to help and willingness to share their knowledge and perspectives, and who were truly inspirational and fun to work with. In particular, I would like to thank Dr. Kerri Hickenbottom for her assistance in helping me understand the fundamental principles of membrane distillation during the initial phases of my research, and Dr. Stephanie Riley for her assistance with nanofiltration experimental system design. Special thanks to Christopher Marks, Emily Gustafson, and Christopher Waechter as well for providing valuable assistance in the conduction of experiments and data analysis.

Finally, I would like to express my deepest gratitude to my family and friends for their support and encouragement over the past several years. I especially thank my father, Tom Bush,

and my best friend and life partner, Rachel Moyle, for their incredible emotional and physical support during the most difficult times of my graduate studies. They were always there to encourage me and at times believed in me more than I believed in myself, and I truly could not have completed this dissertation without them.

CHAPTER 1
INTRODUCTION

Membrane distillation (MD) is an emerging thermally-driven membrane separation process that utilizes a vapor pressure difference through a porous, hydrophobic membrane to drive mass transport. Unlike pressure-driven membrane desalination processes such as reverse osmosis (RO), MD is not limited by osmotic pressure differential between the two solutions, allowing production of high quality water from brines up to and exceeding saturation concentration of dissolved salts. Thus, MD has attracted interest in recent years as a potential strategy to increase the overall water recovery of desalination processes. However, while MD is generally considered to be more resistant to fouling than RO, it still suffers from scaling and fouling problems, which are one of the primary technical challenges that limit commercial applications.

1.1 Problem Statement and Significance

Water resources are increasingly threatened around the world. As demand for potable water continues to increase due to factors such as population growth, industrial development, and expansion of agriculture, many traditional water resources are becoming depleted, contaminated, or impacted by climate change [1]. Desalinated water is an option in many regions, and desalination has expanded rapidly in recent decades due to advances in technologies that have reduced the costs of desalination, particularly membrane desalination technologies such as RO [2]. While desalination of seawater represents the majority of current global capacity, desalination of inland brackish groundwater sources using RO and nanofiltration (NF) is increasingly considered as an alternative to conventional water resources [3-5]. However, desalination of inland brackish resources is often limited by the need to achieve very high water recoveries due to the technical challenges and environmental impacts associated with brine disposal [6, 7].

Most desalination technologies are energy intensive and possess several factors that limit water recovery, which is the ratio of fresh water produced to the total source inflow. Thermal desalination such as multi-stage flash distillation (MSF) and multiple-effect distillation (MED) are prone to mineral scaling of heat exchanger surfaces due to the high temperatures involved,

and typically operate in the range of 10–30% water recovery for seawater desalination [8]. RO may achieve higher recovery, typically about 50% for seawater; however, due to the increased osmotic pressure of the feed solution as it is concentrated, RO systems are subject to thermodynamic restrictions that limit water recovery [9]. Scaling on heat exchanger and membrane surfaces is also a major problem with high water recovery in both thermal distillation and membrane desalination processes as minerals are concentrated beyond their solubility limits [10-14]. Chemical antiscalants are frequently used to reduce scaling tendencies and increase water recovery, however these chemicals are also concentrated in the brine and may cause additional impacts associated with brine disposal, which can impact the local ecosystem if released to the environment [6, 15]. To address these limitations, it is important to develop new technologies that are capable of efficient operation at high salinities and which are less impacted by mineral scaling. Additionally, it is important that new technologies be compatible with existing technologies to maximize the overall efficiency of desalination processes.

MD is a thermally-driven process that utilizes a temperature difference to induce vapor transport through commercially-available, hydrophobic microfiltration membranes. The most common configuration, known as direct contact MD (DCMD), involves both the feed solution and distillate in direct contact with the two membrane surfaces, and vapor pressure difference is established by maintaining the feed solution at a higher temperature than the distillate. The hydrophobicity of the membranes and low-pressure operation prevent liquid transport, producing high quality distillate and almost total rejection of nonvolatile solutes, even at much lower operating temperatures than conventional distillation processes [16]. Unlike pressure-driven membrane processes, MD is not limited by osmotic pressure and is capable of desalinating feed water of very high salinity [17-20]. Because of this, MD is unique in its potential as a desalination process for hypersaline brines, and has been successfully tested using reject streams from RO [21-25], NF [26-28], and naturally occurring hypersaline brines such as water from the Great Salt Lake [29]. MD has also been utilized to concentrate salt solutions to the saturation limit and combined with crystallization methods in a process termed membrane distillation crystallization (MDC) [30] to recover valuable salts from brines, including NaCl [26, 31-34], $CaCO_3$ and $MgSO_4$ [26], and Na_2SO_4 [27, 34]. For the most part, efforts to date have used synthetic solutions, which may perform quite differently than natural brines. For example, in an MDC study using RO concentrate from natural seawater, Ji et al. [21] reported reduced

transmembrane flux, a 20% reduction of salts crystallized, and a 15-23% reduction in crystal growth rate (compared to artificial concentrates) due to dissolved organic matter. The incorporation of MDC in desalination suggests the potential for further enhancement of water recovery by separation of minerals from the water, which may improve the overall process efficiency of pretreatment and approach a zero-liquid discharge (ZLD) desalination process [35]. Despite its potential, MD and MDC have yet to achieve commercialization, and additional studies are needed to address the scaling and fouling issues associated with the complex solutions of natural water resources at high concentration factors, optimize operating and maintenance procedures, and evaluate the benefits of integration with existing processes.

The driving force and operating conditions of MD are quite different than pressure-driven membrane processes, and it is generally considered to be more resistant to fouling than RO [36, 37]. However, MD is impacted by scaling and fouling, and a more comprehensive understanding of fouling behavior and its impact on MD are crucial to its implementation as a viable treatment strategy for water resources with high fouling potential. Inorganic mineral scaling is of particular concern in the desalination of inland brackish resources. Scaling by sparingly soluble salts such as $CaCO_3$, $CaSO_4$, and silica [38-43] are known to cause substantial flux decline in MD. However, in some cases it has been shown that the scale layer formed on the feed side of MD membranes is relatively porous and does not completely prevent water flux [42] and may be removed with simple cleaning processes [29, 40, 44]. Also, employing management strategies such as periodic flushing of the membrane with deionized water [41] or periodic reversal of the temperature difference across the membrane [29] can interrupt the crystallization process before sufficient induction time has passed and may mitigate scale formation. Also, while scaling by sparingly soluble salts typically forms on the membrane surface only and does not affect salt rejection, scaling by NaCl on the membrane surface itself has been shown to aggravate pore wetting [31, 44], which reduces water flux due to the loss of driving force and can also reduce salt rejection, and may lead to crystallization inside the pores themselves [32]. Crystallization on membrane surfaces may also affect membrane properties such as surface hydrophobicity and mechanical strength [45].

While MD can operate at much higher concentrations than any other desalination strategy currently in use, it is nonetheless impacted by the salinity of feed solutions. Notably, the partial pressure of water vapor decreases with increased ionic strength, which decreases the driving

force for a given temperature difference. Thermodynamic properties of the brine such as viscosity and thermal conductivity are also affected by increased concentration and this may also impact performance. An adequate assessment of the viability of MD at extreme concentration requires knowledge of how these factors affect water flux, thermal efficiency, and salt rejection. Although effects of salinity on water flux and salt rejection of MD and MDC processes have been well documented [22, 29, 31, 32, 34, 46], few studies have addressed its effects on thermal efficiency. A theoretical study by Al-Obaidani et al. predicted a decline from 58% to 40% thermal efficiency as concentration was increased from 35 to 350 g/L NaCl for a Microdyne-Nadir MD020CP2N membrane operating with T_f = 55 °C and T_d = 25 °C, but these results were not validated experimentally [47].

1.2 Objective and scope of work

The goal of the dissertation is to evaluate membrane distillation as a potential technology to enhance overall water recovery in desalination processes from water resources and hypersaline brines with high scaling potential. To achieve this goal, bench-scale experimental results were evaluated to determine performance, thermal efficiency, and salt rejection of the MD process with brines supersaturated with various salts and minerals common to natural water supplies. Both synthetic solutions and natural water samples were tested to evaluate short-term and long-term effects of concentration and scaling on MD performance. Scale mitigation and cleaning strategies are investigated to determine robustness of the process and assess practical limitations to water recovery. Due to the unique ability of MD to desalinate highly concentrated water resources with high scaling potential, solution composition relevant to inland water resources were emphasized due to the importance of high water recovery and challenges of brine disposal relevant to inland desalination. Such resources include brackish groundwater and geothermal water, which are often high in silica, calcium, magnesium, sulfates, and carbonates. Specific research objectives and methods included:

1. Assess the efficacy of membrane distillation as a direct substitute for currently available nanofiltration (NF) technologies for removal of silica and calcium from groundwater resources. Performance, efficiency, and rejection are experimentally determined for each

process using similar solution chemistries and operating conditions and compared. Effects of scaling on performance and effectiveness of cleaning strategies are assessed for each process.

2. Investigate the influence of pH on silica polymerization and scaling behavior during the MD process with respect to performance, efficiency, and rejection. Identify conditions which best delay or prevent membrane fouling, assess effectiveness of scale mitigation and cleaning strategies for fouled membranes.
3. Investigate the influence of polyvalent ions, specifically calcium (Ca^{2+}) and magnesium (Mg^{2+}), on silica polymerization and fouling behavior during the MD process with respect to performance, efficiency, and rejection. Identify conditions, which best delay or prevent membrane fouling, assess effectiveness of scale mitigation and cleaning strategies for fouled membranes.
4. Evaluate performance and efficiency of MD for desalination of natural hypersaline brine containing silica and other minerals. Determine effects of increased concentration on performance and scaling behavior. Perform parallel experiments with synthetic solutions containing pure NaCl to isolate and compare effects of salinity and NaCl scaling on performance with effects of mineral scaling.

The objectives of the research are achieved through the completion of four distinct studies, with the overall focus of the study being the assessment of performance and efficiency of membrane distillation for desalination of water resources and brines with high silica and mineral content.

1.3 Structure of dissertation

This dissertation investigates MD as a potential technology to enhance overall water recovery in desalination of water resources and brines with high silica and mineral content. Specifically, effects of increased concentration of synthetic and natural solutions on water flux, thermal efficiency, salt rejection, and scaling behavior are experimentally investigated. The dissertation consists of four chapters, each consisting of a distinct study focused on a specific aspect of the overall research goals. Chapter 2 is a comparative study of MD and NF processes applied to the treatment of silica-saturated water and was submitted to the *Journal of Membrane Science*. Chapter 3 investigates pH modification as a strategy to prevent and mitigate silica

scaling of MD membranes for solutions concentrated above the solubility limit of silica and was published in the *Journal of Membrane Science*. Chapter 4 investigates the influence of divalent cations, carbonate alkalinity, and pH on silica polymerization and scaling behavior during the MD process and explores optimization of feed temperature to minimize silica scaling for solution chemistries where pH adjustment may not be desired or effective. This chapter is currently under internal review and will be submitted to *Environmental Science: Water Research & Technology*. Chapter 4 is an experimental investigation that compares scaling behavior and its impacts on MD of pure NaCl solutions with those of naturally hypersaline brines that also possess high potential of mineral scaling and organic fouling, and was published in *Separation and Purification Technology*.

1.3.1 Experimental comparison of MD and NF for removal of silica and calcium

NF is a commercially available technology that exhibits high rejection of polyvalent ions such as calcium and magnesium, which are commonly found in groundwater resources. Because NF operates at lower pressures than RO, it may possess some advantages for treatment of freshwater resources with sufficient mineral content to require desalination and that pose a significant scaling risk to RO. However, NF processes are also prone to scaling as concentration exceeds saturation, and may achieve relatively low rejection of monovalent ions and silica. Due to its high rejection of salts and minerals ability to operate at high salinity, MD may an attractive option for the treatment of NF concentrate brine to enhance overall recovery of brackish water desalination or possibly as a standalone alternative to NF or RO.

To date, few studies have directly compared fouling behavior in MD with pressure-driven membrane processes at similar conditions. This chapter compares MD with NF as treatment strategies for silica-saturated water at similar concentrations and temperatures. Water flux was impacted by silica scaling in both MD and NF processes; however, an induction time was observed before flux decline occurred during MD experiments, which was not observed for NF. Salt rejection during MD was >99.8% for all solutions tested and was unaffected by scaling, whereas rejection during NF was between 78-90% and tended to decrease after scaling. Attempts to clean the fouled membranes for both processes by rinsing with an NaOH solution at pH >11 were partially effective at restoring water flux but unable to completely remove the silica scale layer.

1.3.2 Prevention and management of silica scaling in MD using pH adjustment

Modification of feed water pH has been successfully demonstrated as a strategy to minimize silica scaling in RO processes [48, 49], but in some cases water recovery may still be limited by osmotic pressure. In this investigation, pH adjustment was tested as a strategy to reduce silica scaling risk in the MD process. With feed water pH less than 5 or higher than 10, scaling impacts were negligible at silica concentrations up to 600 mg/L. Scaling rates were highest at neutral pH between 6 and 8. Cleaning strategies were also explored to remove silica scale from membranes. Cleaning using NaOH solutions at pH higher than 11 to induce dissolution of silica scale was effective at temporarily restoring performance; however, some silica remained on membrane surfaces and scaling upon re-exposure to supersaturated silica concentrations occurred faster than with new membranes.

1.3.3 Influence of cation concentration on silica fouling in MD and process optimization

Brackish groundwater resources often contain relatively high concentration of divalent ions such as calcium and magnesium, which may also be associated with carbonate alkalinity due to the weathering of minerals. Divalent cations are known to catalyze and accelerate silica polymerization, and carbonate alkalinity increases buffering capacity. Thus, mitigation strategies such as pH modification of natural water supplies may not be desired or effective depending on overall solution composition. However, feed temperature also plays a key role in scaling behavior during MD processes due to its effect on crystallization and polymerization processes as well as its effect on water flux, concentration polarization, and temperature polarization. In this investigation, the influence of cation concentration and alkalinity on silica scaling behavior and its impacts on MD are evaluated for solutions supersaturated with silica. Scaling rates increased with the inclusion of either calcium or magnesium, but the influence of calcium is reduced by carbonate alkalinity. The effect of feed temperature on scaling behavior for solutions containing silica and calcium are also investigated. Operation at lower feed temperatures is found to dramatically reduced the relative impacts of silica scaling.

1.3.4 MD for concentration of hypersaline brine with high mineral content

This study investigated the scaling and fouling behavior of a hypersaline brine collected from the North Arm of the Great Salt Lake (GSL), which was nearly saturated with respect to NaCl, and also contained high concentrations of dissolved minerals and organic carbon. Effects on water flux, thermal efficiency, and salt rejection were measured, and membranes used were analyzed before and after testing to evaluate potential causes of these effects. Scaling by NaCl crystallization on the membrane surface limited water recovery to approximately 10%, and also caused damage to the internal pore structure of the membrane when the temperature difference (ΔT) between the feed and distillate was greater than 20 °C. Analysis of the solution chemistry of the GSL water was effective in predicting the scaling tendency of NaCl, but inadequate in predicting the scaling tendency of other salts. Amorphous scaling structures on the membrane surfaces containing magnesium and oxygen were implied as the dominant factors contributing to performance decline at concentrations below NaCl saturation, and the result of fouling due to interactions between organic matter and magnesium. Operation at a maximum water recovery of 8% combined with intermittent reversal of the temperature gradient were effective strategies to prevent both scaling and fouling and maintain long-term performance.

1.4 References

[1] S.B. Roy, L. Chen, E.H. Girvetz, E.P. Maurer, W.B. Mills, T.M. Grieb, Projecting Water Withdrawal and Supply for Future Decades in the U.S. under Climate Change Scenarios, Environmental Science & Technology, 46 (2012) 2545-2556.

[2] N. Ghaffour, T.M. Missimer, G.L. Amy, Technical review and evaluation of the economics of water desalination: Current and future challenges for better water supply sustainability, Desalination, 309 (2013) 197-207.

[3] L.F. Greenlee, D.F. Lawler, B.D. Freeman, B. Marrot, P. Moulin, Reverse osmosis desalination: Water sources, technology, and today's challenges, Water Research, 43 (2009) 2317-2348.

[4] I. Munoz, A.R. Fernandez-Alba, Reducing the environmental impacts of reverse osmosis desalination by using brackish groundwater resources, Water Res, 42 (2008) 801-811.

[5] M. Badruzzaman, A. Subramani, J. DeCarolis, W. Pearce, J.G. Jacangelo, Impacts of silica on the sustainable productivity of reverse osmosis membranes treating low-salinity brackish groundwater, Desalination, 279 (2011) 210-218.

[6] A.M.O. Mohamed, M. Maraqa, J. Al Handhaly, Impact of land disposal of reject brine from desalination plants on soil and groundwater, Desalination, 182 (2005) 411-433.

[7] M. Ahmed, W.H. Shayya, D. Hoey, J. Al-Handaly, Brine disposal from reverse osmosis desalination plants in Oman and the United Arab Emirates, Desalination, 133 (2001) 135-147.

[8] O.J. Morin, Design and Operating Comparison of Msf and Med Systems, Desalination, 93 (1993) 69-109.

[9] L.F. Song, J.Y. Hu, S.L. Ong, W.J. Ng, M. Elimelech, M. Wilf, Performance limitation of the full-scale reverse osmosis process, Journal of Membrane Science, 214 (2003) 239-244.

[10] T.R. Bott, Aspects of crystallization fouling, Experimental Thermal and Fluid Science, 14 (1997) 356-360.

[11] A. Helalizadeh, H. Muller-Steinhagen, M. Jamialahmadi, Mixed salt crystallisation fouling, Chemical Engineering and Processing, 39 (2000) 29-43.

[12] T. Koo, Y.J. Lee, R. Sheikholeslami, Silica fouling and cleaning of reverse osmosis membranes, Desalination, 139 (2001) 43-56.

[13] R. Sheikholeslami, Mixed salts—scaling limits and propensity, Desalination, 154 (2003) 117-127.

[14] R. Sheikholeslami, Assessment of the scaling potential for sparingly soluble salts in RO and NF units, Desalination, 167 (2004) 247-256.

[15] D.A. Roberts, E.L. Johnston, N.A. Knott, Impacts of desalination plant discharges on the marine environment: A critical review of published studies, Water Res, 44 (2010) 5117-5128.

[16] K.W. Lawson, D.R. Lloyd, Membrane distillation, Journal of Membrane Science, 124 (1997) 1-25.

[17] Y.B. Yun, R.Y. Ma, W.Z. Zhang, A.G. Fane, J.D. Li, Direct contact membrane distillation mechanism for high concentration NaCl solutions, Desalination, 188 (2006) 251-262.

[18] F. He, J. Gilron, K.K. Sirkar, High water recovery in direct contact membrane distillation using a series of cascades, Desalination, 323 (2013) 48-54.

[19] M. Safavi, T. Mohammadi, High-salinity water desalination using VMD, Chemical Engineering Journal, 149 (2009) 191-195.

[20] A. Alkhudhiri, N. Darwish, N. Hilal, Treatment of high salinity solutions: Application of air gap membrane distillation, Desalination, 287 (2012) 55-60.

[21] X. Ji, E. Curcio, S. Al Obaidani, G. Di Profio, E. Fontananova, E. Drioli, Membrane distillation-crystallization of seawater reverse osmosis brines, Separation and Purification Technology, 71 (2010) 76-82.

[22] C.R. Martinetti, A.E. Childress, T.Y. Cath, High recovery of concentrated RO brines using forward osmosis and membrane distillation, Journal of Membrane Science, 331 (2009) 31-39.

[23] A. Pérez-González, A.M. Urtiaga, R. Ibáñez, I. Ortiz, State of the art and review on the treatment technologies of water reverse osmosis concentrates, Water Research, 46 (2012) 267-283.

[24] D. Qu, J. Wang, B. Fan, Z.K. Luan, D.Y. Hou, Study on concentrating primary reverse osmosis retentate by direct contact membrane distillation, Desalination, 247 (2009) 540-550.

[25] T.Y. Cath, Osmotically and thermally driven membrane processes for enhancement of water recovery in desalination processes, Desalin Water Treat, 15 (2010) 279-286.

[26] E. Drioli, E. Curcio, A. Criscuoli, G.D. Profio, Integrated system for recovery of CaCO3, NaCl and MgSO4·7H2O from nanofiltration retentate, Journal of Membrane Science, 239 (2004) 27-38.

[27] E. Curcio, X. Ji, A.M. Quazi, S. Barghi, G. Di Profio, E. Fontananova, T. Macleod, E. Drioli, Hybrid nanofiltration–membrane crystallization system for the treatment of sulfate wastes, Journal of Membrane Science, 360 (2010) 493-498.

[28] F. Macedonio, E. Drioli, E. Curcio, G. Di Profio, Experimental and economical evaluation of a membrane crystallizer plant, Desalin Water Treat, 9 (2009) 49-53.

[29] K.L. Hickenbottom, T.Y. Cath, Sustainable operation of membrane distillation for enhancement of mineral recovery from hypersaline solutions, Journal of Membrane Science, 454 (2014) 426-435.

[30] E. Drioli, G. Di Profio, E. Curcio, Progress in membrane crystallization, Current Opinion in Chemical Engineering, 1 (2012) 178-182.

[31] M. Gryta, Concentration of NaCl solution by membrane distillation integrated with crystallization, Separation Science and Technology, 37 (2002) 3535-3558.

[32] M. Gryta, Direct contact membrane distillation with crystallization applied to NaCl solutions, Chem Pap-Chem Zvesti, 56 (2002) 14-19.

[33] F. Edwie, T.-S. Chung, Development of simultaneous membrane distillation–crystallization (SMDC) technology for treatment of saturated brine, Chemical Engineering Science, 98 (2013) 160-172.

[34] C.M. Tun, A.G. Fane, J.T. Matheickal, R. Sheikholeslami, Membrane distillation crystallization of concentrated salts - flux and crystal formation, Journal of Membrane Science, 257 (2005) 144-155.

[35] F. Macedonio, L. Katzir, N. Geisma, S. Simone, E. Drioli, J. Gilron, Wind-Aided Intensified eVaporation (WAIV) and Membrane Crystallizer (MCr) integrated brackish water desalination process: Advantages and drawbacks, Desalination, 273 (2011) 127-135.

[36] D.M. Warsinger, J. Swaminathan, E. Guillen-Burrieza, H.A. Arafat, J.H. Lienhard V, Scaling and fouling in membrane distillation for desalination applications: A review, Desalination, 356 (2015) 294-313.

[37] L.D. Tijing, Y.C. Woo, J.-S. Choi, S. Lee, S.-H. Kim, H.K. Shon, Fouling and its control in membrane distillation—A review, Journal of Membrane Science, 475 (2015) 215-244.

[38] M. Gryta, Alkaline scaling in the membrane distillation process, Desalination, 228 (2008) 128-134.

[39] M. Gryta, Long-term performance of membrane distillation process, Journal of Membrane Science, 265 (2005) 153-159.

[40] E. Curcio, X.S. Ji, G. Di Profio, A. Sulaiman, E. Fontananova, E. Drioli, Membrane distillation operated at high seawater concentration factors: Role of the membrane on CaCO3 scaling in presence of humic acid, Journal of Membrane Science, 346 (2010) 263-269.

[41] L.D. Nghiem, T. Cath, A scaling mitigation approach during direct contact membrane distillation, Separation and Purification Technology, 80 (2011) 315-322.

[42] F. He, K.K. Sirkar, J. Gilron, Studies on scaling of membranes in desalination by direct contact membrane distillation: CaCO3 and mixed CaCO3/CaSO4 systems, Chemical Engineering Science, 64 (2009) 1844-1859.

[43] J. Gilron, Y. Ladizansky, E. Korin, Silica Fouling in Direct Contact Membrane Distillation, Ind Eng Chem Res, 52 (2013) 10521-10529.

[44] M. Gryta, Fouling in direct contact membrane distillation process, Journal of Membrane Science, 325 (2008) 383-394.

[45] E. Guillen-Burrieza, R. Thomas, B. Mansoor, D. Johnson, N. Hilal, H. Arafat, Effect of Dry-out on the Fouling of PVDF and PTFE Membranes under Conditions Simulating Intermittent Seawater Membrane Distillation (SWMD), Journal of Membrane Science, (2013).

[46] L. Mariah, C.A. Buckley, C.J. Brouckaert, E. Curcio, E. Drioli, D. Jaganyi, D. Ramjugernath, Membrane distillation of concentrated brines - Role of water activities in the evaluation of driving force, Journal of Membrane Science, 280 (2006) 937-947.

[47] S. Al-Obaidani, E. Curcio, F. Macedonia, G. Di Profio, Al-Hinai, E. Drioli, Potential of membrane distillation in seawater desalination: Thermal efficiency sensitivity study and cost estimation, Journal of Membrane Science, 323 (2008) 85-98.

[48] P.V. Brady, S.J. Altman, L.K. McGrath, J.L. Krumhansl, H.L. Anderson, pH modification for silica control, Desalin Water Treat, 51 (2013) 5901-5908.

[49] R.Y. Ning, A.J. Tarquin, J.E. Balliew, Seawater RO treatment of RO concentrate to extreme silica concentrations, Desalin Water Treat, 22 (2010) 286-291.

CHAPTER 2

COMPARISON OF MEMBRANE DISTILLATION AND HIGH-TEMPERATURE NANOFILTRATION PROCESSES FOR TREATMENT OF SILICA-SATURATED WATER

Submitted for possible publication in *Journal of Membrane Science*

John A. Bush[1❖], Johan Vanneste[1], Tzahi Y. Cath[1*]

2.1 Abstract

Desalination of inland water resources such as brackish groundwater or geothermal water must achieve high water recovery to minimize reject brine volume and costs associated with its disposal. Pressure-driven membrane processes such as reverse osmosis (RO) and nanofiltration (NF) are presently the most commonly used technology for desalination of brackish water; however, water recovery is often limited due to high scaling potential by silica, calcium, magnesium, and other minerals. Membrane distillation (MD), a thermally driven membrane process, is commonly tolerant to high salinity and may be less prone to irreversible fouling by mineral scaling. This investigation compared performance and fouling behavior of MD and NF during concentration of silica-containing solutions from 225 mg/L to 600 mg/L SiO_2 at comparable operating conditions. Water flux was impacted by silica scaling in both MD and NF processes; however, an induction time was observed before flux decline occurred during MD experiments, which was not observed for NF. Salt rejection during MD was >99.8% for all solutions tested and was unaffected by scaling, whereas rejection during NF was between 78-90% and tended to decrease after scaling. Attempts to clean the fouled membranes for both processes by rinsing with an NaOH solution at pH >11 were partially effective at restoring water flux but unable to completely remove the silica scale layer.

[1]Colorado School of Mines, Golden, CO, USA
[❖]Primary researcher and author
[*]Corresponding author: email: tcath@mines.edu; phone: (303) 273-3402; fax: (303) 273-3413

2.2 Introduction

Desalination has expanded rapidly in recent years due to increase in demand and advances in technology that have made desalinated water cost-competitive with other water resources. The most significant recent technological advances have involved membrane desalination processes, with seawater reverse osmosis (RO) providing most of the global desalinated water produced from the ocean [1]. Considering current and future trends in water demand and scarcity, inland communities are also likely to become more dependent on desalination as a supplement to fresh water resources. Desalination of inland brackish groundwater sources using RO and nanofiltration (NF) is increasingly considered as an alternative to conventional water resources [2-4]. Desalinated geothermal water is another potential resource available in many regions that has potential use as industrial, agricultural, and drinking water [5].

Despite recent advances in membrane technologies, inland desalination is hindered by several factors. High water recoveries are usually required to avoid the technical challenges and costs associated with brine disposal [2]. However, because osmotic pressure increases with concentration, pressure-driven membrane processes consume more energy and possess thermodynamic limits at higher water recoveries [6]. Also, brackish groundwater and geothermal water often possess high scaling potential due to the presence of sparingly soluble minerals such as calcium sulfate, calcium carbonate, barium sulfate, and silica [2]. Scaling severely impacts membrane performance, and many studies have investigated scale mitigation strategies for membrane desalination processes applied to brackish groundwater and geothermal water [4, 7-12]. Scaling due to crystallization of mineral salts can often be managed using techniques that include hardness removal, chemical addition (antiscalants), pH adjustment, and chemical cleaning [2, 13].

Prevention and management of silica scaling remains a major challenge in treatment of brackish groundwater and geothermal resources [4, 7, 8, 12, 14, 15]. The chemistry of silica in aqueous systems is complex and highly influenced by temperature, pH, ionic strength, and the presence of other ions in solution [16]. Interactions with polyvalent ions such as calcium, magnesium, and barium tend to catalyze silica polymerization and accelerate scaling in membrane systems [17, 18]. Once formed, silica scale is resistant to most chemical cleaning and can be very difficult or impossible to completely remove [4, 11]. Pretreatment to remove silica

prior to desalination can reduce scaling [7, 8, 10, 19, 20]; however, some pretreatment processes produce large volumes of sludge and may be prohibitive due to increased labor and disposal costs. Chemical antiscalants specifically designed to stabilize silica may reduce polymerization and scaling [4, 21]; yet, these may themselves become foulants and increase the risk of organic fouling [22, 23]. Thus, the development of new strategies to reduce energy consumption and manage silica scaling at high water recoveries are needed for the economic desalination of inland brackish resources.

Membrane distillation (MD) is an emerging, thermally driven membrane desalination process that uses the difference in partial vapor pressure between a hot feed stream and cool distillate stream to drive mass transport across a porous, hydrophobic membrane. Because mass transfer occurs in the vapor phase, MD is not limited by the osmotic pressure difference between the feed and distillate streams and it is capable of sustaining operation at higher salinities than can be achieved by RO or NF. Also, scaling and fouling behaviors are different in MD than in pressure-driven membrane processes, and MD membranes are generally more resistant to fouling than RO membranes [24]. Scale mitigation techniques [25-29] and mild chemical cleaning strategies [30-32] have been demonstrated as effective methods to manage mineral scaling and organic fouling on MD membranes. Thus, MD has great potential as a desalination technology capable of higher water recoveries than conventional processes, and has been successfully demonstrated in the lab for desalination of natural hypersaline brines [25, 26], reject brines from RO [33-36], and in conjunction with crystallization processes to extract both pure water and minerals from brines [37-41].

As with other distillation processes, MD has a high thermal energy demand; yet, MD can operate at any temperature difference and energy costs could be alleviated by the use of inexpensive thermal energy sources such as low-grade waste heat from thermoelectric power generation and industrial processes [42]. However, water flux in MD is substantially reduced at low feed temperatures due to the exponential relationship between temperature and partial vapor pressure [43], and the use of low-temperature waste heat sources could severely limit rates of water production. In such cases, and if feed salinity is not high, it may be more beneficial to use a commercial pressure-driven membrane process to perform the initial desalination and use MD to treat the smaller volume of reject brine and increase overall water recovery. While most studies involving this type of application have involved reject brines from RO [33, 34, 36, 37],

NF may be a more viable option for the initial desalination of low-salinity brackish and geothermal water. NF requires lower operating pressures than RO and may achieve high rejection of polyvalent ions common to these resources, and in some cases can produce acceptable water quality without the need for RO [44].

A better understanding of silica scaling behavior and its impacts on the MD process is needed to consider its suitability as a treatment strategy for brines from desalination of brackish resources. Although silica was a factor in some investigations involving mixed solutions [33, 34], few studies exist in the literature that focus specifically on silica polymerization and scaling. Gilron et al. reported gradual decline in water flux due to silica fouling in MD membranes and restored performance by rinsing with sodium carbonate, but the long-term effectiveness of cleaning were not investigated [45]. At the same time, development of an integrated NF/MD system for treatment of brackish water and geothermal water might benefit by an improved understanding of silica scaling behavior in the NF process at high temperatures. NF membranes and modules can be designed to operate in a range of temperatures similar to those of MD [46]. A high-temperature NF process would be advantageous in an integrated NF/MD system for treatment of geothermal water to avoid the need to cool and reheat the brine at the different stages of the process. Also, application of low-grade heat prior to the NF stage might be beneficial due to the increased silica solubility with temperature, thus reducing the degree of saturation and polymerization rates early in the process and potentially lowering the scaling risk in the MD stage. High temperatures increase permeability of NF membranes, which can decrease rejection; however, most studies on high-temperature NF processes have primarily focused on applications to industrial wastewater treatment [47-50], and the effects of temperature on rejection and scaling behavior in NF with brackish resources have not been adequately explored.

In this study, MD and NF processes were investigated using silica-saturated water at similar temperatures, concentrations, and initial water flux. The main objectives were to elucidate the potential differences in silica scaling behavior and its impacts on MD performance compared to a pressure-driven membrane process at comparable conditions, to investigate the potential of high-temperature NF as a treatment strategy for feed waters with high silica content, and to compare the influence of divalent cations and alkalinity on silica scaling behavior for each process. Water flux and rejection for each process were measured and compared as solutions were concentrated to similar degrees of supersaturation with respect to silica. The tenacity of the

resulting silica scale on the membrane surfaces were also tested for each process by rinsing with a high-pH NaOH solution and subsequent testing using a new silica solution.

2.3 Materials and methods

2.3.1 Solution chemistry and analytical methods

Synthetic solutions were prepared for all experiments. Solution composition was chosen based on a target concentration of silica of ~225 mg/L, which is near the solubility limit at 60 °C and about twice the solubility limit at 25 °C, based on the calculated scaling tendency using OLI Stream Analyzer (OLI Systems, Inc., Cedar Knolls, NJ). OLI Stream Analyzer calculates scaling tendency as the ratio of the real-solution solubility product to the thermodynamic limit based on the thermodynamic equilibrium constant, K_{SP}, considering the chemical composition, pH, and temperature of the solution. In practice, the solubility of amorphous silica at 25 °C is estimated to be 120 mg/L, although values from 70 to more than 150 mg/L have been reported [16]. Experiments were also conducted incorporating calcium because it is often found in groundwater and geothermal water and because the presence of calcium has been shown to catalyze silica polymerization and accelerate silica scaling in membrane processes [11, 18, 51].

The effects of alkalinity and potential interactions with carbonates were investigated with added bicarbonate. Supersaturated silica solutions were prepared by dissolving $Na_2SiO_3 \cdot 5H_2O$ into deionized water, which is highly soluble in water and forms a stable alkaline solution of sodium and monomeric silicate ions [16]. The sodium silicate solution was then adjusted to neutral pH with concentrated HCl. Neutralization reduces the solubility limit of silica by converting silicate to monosilicic acid, $Si(OH)_4$, which is highly prone to polymerization; therefore, all solutions were prepared immediately prior to NF and MD experiments. When applicable, $CaCl_2 \cdot 2H_2O$ and $NaHCO_3$ were added to provide Ca^{2+} and HCO_3^- in concentrations approximately equal to the molar concentration of silica.

Four different solution chemistries were tested in the study, the compositions of which are listed in Table 2.1. The neutralization of the sodium silicate was performed prior to the addition of bicarbonate, which raised the pH of these solutions slightly to 7.7–7.8. Chemical and physical properties of each solution were calculated using OLI Stream Analyzer. Silica concentration in both the feed and permeate streams were performed using the silicomolybdate method and a Hach spectrophotometer (Model DR 5000, Hach Company, Loveland, CO) to

measure absorbance at 452 nm. The silicomolybdate method is useful for molybdate-reactive silica, which includes dissolved simple silicates, monomeric silica, silicic acid, and an undetermined amount of polymeric silica [52]. Colloidal polymeric silica is not measured by the method due to its unreactive nature; however, this form of silica behaves more like a solid than a dissolved form and almost complete rejection by both MD and NF was assumed. Samples analyzed using the silicomolybdate method were acidified to pH ~1 using concentrated HCl immediately after collection to halt additional polymerization. Total silica (including reactive and polymeric silica) and cation concentrations were measured following experiments by diluting and filtering samples through a 0.45 micron filter and analyzed with an inductively coupled plasma atomic emission spectrometer (ICP-AES) (Optima 5300 DV, PerkinElmer Inc., Waltham, MA).

Table 2.1. Composition of synthetic solutions tested, and predicted concentration of major dissolved species based on OLI simulation at 25 °C assuming no solids precipitation and neutralization with HCl to pH 7.

Solution	**Reagent added (mg/L)**			**Predicted species concentration (mg/L)**				
	$Na_2SiO_3 \cdot 5H_2O$	$CaCl_2 \cdot 2H_2O$	$NaHCO_3$	SiO_2	Ca^{2+}	Na^+	Cl^-	HCO_3^-
SiO_2	800			226		173	267	
SiO_2–HCO_3^-	800		312.5	221		257	267	217
SiO_2–Ca^{2+}	800	550		226	150	173	532	
SiO_2–Ca^{2+}–HCO_3^-	800	550	312.5	223	143	257	532	204

2.3.2 Membranes and modules

Hydrophobic, microporous polypropylene membrane manufactured by 3M (St. Paul, MN) was used for MD experiments. The membrane is symmetric and isotropic with a nominal pore size of 0.2 μm, a porosity of 85%, and a thickness of 110 μm. The new membrane was determined to have a contact angle of 124° using the sessile drop method and a Standard Goniometer (Model 200, Ramé-Hart Instrument, CO, Succasunna, NJ). Custom acrylic flow cells were fabricated for the MD experiments featuring ten 18 cm long, by 6.35 mm wide, by 3.2 mm deep parallel flow channels on the feed and distillate sides, providing a total membrane surface area of 125 cm^2. No spacers were used to simplify and ensure consistency in the hydrodynamic conditions near the membrane surface.

Commercial NF membrane was used in the study (NF90, DOW Chemical Company, Midland, MI). The membrane is a polyamide thin-film composite membrane designed for commercial systems, and was chosen primarily due to its low operating pressure and high rejection of silica [53]. The NF90 membrane elements are rated for a maximum operating temperature of 45 °C and a maximum operating pressure of 4.14 MPa (600 psi). However, per the manufacturer this is largely due to the materials and glue used in the spiral-wound membrane elements. The flat sheet membrane coupons themselves are tolerant of higher temperatures. Custom acrylic flow cells were fabricated for the NF experiments featuring feed channels identical to the feed channel geometry of the MD flow cell. The permeate side consisted of a single channel, 1 mm in thickness, and a tricot spacer was installed in the channel to provide support for the membrane and allow the permeate to flow out of the cell.

2.3.3 System description

Experiments were conducted using an automated, closed-loop, bench-scale system capable of conducting both MD and NF experiments. Temperature was monitored using silicon-type temperature sensors (Model EI1034, Electronic Innovations Corp., Lakewood, CO) and feed temperature was maintained using a heat exchanger with water as the working fluid heated with a 1500 W electric heater (Model 1019, Hotwatt, Danvers, MA). Conductivity was monitored continuously in both feed and permeate solutions to track salt rejection using a toroidal sensor (Model TCSMA, Sensorex, Garden Grove, CA) and a conductivity probe (Model T-35820-62, Cole-Parmer, Vernon Hills, IL), respectively. Water flux across the membrane was calculated by measuring the change in height of the water column in the permeate tank over time using a 0–7 kPa (0–1 psi) pressure transducer (Model PX309-001G5V, Omegadyne Inc., Sunbury, OH). The permeate tank was also fitted with a solenoid valve to allow collected distillate to drain back into the feed tank when the permeate reached a specified volume during experiments, allowing for extended operation within a specified feed concentration range. Data collection and operating conditions were controlled using Labview software (National Instruments) and a multichannel DAQ (U6, Labjack, Lakewood, CO).

During MD experiments (Figure 2.1), feed and distillate were pumped continuously through the system using positive-displacement gear pumps (Micropump Integral Series, IDEX Corp. Vancouver, WA). Temperature of the distillate was maintained using a chilled glycol

solution and a heat exchanger, with the flow rate of the glycol solution controlled using a proportional valve (Model EPV-SS-6L, Hass Manufacturing Company, Averill Park, NY).

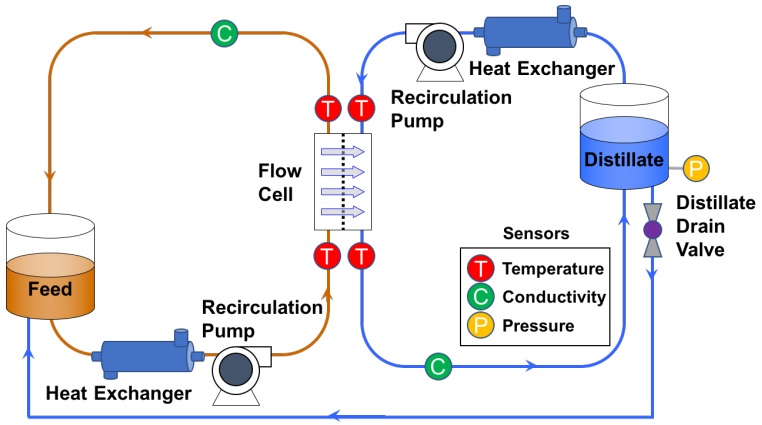

Figure 2.1. System schematic configured for MD. Feed and distillate were circulated at constant 2.0 L/min in countercurrent flow configuration. Feed and distillate temperatures were monitored at the inlet and outlet of the flow cell. Conductivity was monitored in both feed and distillate streams between the flow cell and tanks. Volume of collected distillate was measured using a pressure transducer in the bottom of the distillate tank. Feed concentration was controlled by periodically returned collected distillate back to feed tank using an automated solenoid valve.

Temperatures of the feed and distillate solutions were measured at both the inlet and outlet of the flow cell to enable calculation of thermal efficiency, which is defined in MD as the ratio of the latent heat transfer associated with vapor flux through the membrane to the total heat transfer across the membrane:

$$\eta_{th} = \frac{Q_{vap}}{Q_{vap}+Q_{cond}} \tag{2.1}$$

where η_{th} is the thermal efficiency, Q_{vap} is the latent heat transfer associated with the vapor transport through the membrane and Q_{cond} is the conduction heat transfer. Experimentally, the total heat transfer can be calculated using the change in enthalpy between the inlet and outlet of the flow cell. In this study, thermal efficiency was calculated using the measured enthalpy change of the distillate because it was approximately equal to the ambient temperature and heat transfer through the flow cell to the environment was negligible:

$$\eta_{th} = \frac{\dot{m}_m \Delta H_{vap}}{c_p[(\dot{m}_d + \dot{m}_m)T_{d,out} - \dot{m}_d T_{d,in}]} \quad (2.2)$$

where $\dot{m}_m$ is the mass flow rate through the membrane, $\dot{m}_d$ is the mass flow rate of the distillate, ΔH_{vap} is the latent enthalpy of vaporization of water, and c_p is the constant-pressure specific heat of pure water. $T_{d,in}$ and $T_{d,out}$ are the temperature of the distillate at the inlet and outlet of the flow cell, respectively.

During NF experiments (Figure 2.2) a high-pressure pump was used to circulate the feed solution at constant flow rate of 2.0 L/min, with constant pressure maintained using an automated proportional valve to restrict flow (Model EPV-SS-6L, Hass Manufacturing Company, Averill Park, NY). Pressure was monitored at the outlet of the feed channel using a 0–1.7 MPa (0–250 psi) pressure transducer (Model EW-68075-50, Cole-Parmer, Vernon Hills, IL).

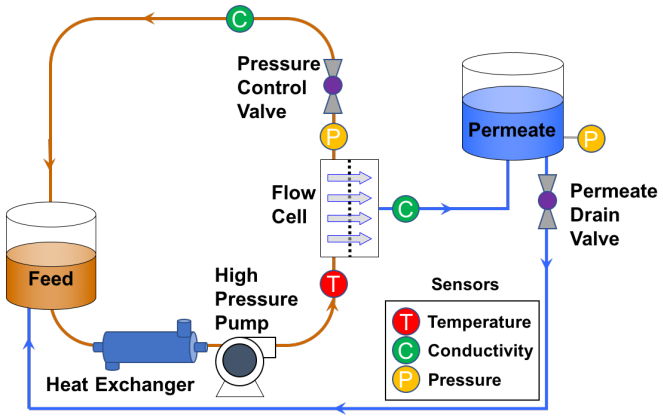

Figure 2.2. System schematic configured for NF. Feed was circulated using a high-pressure pump at constant 2.0 L/min. Feed temperature was measured at the inlet of the flow cell. Feed pressure was measured at the outlet of the flow cell and controlled using an automated proportional valve. Conductivity was measured in both feed and permeate. Volume of collected permeate was measured using a pressure transducer located on the bottom of the permeate tank. Feed concentration was controlled by periodically returning collected permeate back to feed tank using an automated solenoid valve.

2.3.4 Experimental procedures

Both MD and NF experiments were performed using synthetic solutions with initial feed volume of 4 L and new membrane samples. Feed flow rate was maintained constant at 2.0 L/min, providing a flow velocity of 16.6 cm/s and Reynolds number of 680–1670, dependent on

temperature. In each experiment, the feed solution was concentrated until a maximum of 2.5 L of permeate/distillate was collected, at which point 0.5 L of permeate/distillate was returned to the feed tank. This procedure continued for the duration of the experiment, maintaining the concentration factor ($CF = V_o / (V_o–V_p)$) of the feed solution between 2 and 2.67. Based on the initial concentration of sodium silicate added, the concentration of silica of the test solutions reached as high as 600 mg/L and was not lower than 450 mg/L once reaching the maximum feed concentration.

2.3.4.1 MD Experiments

All MD experiments were conducted in a direct contact MD (DCMD) mode, operated in a countercurrent flow configuration. Feed and distillate flow rate were maintained constant at 2.0 L/min. Baseline performance characterization of the membrane and configuration used were determined using a 1 g/L NaCl feed solutions and temperatures between 30 and 70 °C with distillate temperatures between 20 and 30 °C. Only the 1 g/L NaCl solution was tested because MD is not affected by the osmotic pressure of the feed and the effect of ionic strength on vapor pressure is negligible at the concentrations used in this investigation. MD experiments using solutions containing silica were performed with feed inlet temperature maintained at 60 °C and distillate inlet temperature maintained at 20 °C.

2.3.4.2 NF experiments

All NF membranes used in the study were compacted by operating with deionized water circulated through the system at a constant flow rate of 2.0 L/min and a pressure of 620 kPa (90 psi) to condition the membranes prior to experiments. Baseline performance characteristics of the membrane and configuration used were determined using NaCl solutions as feed. Membranes were tested with feed concentrations of 1 and 4 g/L, temperatures between 25 to 60 °C, and pressures between 207 and 620 kPa (30–90 psi). To investigate the influence of temperature on mineral scaling, parallel NF experiments with SiO_2, SiO_2–Ca^{2+}, and SiO_2–Ca^{2+}–HCO_3^- solutions were conducted with feed temperatures of 25 °C (baseline) and 60 °C, and operating pressures between 207 and 483 kPa (30–70 psi).

2.4 Results and Discussion

2.4.1 Membrane distillation

2.4.1.1 Effects of feed and distillate temperatures on MD performance

Average water flux was ~27 L/m^2/hr for the 1 g/L NaCl feed solution at 60 °C and distillate temperature of 20 °C (Figure 2.3a). As expected, due to the exponential relationship between vapor pressure and temperature, exponential relationship between ΔT (ΔT = $T_{f,in} - T_{d,in}$) and water flux was observed, and water flux was higher at increased overall temperatures for similar ΔT. Despite the increase in water flux with temperature, measured thermal efficiency was not strongly affected by operating conditions, and was relatively constant at approximately 50% (Figure 2.3b). Salt rejection was very high, exceeding 99.8% for almost all conditions tested.

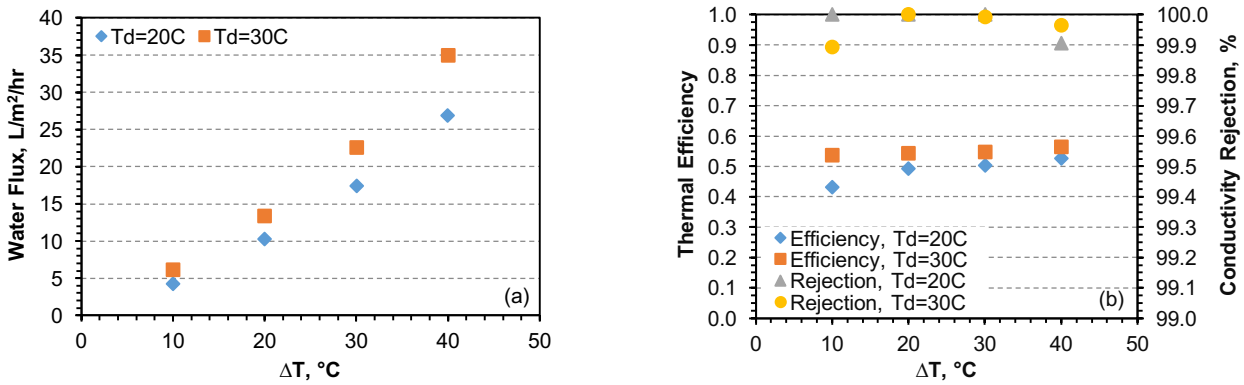

Figure 2.3. Measured (a) water flux and (b) thermal efficiency and conductivity rejection for the 3M MD membrane. Feed solution was 1 g/L NaCl and both feed and distillate were circulated at constant 2.0 L/min. Influence of temperature was evaluated by testing ΔT between 10 and 40 °C with distillate temperature of 20 °C or 30 °C.

2.4.1.2 MD testing: silica removal and membrane fouling

Initial water flux, ranging from 27 to 30 L/m^2/hr for all solutions tested, was not strongly affected by solution composition (Figure 2.4a)—water flux was stable during the initial concentration period for all experiments, regardless of composition. This is because MD is not affected by differences in osmotic pressure between the feed and permeate and water flux is controlled by the partial vapor pressure difference of water. The presence of dissolved ions in solution may impact the partial vapor pressure and viscosity, but the effect is negligible at the low concentrations used in this investigation. After the initial concentration period of relatively

stable operation, water flux declined rapidly because of silica scaling. This suggests the possibility of some initial resistance to scaling; but once scaling begins, it proceeds rapidly and severely impacts water flux. However, induction time for silica polymerization is highly dependent on the degree of supersaturation. For example, Rothbaum and Rohde found that at 60 °C the induction time was between 500–1000 min for 450 mg/L silica but less than 50 min for 600 mg/L silica [54]. Therefore, it is possible that no colloids were present until reaching the maximum concentration factor for the MD experiments.

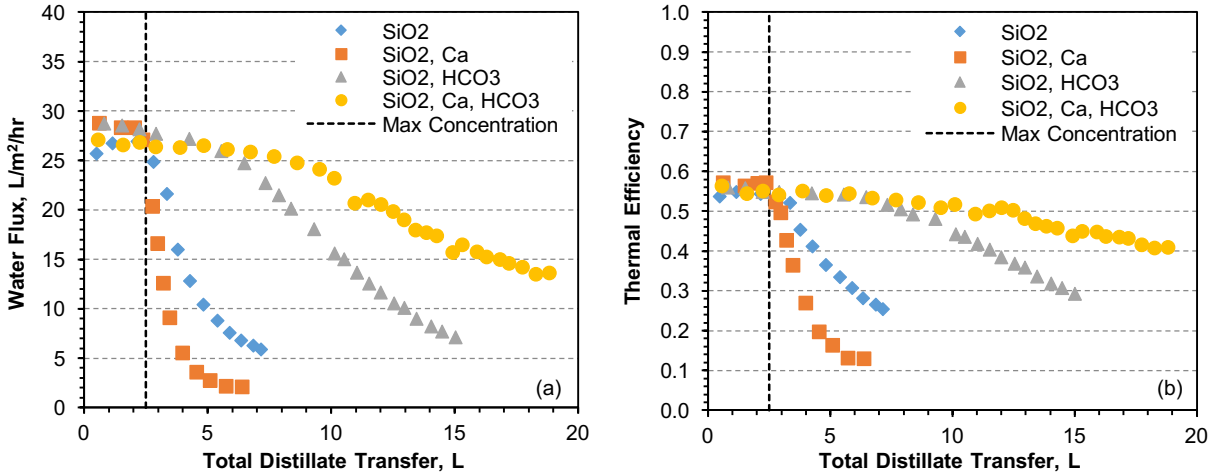

Figure 2.4. Measured (a) water flux and (b) thermal efficiency for MD membranes tested with SiO_2, SiO_2–Ca^{2+}, SiO_2–HCO_3^-, and SiO_2–Ca^{2+}–HCO_3^- solutions. Feed temperature was 60 °C and distillate was 20 °C. Feed and distillate solutions were circulated at constant 2.0 L/min in a countercurrent flow configuration. Feed solutions had initial concentration of ~225 mg/L as silica and equimolar concentrations of Ca^{2+} and HCO_3^- where applicable. Predicted species concentrations are listed in Table 2.1. Vertical dashed line indicates the first time of maximum concentration (CF=2.67). After reaching maximum concentration permeate was periodically returned to feed tank to maintain concentration factor between 2 and 2.67 for the remainder of each experiment.

The presence of calcium increased fouling rate and severity in the MD experiments, while bicarbonate alkalinity appeared to mitigate the effect of scaling. Decline in water flux during experiments containing bicarbonate was slower, and the overall decline in water flux was less severe than in experiments without bicarbonate. Curiously, the mitigating effect of bicarbonate appeared to be enhanced by calcium. The reasons for the reduced flux decline in the experiment using the SiO_2–Ca^{2+}–HCO_3^- as feed are unclear and may be due to removal of

calcium from solution as solid $CaCO_3$. At the conclusion of these experiments, feed water samples were analyzed using ICP-AES, which found lower calcium concentrations in the SiO_2–Ca^{2+}–HCO_3^- solution than expected, based on concentration factor and measured conductivity rejection. This suggests that some calcium precipitated out of solution during the experiments; likely on the heat exchanger surfaces used to maintain feed temperature due to the lower solubility of $CaCO_3$ at high temperature (Table 2.2).

Table 2.2. Dominant scaling tendencies for synthetic silica solutions, calculated using OLI Stream Analyzer. Species concentration for each solution are summarized in Table 2.1.

Species	**Solution**							
	SiO_2		SiO_2–HCO_3^-		SiO_2–Ca^{2+}		SiO_2–Ca^{2+}–HCO_3^-	
	25 °C	60 °C	25 °C	60 °C	25 °C	60 °C	25 °C	60 °C
SiO_2	1.98	1	1.94	1	1.98	1	1.96	1.08
Calcite							4.82	5.46
Aragonite							2.04	3.66

In addition to acting as a catalyst for polymerization, polyvalent cations facilitate deposition of colloidal silica onto surfaces by enhancing collisions and adhesion between the negatively-charged colloids and the surface [16]. However, in MD, liquid water does not enter the membrane pores but instead evaporates off a surface that is supported by the membrane, which may limit the extent of actual contact between the silica colloids and the membrane itself. Also, silica colloids are hydrophilic due to the presence of silanol (SiOH) groups on their surfaces, which inhibits attachment to hydrophobic surfaces [16]. These factors may contribute to the long induction times before impacts of silica scaling were observed in the MD experiments, resulting in high silica concentrations in the bulk solution. Most likely, silica colloids formed by homogeneous polymerization and were forced towards the membrane surface due to permeate drag forces after reaching a critical size. At that point, a scale layer began to form and grew rapidly due to a combination of colloidal deposition and heterogeneous polymerization on the scale layer.

Conductivity rejection was not affected by silica fouling and remained higher than 99.9% for all solutions tested throughout all experiments. Thermal efficiency declined in a similar timeframe as water flux, but the decline was not as severe for any case (Figure 2.4b). For example, in the most extreme case with the SiO_2–Ca^{2+} solution, the water flux dropped from 28

L/m^2/hr to less than 3 L/m^2/hr, a decline of more than 90%. Over the same period, the thermal efficiency declined from 0.57 to 0.15, a decline of less than 74%. Because thermal efficiency is primarily affected by membrane properties, a likely explanation is that the effect of the silica scale layer on thermal resistance is higher than its effect on mass transport resistance.

2.4.2 Nanofiltration

2.4.2.1 Effects of temperature, salinity, and pressure on NF performance

NF performance was strongly affected by both temperature and salinity. Water flux during testing with 1 g/L NaCl feed solution increased almost threefold when temperature was raised from 25 °C to 60 °C, despite constant pressure of 483 kPa (70 psi) (**Error! Reference source not found.**a). Conversely, as little as 4 g/L NaCl feed concentration reduced water flux by 47% at 25 °C and 56% at 60 °C compared to 1 g/L NaCl (Figure 2.5a).

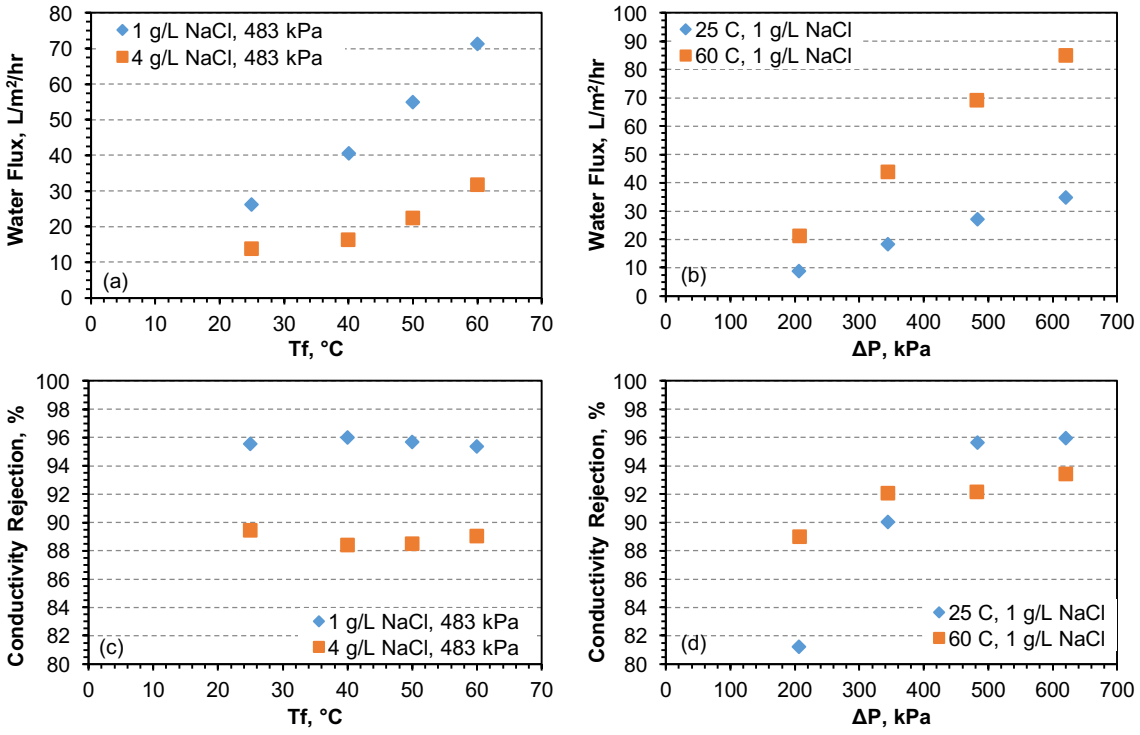

Figure 2.5. Measured (a, b) water flux and (c, d) conductivity rejection for NF90 membranes tested with NaCl solutions. Feed velocity was constant 16.6 cm/s. Influence of feed temperature was evaluated by testing solutions of constant 1, or 4 g/L NaCl and constant 483 kPa between temperatures of 25 and 60 °C (a, c). Influence of feed pressure was evaluated by testing solutions of constant 1 g/L and constant temperature of 25 °C or 60 °C between pressures of 207 kPa (30 psi) and 621 kPa (90 psi) (b, d).

Water flux increased with temperature due to the increased permeability of NF membranes and reduced feed water viscosity at increased temperature (Table 2.3). Viscosity is not strongly impacted at low concentrations; however, the osmotic pressure increases almost fourfold between 1 and 4 g/L NaCl at both 25 °C and 60 °C, leading to reduced driving force for mass transport with increased salinity. As expected, the relationship between operating pressure and water flux are linear, with a steeper slope at higher temperature (Figure 2.5b). Salt rejection was not affected substantially by temperature but was impacted by increased salinity (Figure 2.5c). And lastly, operating pressure was found to have a larger impact on salt rejection, with a marked decrease in rejection observed below 345 kPa (50 psi) (Figure 2.5d).

Table 2.3. Calculated viscosity and osmotic pressure of pure water, 1 g/L NaCl, and 4 g/L solutions at 25 °C and 60 °C.

Solution	**Viscosity, Pa-s**		**Osmotic Pressure, kPa (psi)**	
	25 °C	60 °C	25 °C	60 °C
Pure water	8.91E-04	4.67E-04	0 (0)	0 (0)
1 g/L NaCl	8.93E-04	4.68E-04	81.5 (11.8)	89.6 (13.0)
4 g/L NaCl	8.97E-04	4.71E-04	319.0 (46.3)	349.8 (50.7)

2.4.2.2 NF testing: silica removal and membrane fouling

The influence of temperature on performance and rejection in the NF processing using silica solutions were determined by performing experiments at 25 °C and 60 °C using and operating pressure of 483 kPa (70 psi). Initial water flux for NF experiments with SiO_2 and SiO_2–Ca^{2+} feed solutions at 25 °C were much higher than the SiO_2–Ca^{2+}–HCO_3^- feed solution (Figure 2.6a). This is likely a result of the lower osmotic pressure of the sodium silicate—for example, the osmotic pressure of the SiO_2 solution at the beginning of the experiment was 45.6 kPa (6.6 psi) at 25 °C compared to 111.7 kPa (16.2 psi) for the SiO_2–Ca^{2+}–HCO_3^- solution (Table 2.4).

The induction time observed in MD experiments did not occur with NF, and water flux for all three solutions rapidly declined during the period when solutions were initially concentrated to the maximum concentration factor of 2.67. The rate of flux decline was most severe for the SiO_2–Ca^{2+} solution and least severe for the SiO_2–Ca^{2+}–HCO_3^- solution, although the initial water flux for the latter was notably lower than either of the other solutions tested. Considering the impact of salinity on water flux for NF, the initial flux decline may partially be

attributed to the increase in concentration of the feed solutions. The impact of increased osmotic pressure was especially prominent for the SiO_2–Ca^{2+}–HCO_3^- solution, which had a distinct reduction in the rate of flux decline after reaching the maximum concentration and permeate cycling began. No immediate changes in rate of flux decline were observed for the SiO_2 and SiO_2–Ca^{2+} solutions after reaching maximum concentration, suggesting that fouling also contributed to flux decline during the initial concentration for these experiments and probably played a more important role than the effect of increasing osmotic pressure.

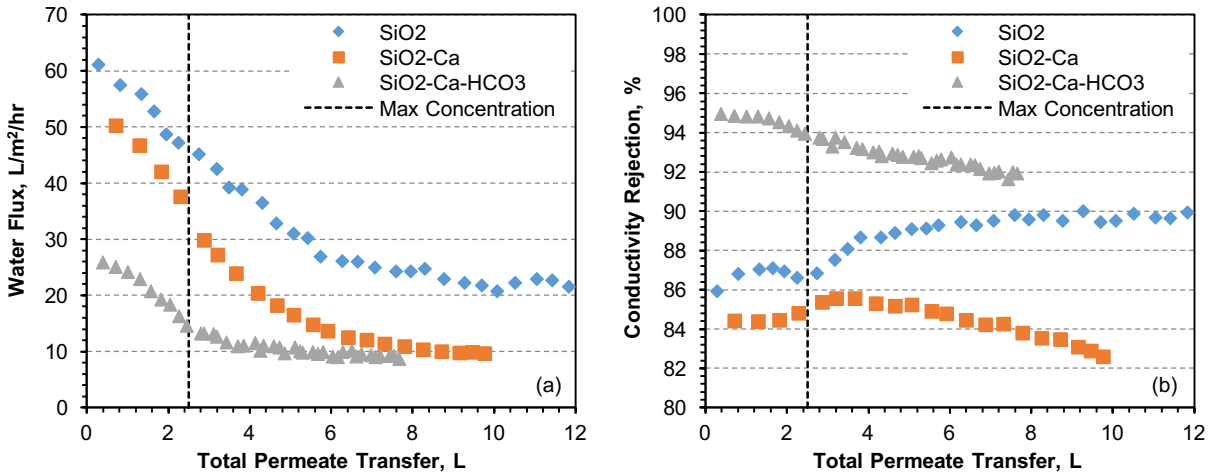

Figure 2.6. Measured (a) water flux and (b) conductivity rejection for NF membranes tested with SiO_2, SiO_2–Ca^{2+}, and SiO_2–Ca^{2+}–HCO_3^- solutions at constant **25 °C** and 483 kPa (70 psi). Feed solutions were circulated at constant 2.0 L/min. Feed solutions had initial concentration of ~225 mg/L as silica and equimolar concentrations of Ca^{2+} and HCO_3^- where applicable. Predicted species concentrations are listed in Table 2.1. Vertical dashed line indicates the first time of maximum concentration (CF=2.67). After reaching maximum concentration permeate was periodically returned to feed tank to maintain concentration factor between 2 and 2.67 for the remainder of each experiment.

Water flux for all solutions continued to slightly decline after the initial concentration period, with the concentration factor maintained between 2.0 and 2.67, but approached a relatively stable flux after sufficient time. After each experiment, a beige deposit was observed on the membrane surface, suggesting that scaling occurred by indirect deposition of colloidal silica. Monomeric silica, $Si(OH)_4$, requires specific conditions to deposit directly onto surfaces, particularly the presence of OH^- groups with which to react [16]. Such deposition is rare and when it does occur it tends to form an impermeable, glassy surface. Rather, when present in

water at concentrations exceeding solubility it tends to polymerize in solution, eventually forming colloids that collide and attach to each other and surfaces. Deposits formed in this manner tend to form an opaque and somewhat porous layer.

Both the SiO_2–Ca^{2+} and SiO_2–Ca^{2+}–HCO_3^- solutions appeared to converge to a similar steady water flux despite a substantial difference in initial osmotic pressure (Table 2.4). This is not surprising because colloidal fouling in membrane processes is highly influenced by permeate drag forces, which determine the rate at which particles can be driven towards the membrane surface [55]. As water flux decreases, eventually the permeate drag forces are reduced to a critical value and cake development ceases, which restricts the extent of impacts fouling can have on water flux. The minimum flux of the SiO_2–Ca^{2+} and SiO_2–Ca^{2+}–HCO_3^- solutions was substantially lower than the final flux of the SiO_2 solution and may be due to increased polymerization rate catalyzed by the Ca^{2+} ions, or the role of Ca^{2+} ions in attaching silica colloids to the membrane surface and eventually the silica scale itself. The presence of calcium has a negligible effect on silica solubility, but has been shown to accelerate polymerization of colloidal silica and accelerate silica fouling in RO membranes [11, 18, 51].

Initial conductivity rejection for the SiO_2–Ca^{2+}–HCO_3^- solution was similar to the measured conductivity rejection of 1 g/L NaCl solution at similar temperature and pressure, whereas the initial conductivity rejections for both the SiO_2 and SiO_2–Ca^{2+} solutions were substantially lower (Figure 2.6b). Conductivity rejection of both solutions containing calcium declined over the duration of the experiment, whereas rejection in the SiO_2 solution increased and eventually stabilized. It is important to note that at neutral pH, soluble silica primarily exists as neutral monomeric silicic acid and does not contribute substantially to measured conductivity rejection. Conductivity rejection for the solutions with no added calcium is therefore likely to be a measurement of NaCl rejection, and its increase may be attributed to the silica scaling.

Table 2.4. Calculated viscosity and osmotic pressure for synthetic silica solutions. Species concentration for each solution are listed in Table 2.1.

Solution	**Viscosity, Pa-s**		**Osmotic Pressure, kPa (psi)**	
	25 °C	60 °C	25 °C	60 °C
SiO_2	8.92E-04	4.67E-04	45.6 (6.6)	50.0 (7.2)
SiO_2–HCO_3^-	8.93E-04	4.68E-04	74.3 (10.8)	82.3 (11.9)
SiO_2–Ca^{2+}	8.93E-04	4.68E-04	81.8 (11.9)	90.0 (13.1)
SiO_2–Ca^{2+}–HCO_3^-	8.95E-04	4.69E-04	111.7 (16.2)	124.3 (18.0)

The decline in water flux during experiments with SiO_2 and SiO_2–Ca^{2+}–HCO_3^- feed solutions tested at 60 °C followed a similar trend as during experiments conducted at 25 °C. As expected, initial water flux for all feed solutions was much higher with feed temperature of 60 °C than with 25 °C (Figure 2.7a). Water flux declined rapidly for the SiO_2, SiO_2–Ca^{2+}, and SiO_2–Ca^{2+}–HCO_3^- solutions despite the increased solubility of silica at elevated temperature, which at 60 °C may exceed 300 mg/L [56], well above the initial concentration of 225 mg/L used in the present investigation.

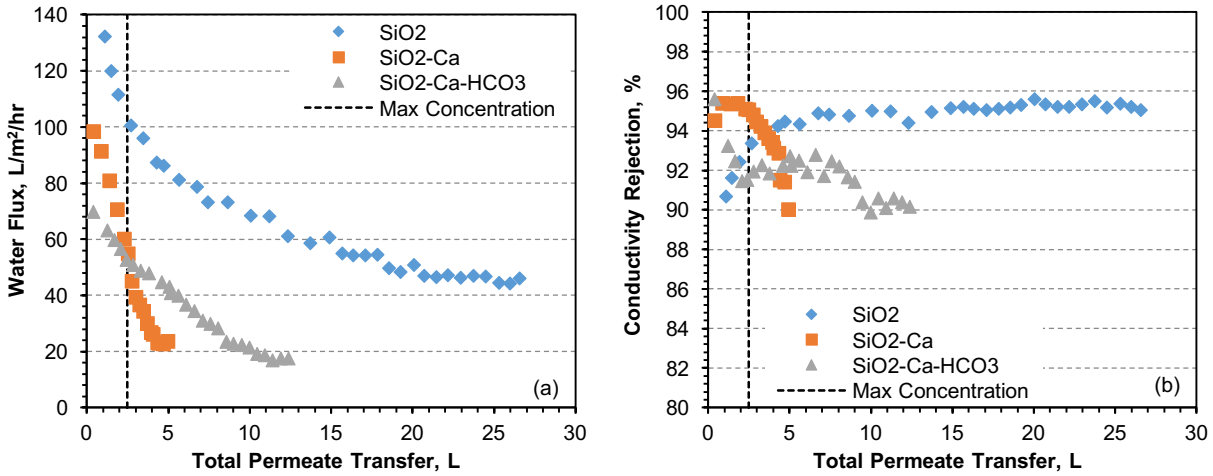

Figure 2.7. Measured (a) water flux and (b) conductivity rejection for NF membranes tested with SiO_2, SiO_2–Ca^{2+}, and SiO_2–Ca^{2+}–HCO_3^- solutions at constant **60 °C** and 483 kPa (70 psi). Feed solutions were circulated at constant 2.0 L/min. Feed solutions had initial concentration of ~225 mg/L as silica and equimolar concentrations of Ca^{2+} and HCO_3^- where applicable. Predicted species concentrations are listed in Table 2.1. Vertical dashed line indicates the first time of maximum concentration (CF=2.67). After reaching maximum concentration permeate was periodically returned to feed tank to maintain concentration factor between 2 and 2.67 for the remainder of each experiment.

Also, unlike the experiments performed at 25 °C, no immediate reduction in the rate of flux decline was observed for the SiO_2–Ca^{2+}–HCO_3^- after reaching maximum concentration. The immediate and rapid flux decline was the result of several factors. The higher initial flux of these experiments led to increased concentration polarization and higher degrees of supersaturation at the membrane surface, which leads to shorter induction times and higher rates of polymerization [54]. Also, the size of the initial polymers formed tends to increase with temperature [54], which coupled with the increased permeate drag forces associated with higher water flux led to a more

rapid agglomeration of silica polymers at the membrane surface. The influence of calcium on silica scaling behavior was also affected by temperature, and rate of flux decline during experiments with the SiO_2–Ca^{2+} feed solution was notably more severe. Similar to what was observed in the MD experiments, the influence of calcium was reduced slightly by alkalinity at 60 °C, and a lower water flux was reached with the SiO_2–Ca^{2+} solution much earlier than the SiO_2–Ca^{2+}–HCO_3^- feed solution.

Initial conductivity rejection at 60 °C was higher than at 25 °C for the SiO_2 and SiO_2–Ca^{2+} solutions, and similar for the SiO_2–Ca^{2+}–HCO_3^- solution (Figure 2.7b). Initial conductivity rejection for all solutions was between 90 and 95%, and followed similar trends as observed for experiments conducted at 25 °C—decreasing slightly for the SiO_2–Ca^{2+} and SiO_2–Ca^{2+}–HCO_3^- solutions and increasing for the SiO_2 solution.

2.4.3 Comparison of MD and NF

To facilitate a closer comparison between the two processes, additional NF experiments were conducted with similar feed solution composition as used in the MD experiments but with the *pressure* adjusted to match the initial water flux of the MD experiments (27–30 L/m^2/hr). This ensured similar concentration polarization in the feed channels, and transport of silica colloids towards the membrane surface. Temperature had a stronger effect than the presence of calcium, with slightly faster flux decline at 25 °C than at 60 °C (Figure 2.8a).

This is possibly a result of the reduced solubility of silica at lower temperatures, resulting in a higher degree of supersaturation with concentration and a larger quantity of colloidal silica formed at lower temperatures. Decline in water flux began immediately, although at a lower rate than occurred during the 483 kPa (70 psi) experiments. The influence of increased osmotic pressure with concentration was also more substantial compared to experiments performed at higher feed pressure; the rate of flux decline decreased slightly for all experiments after reaching the maximum concentration and the initiation of permeate cycling. Water flux continued to slowly decline with the concentration factor maintained between 2 and 2.67, but the rates of flux decline and the extent of flux decline (relative to the initial flux) were both lower than the higher pressure NF or MD experiments performed with similar solution chemistry. Both solutions at 60 °C showed higher conductivity rejection than the tests at 25 °C despite having similar initial flux and using a lower operating pressure of 207 kPa (30 psi) compared to 276–310 kPa (40–45 psi)

for the 25 °C experiments (Figure 2.8b)—this is expected due to the higher water flux in these experiments.

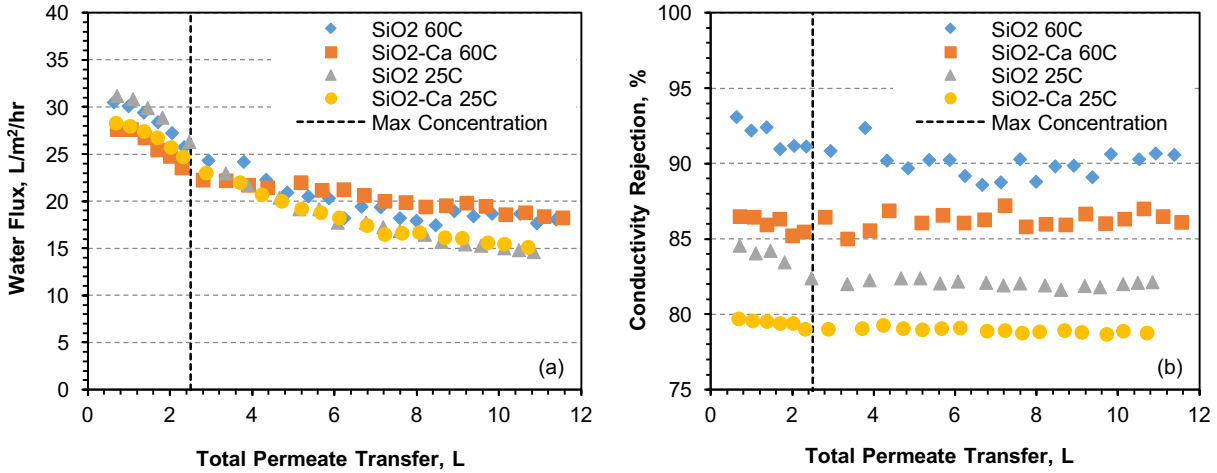

Figure 2.8. Measured (a) water flux and (b) conductivity rejection for NF membranes tested with SiO_2 and SiO_2–Ca^{2+} solutions at constant 25 °C or 60 °C and operating pressure adjusted between 207 and 310 kPa (30–45 psi) to obtain an initial water flux of ~30 L/m^2/hr. Feed solutions were circulated at constant 2.0 L/min. Feed solutions had initial concentration of ~225 mg/L as silica and equimolar concentrations of Ca^{2+} where applicable. Predicted species concentrations are listed in Table 2.1. Vertical dashed line indicates the first time of maximum concentration (CF=2.67). After reaching maximum concentration permeate was periodically returned to feed tank to maintain concentration factor between 2 and 2.67 for the remainder of each experiment.

NF experiments performed at 60 °C and 207 kPa (30 psi) had similar patterns of water flux for all feed solutions (Figure 2.9a). This is because the initial water flux of ~30 L/m^2/hr in the NF experiments was very close to the critical minimum flux for the experimental conditions, as evidenced by the fact that the NF experiments performed with SiO_2–Ca^{2+} and SiO_2–Ca^{2+}–HCO_3^- at 60 °C and 483 kPa (70 psi) both stabilized at a similar minimum flux of about 20 L/m^2/hr (Figure 2.9a). Thus, the influence of solution chemistry on silica polymerization and scaling behavior for these experiments was negligible. Conductivity rejection of the NF membrane at 60 °C and 207 (30 psi) was mostly a function of solution composition, and did not change much over the course of experiments (Figure 2.9b).

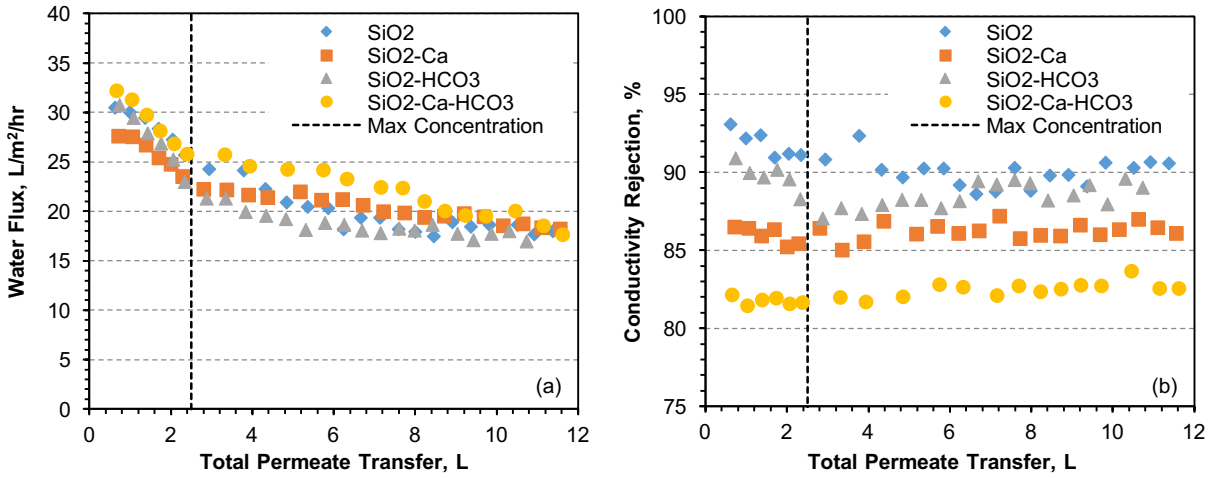

Figure 2.9. Measured (a) water flux (with a tab of Fig. 4a) and (b) conductivity rejection for NF membranes tested with SiO_2, SiO_2–Ca^{2+}, SiO_2–HCO_3^-, and SiO_2–Ca^{2+}–HCO_3^- solutions at constant 60 °C and operating pressure of 207 kPa (30 psi) to obtain an initial water flux of ~30 L/m^2/hr. Feed solutions were circulated at constant 2.0 L/min. Feed solutions had initial concentration of ~225 mg/L as silica and equimolar concentrations of Ca^{2+} and HCO_3^- where applicable. Predicted species concentrations are listed in Table 2.1. Vertical dashed line indicates the first time of maximum concentration (CF=2.67). After reaching maximum concentration permeate was periodically returned to feed tank to maintain concentration factor between 2 and 2.67 for the remainder of each experiment.

The similarity in patterns of flux decline in the NF experiments are in sharp contrast to the rather substantial differences in patterns of flux decline observed in MD experiments (Figure 2.4a). Due to the similar chemistry, temperature, and hydrodynamics of these experiments, it is unlikely that there were substantial differences in silica polymerization behavior between the two processes. However, unlike the NF experiments, rapid and severe flux decline was observed in MD experiments performed with SiO_2 and SiO_2–Ca^{2+} solutions, while much lower rates of flux decline were observed for the SiO_2–HCO_3^- and SiO_2–Ca^{2+}–HCO_3^- solutions. These results suggest that the processes that govern silica scaling and its impacts on MD performance are fundamentally different than those for pressure driven-processes and these differences should be explored in future research to better understand silica scaling behavior and management in MD.

Soluble silica is nonionic in neutral and slightly acidic solutions [16]. To assess the potential correlations between conductivity rejection and soluble silica rejection in NF, feed and permeate samples from the 60 °C and 207 kPa (30 psi) experiments were analyzed for reactive silica using the silicomolybdate method. Initial feed and permeate silica concentrations were

measured after the conductivity of the permeate stabilized, 1–2 hours after starting the experiment, and silica concentration was measured in the feed and permeate at the end of each experiment (feed CF of 2.0 (50% batch recovery)). There was a notable correlation between feed conductivity and silica rejection, with the highest rejection observed in the silica solution and the lowest rejection in the SiO_2–Ca^{2+}–HCO_3^- solution, which had the lowest and highest feed conductivity, respectively. Except for the case of the silica solution with no other added ions, initial silica rejection was generally similar to initial conductivity rejection, and a slight decline was noted between the initial rejection of clean membranes and the final rejection of the scaled membranes (Figure 2.10).

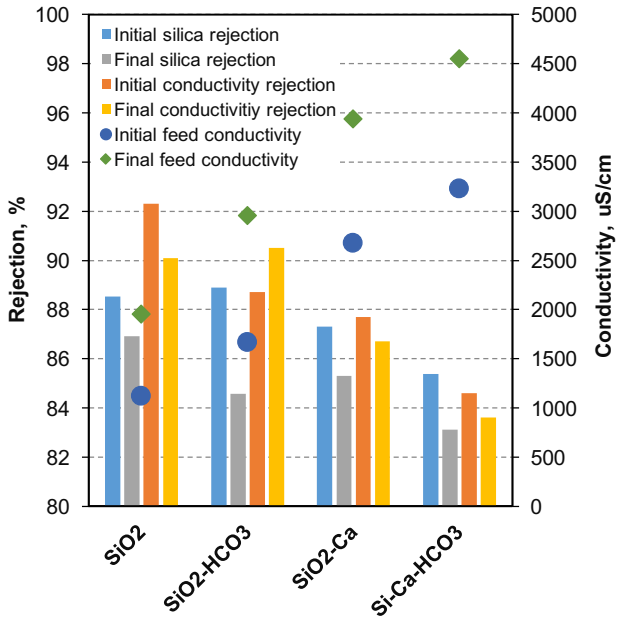

Figure 2.10. Measured initial and final feed conductivity, conductivity rejection, and silica rejection for NF experiments performed at constant temperature of 60 °C and constant temperature of 30 psi. Feed solutions were circulated at constant 2.0 L/min. Feed solutions had initial concentration of ~225 mg/L as silica and equimolar concentrations of Ca^{2+} and HCO_3^- where applicable. Predicted species concentrations are listed in Table 2.1.

Measured reactive silica concentrations for feed samples are summarized in Table 2.5. Due to polymerization into colloidal silica, final reactive silica concentrations were much lower than might be expected based on measured silica rejection and concentration factor. Interestingly, the silica solution had the lowest final silica concentration in the feed, which was

equal to the initial measured concentration and close to the solubility limit of silica at 60 °C, despite all four solutions having similar silica rejection. The other three feed solutions all contained higher final silica concentrations, with the SiO_2–HCO_3 being the highest at 350 mg/L, and no difference between the SiO_2–Ca^{2+} and SiO_2–Ca^{2+}–HCO_3^- solutions.

Table 2.5. Initial and final measured feed silica concentration, silica rejection, and conductivity rejection for NF experiments conducted at 60 °C and 30 psi.

Solution	***Feed silica (mg/L)***		***Silica Rejection (%)***		***Conductivity Rejection (%)***	
	Initial	Final	Initial	Final	Initial	Final
SiO_2	270	260	88.5	86.9	92.3	90.1
SiO_2–HCO_3^-	270	350	88.9	84.6	88.7	90.5
SiO_2–Ca^{2+}	260	320	87.3	85.3	87.7	86.7
SiO_2–Ca^{2+}–HCO_3^-	260	320	85.4	83.1	84.6	83.6

2.4.4 Membrane cleaning

Silica scale is typically very difficult to remove, and mitigation strategies in membrane desalination processes primarily emphasize prevention. However, silica solubility increases dramatically above pH 11 and depolymerization of colloidal silica will occur in highly alkaline solutions [16, 29]. To compare the ability of a high-pH solution to dissolve silica scale and restore performance in the MD and NF processes, a cleaning procedure consisting of rinsing with deionized water followed by recirculation with a NaOH solution of pH 11 was tested on two membranes used with the SiO_2–Ca^{2+} solutions. After cleaning, each membrane was tested with deionized water feed and again with a new SiO_2–Ca^{2+} feed solution to determine the effectiveness of the cleaning procedure.

In the case of MD, the NaOH solution was recirculated at 60 °C with distillate at 20 °C. Additional NaOH was added periodically to maintain a pH of above 11. Because of the nature of the MD process, water vapors permeated through the membrane during the cleaning process and the flux was observed to slightly increase each time NaOH was added, and reached a maximum of 25 L/m^2/hr, which is only slightly lower than the initial clean membrane flux of 28 L/m^2/hr. However, upon subsequent testing with a new SiO_2–Ca^{2+} solution, the water flux slightly declined to 23 L/m^2/hr and began to sharply decline immediately (Figure 2.11a). The induction

time prior to flux decline due to silica scaling noted in the previous MD test with a new membrane was not observed in the second fouling cycle after cleaning.

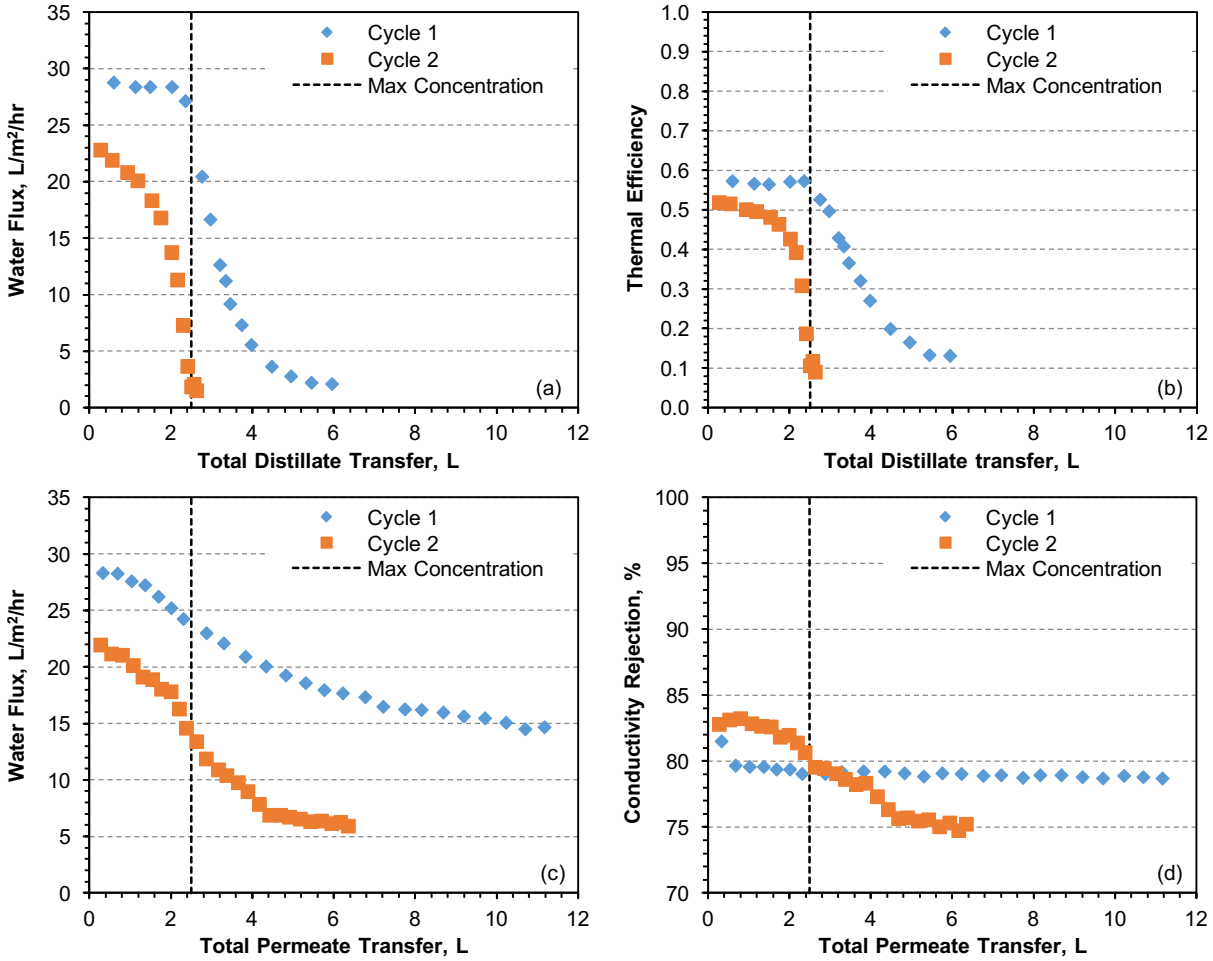

Figure 2.11. Measured (a) water flux and (b) thermal efficiency for MD membranes, and measured (c) water flux and (d) conductivity rejection for NF membranes over two concentration cycles of SiO_2–Ca^{2+} solution with initial concentration of ~225 mg/L as silica and equimolar concentrations of Ca^{2+}. Predicted species concentrations are listed in Table 2.1. A new synthetic solution was used for each cycle. Between the two cycles, the membranes were rinsed with deionized water and cleaned using a NaOH solution at pH >11. Vertical dashed line indicates the first time of maximum concentration (CF=2.67). After reaching maximum concentration permeate was periodically returned to feed tank to maintain concentration factor between 2 and 2.67 for the remainder of each experiment.

In the case of NF, the membrane used at 25 °C was cleaned with a 25 °C NaOH solution for one hour, with additional concentrated NaOH added periodically to maintain a pH of above 11. This process appeared to be effective and when tested with deionized water feed at the

operating pressure of 310 kPa (45 psi), the water flux was restored to about 27 L/m^2/hr. However, upon subsequent testing with a new SiO_2–Ca^{2+} solution (~1,100 mg/L TDS), the water flux was only 21 L/m^2/hr and immediately began to decline. Membrane fouling followed a similar pattern as the initial testing, except both initial and final water flux were lower than that of the clean membrane (Figure 2.11c).

The results of both MD and NF suggest that exposure to a NaOH solution above pH 11 does partially remove the silica scale from membrane surfaces, but the remaining silica increases scaling propensity and leads to increased fouling rates in both processes. However, the MD membrane retained high rejection after the cleaning procedure, and the relationships between water flux and thermal efficiency during the second fouling cycle were similar to those of a new membrane (Figure 2.11b), whereas rejection declined in the NF membrane from more than 79% to approximately 75% after cleaning (Figure 2.11d). Thus, while a practical and effective cleaning procedure for silica scale remains a difficult challenge, the results of this investigation suggest that MD membranes are more resilient to chemical cleaning of silica scale than NF membranes.

2.5 Conclusion

In this investigation, scaling behavior and its impacts on a thermally driven membrane process (MD) were compared to a pressure driven process (NF) applied for treatment of silica-saturated water in combinations that included Si, Si + Ca^{2+}, Si + HCO_3^-, and Si + Ca^{2+} + HCO_3^-. Despite similar initial water flux and hydrodynamic conditions, there were substantial differences between the two processes. Water flux declined immediately in NF due to silica scaling as concentration in the feed water exceeded saturation. In contrast, MD membranes were initially resistant to scaling impacts and all solutions were concentrated to more than twice the solubility limit of silica before performance declined. This was attributed to the hydrophobic nature of the membranes used in MD, which are not receptive to heterogeneous nucleation by silica. However, after the initial induction time the impacts of scaling tended to be more severe in MD, except for solutions containing HCO_3^-. Thus, MD may be better suited for desalination of water resources supersaturated with silica than pressure driven processes if the desired water recovery can be achieved before silica colloids develop sufficient size to cause scaling. While this might require a large amount of MD membrane, the overall footprint of a treatment system

could in some cases be reduced by pretreatment with NF, which was capable of much higher water flux than MD. Additionally, NF performance was improved at increased temperatures, suggesting the possibility of high-temperature NF as a pretreatment strategy for hot brines, i.e. geothermal. Preheating brines prior to NF might also reduce silica scaling risk in MD by reducing the time available for silica polymerization to occur between the two stages of a hybrid NF/MD treatment train. However, silica scaling was notably more severe in NF with increased initial flux; therefore, care must be taken to ensure that feed concentration does not exceed saturation in the NF stage.

2.6 References

[1] N. Ghaffour, T.M. Missimer, G.L. Amy, Technical review and evaluation of the economics of water desalination: Current and future challenges for better water supply sustainability, Desalination, 309 (2013) 197-207.

[2] L.F. Greenlee, D.F. Lawler, B.D. Freeman, B. Marrot, P. Moulin, Reverse osmosis desalination: Water sources, technology, and today's challenges, Water Research, 43 (2009) 2317-2348.

[3] I. Munoz, A.R. Fernandez-Alba, Reducing the environmental impacts of reverse osmosis desalination by using brackish groundwater resources, Water Res, 42 (2008) 801-811.

[4] M. Badruzzaman, A. Subramani, J. DeCarolis, W. Pearce, J.G. Jacangelo, Impacts of silica on the sustainable productivity of reverse osmosis membranes treating low-salinity brackish groundwater, Desalination, 279 (2011) 210-218.

[5] D.L. Gallup, Treatment of geothermal waters for production of industrial, agricultural or drinking water, Geothermics, 36 (2007) 473-483.

[6] L.F. Song, J.Y. Hu, S.L. Ong, W.J. Ng, M. Elimelech, M. Wilf, Performance limitation of the full-scale reverse osmosis process, Journal of Membrane Science, 214 (2003) 239-244.

[7] P. Sanciolo, N. Milne, K. Taylor, M. Mullet, S. Gray, Silica scale mitigation for high recovery reverse osmosis of groundwater for a mining process, Desalination, 340 (2014) 49-58.

[8] N.A. Milne, T. O'Reilly, P. Sanciolo, E. Ostarcevic, M. Beighton, K. Taylor, M. Mullett, A.J. Tarquin, S.R. Gray, Chemistry of silica scale mitigation for RO desalination with particular reference to remote operations, Water Research, 65 (2014) 107-133.

[9] M. Uchymiak, A.R. Bartman, N. Daltrophe, M. Weissman, J. Gilron, P.D. Christofides, W.J. Kaiser, Y. Cohen, Brackish water reverse osmosis (BWRO) operation in feed flow

reversal mode using an ex situ scale observation detector (EXSOD), Journal of Membrane Science, 341 (2009) 60-66.

[10] R. Sheikholeslami, I.S. Al-Mutaz, S. Tan, S.D. Tan, Some aspects of silica polymerization and fouling and its pretreatment by sodium aluminate, lime and soda ash, Desalination, 150 (2002) 85-92.

[11] T. Koo, Y.J. Lee, R. Sheikholeslami, Silica fouling and cleaning of reverse osmosis membranes, Desalination, 139 (2001) 43-56.

[12] B. Tomaszewska, M. Bodzek, Desalination of geothermal waters using a hybrid UF-RO process. Part II: Membrane scaling after pilot-scale tests, Desalination, 319 (2013) 107-114.

[13] A. Al-Amoudi, R.W. Lovitt, Fouling strategies and the cleaning system of NF membranes and factors affecting cleaning efficiency, Journal of Membrane Science, 303 (2007) 4-28.

[14] T. Tong, S. Zhao, C. Boo, S.M. Hashmi, M. Elimelech, Relating Silica Scaling in Reverse Osmosis to Membrane Surface Properties, Environmental Science & Technology, 51 (2017) 4396-4406.

[15] R.Y. Ning, A.J. Tarquin, J.E. Balliew, Seawater RO treatment of RO concentrate to extreme silica concentrations, Desalin Water Treat, 22 (2010) 286-291.

[16] R.K. Iler, The chemistry of silica: solubility, polymerization, colloid and surface properties, and biochemistry, Wiley, 1979.

[17] R. Sheikholeslami, I.S. Al-Mutaz, T. Koo, A. Young, Pretreatment and the effect of cations and anions on prevention of silica fouling, Desalination, 139 (2001) 83-95.

[18] R. Sheikholeslami, S. Zhou, Performance of RO membranes in silica bearing waters, Desalination, 132 (2000) 337-344.

[19] W. Den, C.-J. Wang, Removal of silica from brackish water by electrocoagulation pretreatment to prevent fouling of reverse osmosis membranes, Separation and Purification Technology, 59 (2008) 318-325.

[20] R. Sheikholeslami, J. Bright, Silica and metals removal by pretreatment to prevent fouling of reverse osmosis membranes, Desalination, 143 (2002) 255-267.

[21] E. Neofotistou, K.D. Demadis, Use of antiscalants for mitigation of silica (SiO2) fouling and deposition: fundamentals and applications in desalination systems, Desalination, 167 (2004) 257-272.

[22] A. Sweity, T.R. Zere, I. David, S. Bason, Y. Oren, Z. Ronen, M. Herzberg, Side effects of antiscalants on biofouling of reverse osmosis membranes in brackish water desalination, Journal of Membrane Science, 481 (2015) 172-187.

[23] A. Antony, J.H. Low, S. Gray, A.E. Childress, P. Le-Clech, G. Leslie, Scale formation and control in high pressure membrane water treatment systems: A review, Journal of Membrane Science, 383 (2011) 1-16.

[24] D.M. Warsinger, J. Swaminathan, E. Guillen-Burrieza, H.A. Arafat, J.H. Lienhard V, Scaling and fouling in membrane distillation for desalination applications: A review, Desalination, 356 (2015) 294-313.

[25] J.A. Bush, J. Vanneste, T.Y. Cath, Membrane distillation for concentration of hypersaline brines from the Great Salt Lake: Effects of scaling and fouling on performance, efficiency, and salt rejection, Separation and Purification Technology, 170 (2016) 78-91.

[26] K.L. Hickenbottom, T.Y. Cath, Sustainable operation of membrane distillation for enhancement of mineral recovery from hypersaline solutions, Journal of Membrane Science, 454 (2014) 426-435.

[27] L.D. Nghiem, T. Cath, A scaling mitigation approach during direct contact membrane distillation, Separation and Purification Technology, 80 (2011) 315-322.

[28] F. He, K.K. Sirkar, J. Gilron, Effects of antiscalants to mitigate membrane scaling by direct contact membrane distillation, Journal of Membrane Science, 345 (2009) 53-58.

[29] J.A. Bush, J. Vanneste, E.M. Gustafson, C.A. Waechter, D. Jassby, C.S. Turchi, T.Y. Cath, Prevention and management of silica scaling in membrane distillation using pH adjustment, Journal of Membrane Science, 554 (2018) 366-377.

[30] E. Curcio, X.S. Ji, G. Di Profio, A. Sulaiman, E. Fontananova, E. Drioli, Membrane distillation operated at high seawater concentration factors: Role of the membrane on CaCO3 scaling in presence of humic acid, Journal of Membrane Science, 346 (2010) 263-269.

[31] S. Srisurichan, R. Jiraratananon, A.G. Fane, Humic acid fouling in the membrane distillation process, Desalination, 174 (2005) 63-72.

[32] M. Gryta, M. Tomaszewska, J. Grzechulska, A.W. Morawski, Membrane distillation of NaCL solution containing natural organic matter, Journal of Membrane Science, 181 (2001) 279-287.

[33] C.R. Martinetti, A.E. Childress, T.Y. Cath, High recovery of concentrated RO brines using forward osmosis and membrane distillation, Journal of Membrane Science, 331 (2009) 31-39.

[34] D. Qu, J. Wang, B. Fan, Z.K. Luan, D.Y. Hou, Study on concentrating primary reverse osmosis retentate by direct contact membrane distillation, Desalination, 247 (2009) 540-550.

[35] M. Osman, J.J. Schoeman, L. Baratta, Desalination/concentration of reverse osmosis and electrodialysis brines with membrane distillation, Desalin Water Treat, 24 (2010) 293-301.

[36] J.P. Mericq, S. Laborie, C. Cabassud, Vacuum membrane distillation of seawater reverse osmosis brines, Water Res, 44 (2010) 5260-5273.

[37] X. Ji, E. Curcio, S. Al Obaidani, G. Di Profio, E. Fontananova, E. Drioli, Membrane distillation-crystallization of seawater reverse osmosis brines, Separation and Purification Technology, 71 (2010) 76-82.

[38] F. Edwie, T.-S. Chung, Development of simultaneous membrane distillation–crystallization (SMDC) technology for treatment of saturated brine, Chemical Engineering Science, 98 (2013) 160-172.

[39] G.Q. Guan, R. Wang, F. Wicaksana, X. Yang, A.G. Fane, Analysis of Membrane Distillation Crystallization System for High Salinity Brine Treatment with Zero Discharge Using Aspen Flowsheet Simulation, Ind Eng Chem Res, 51 (2012) 13405-13413.

[40] M. Gryta, Direct contact membrane distillation with crystallization applied to NaCl solutions, Chem Pap-Chem Zvesti, 56 (2002) 14-19.

[41] M. Gryta, Concentration of NaCl solution by membrane distillation integrated with crystallization, Separation Science and Technology, 37 (2002) 3535-3558.

[42] J. Vanneste, J.A. Bush, K.L. Hickenbottom, C.A. Marks, D. Jassby, C.S. Turchi, T.Y. Cath, Novel thermal efficiency-based model for determination of thermal conductivity of membrane distillation membranes, Journal of Membrane Science, 548 (2018) 298-308.

[43] R.W. Schofield, A.G. Fane, C.J.D. Fell, Heat and mass transfer in membrane distillation, Journal of Membrane Science, 33 (1987) 299-313.

[44] W.L. Ang, A.W. Mohammad, N. Hilal, C.P. Leo, A review on the applicability of integrated/hybrid membrane processes in water treatment and desalination plants, Desalination, 363 (2015) 2-18.

[45] J. Gilron, Y. Ladizansky, E. Korin, Silica Fouling in Direct Contact Membrane Distillation, Ind Eng Chem Res, 52 (2013) 10521-10529.

[46] M.J.H. Snow, D. de Winter, R. Buckingham, J. Campbell, J. Wagner, New techniques for extreme conditions: high temperature reverse osmosis and nanofiltration, Desalination, 105 (1996) 57-61.

[47] M. Mänttäri, A. Pihlajamäki, E. Kaipainen, M. Nyström, Effect of temperature and membrane pre-treatment by pressure on the filtration properties of nanofiltration membranes, Desalination, 145 (2002) 81-86.

[48] N. Ben Amar, H. Saidani, J. Palmeri, A. Deratani, Effect of temperature on the rejection of neutral and charged solutes by Desal 5 DK nanofiltration membrane, Desalination, 246 (2009) 294-303.

[49] H.Q. Dang, W.E. Price, L.D. Nghiem, The effects of feed solution temperature on pore size and trace organic contaminant rejection by the nanofiltration membrane NF270, Separation and Purification Technology, 125 (2014) 43-51.

[50] M. Nilsson, G. Trägårdh, K. Östergren, The influence of pH, salt and temperature on nanofiltration performance, Journal of Membrane Science, 312 (2008) 97-106.

[51] R. Sheikholeslami, S. Tan, Effects of water quality on silica fouling of desalination plants, Desalination, 126 (1999) 267-280.

[52] ASTM D859-16, Standard Test Method for Silica in Water, in, ASTM International, West Conshohocken, PA, 2016.

[53] H. Koseoglu, B.I. Harman, N.O. Yigit, E. Guler, N. Kabay, M. Kitis, The effects of operating conditions on boron removal from geothermal waters by membrane processes, Desalination, 258 (2010) 72-78.

[54] H.P. Rothbaum, A.G. Rohde, Kinetics of silica polymerization and deposition from dilute solutions between 5 and 180°C, Journal of Colloid and Interface Science, 71 (1979) 533-559.

[55] M.A. Al Mamun, S. Bhattacharjee, D. Pernitsky, M. Sadrzadeh, Colloidal Fouling of Nanofiltration Membranes: Development of a Standard Operating Procedure, Membranes, 7 (2017) 4.

[56] G. Okamoto, T. Okura, K. Goto, Properties of silica in water, Geochimica et Cosmochimica Acta, 12 (1957) 123-132.

CHAPTER 3

PREVENTION AND MANAGEMENT OF SILICA SCALING IN MEMBRANE DISTILLATION USING PH ADJUSTMENT

Modified from an article published in *Journal of Membrane Science*[1]

John A. Bush[2❖], Johan Vanneste[2], Emily M. Gustafson[2], Christopher A. Waechter[3], David Jassby[4], Craig S. Turchi[5], Tzahi Y. Cath[2*]

3.1 Abstract

Membrane scaling by silica is a major challenge in desalination, particularly for inland desalination of brackish groundwater or geothermal resources, which often contain high concentrations of silica and dissolved solids. Adjustment of feed pH may reduce silica scaling risk, which is important for inland facilities that operate at high water recoveries to reduce brine disposal costs. However, water recovery of reverse osmosis is also limited due to increased osmotic pressure with feed water concentration. Membrane distillation (MD) is a thermally driven membrane desalination technique that is not limited by increased osmotic pressure of the feed. In this investigation, pH adjustment was tested as a strategy to reduce silica scaling risk in the MD process. With feed water pH less than 5 or higher than 10, scaling impacts were negligible at silica concentrations up to 600 mg/L. Scaling rates were highest at neutral pH between 6 and 8. Cleaning strategies were also explored to remove silica scale from membranes. Cleaning using NaOH solutions at pH higher than 11 to induce dissolution of silica scale was effective at temporarily restoring performance; however, some silica remained on membrane surfaces and scaling upon re-exposure to supersaturated silica concentrations occurred faster than with new membranes.

---

[1]Reprinted with permission of *Journal of Membrane Science*, 554 (2018) 366-377.
[2]Colorado School of Mines, Golden, Colorado, USA 80401
❖Primary researcher and author
[3]US Bureau of Reclamation, Denver, Colorado, USA 80225
[4]University of California Los Angeles, Los Angeles, California, USA 90095
[5]The National Renewable Energy Laboratory, Golden, Colorado, USA 80401
*Corresponding author: email: tcath@mines.edu; phone: (303) 273-3402; fax: (303) 273-3413

3.2 Introduction

Control and mitigation of silica scaling on membranes is a challenging problem in the treatment of impaired waters requiring desalination. Silica is present in most natural water resources, it has low solubility, and when concentrated beyond its solubility limit of approximately 120 mg/L [1], precipitation may occur and form a hard scale that is extremely difficult to remove. Silica scaling on heat exchanger surfaces in thermal desalination processes increases thermal resistance, which reduces process efficiency and requires costly chemical and mechanical cleaning. In membrane processes such as reverse osmosis (RO) or nanofiltration (NF), silica scaling reduces water flux [2-5], and is resistant to simple cleaning methods used to manage other types of mineral scaling such as acid washing. The effectiveness of commercial cleaners to remove silica scale are limited and risk damaging the membranes [5]. Operating at low water recoveries that keep the concentrate below the solubility limit of silica can reduce the risk of silica scaling, but this may result in the production of large volumes of reject brine, which can be a substantial problem for desalination facilities, particularly in the case of inland desalination where brine disposal is difficult and expensive [6, 7]. Nevertheless, conventional inland water resources are becoming depleted in many parts of the world, and unconventional resources such as brackish groundwater and geothermal water are attracting more interest due to increased demand and technology advances that have reduced the cost of desalination [8]. However, these resources are often particularly high in silica and total dissolved solids (TDS) and must be demineralized before use [7, 9-12].

The chemistry of silica in water is complex and influenced by many factors, including temperature, pH, ionic strength, and interactions with other dissolved ions [1]. Silica scaling in desalination processes is typically the result of silica polymerization and the formation of amorphous colloidal silica. At low concentrations and neutral or acidic pH, soluble silica exists mostly in non-ionic form in as monosilicic acid, $Si(OH)_4$. As concentration increases, the monomeric form undergoes polymerization through a dehydration reaction to form polysilicic acids, which are connected by silica-oxygen bonds [6]. Soluble silica can be removed by pretreatment with sodium aluminate or lime-soda softening, which create precipitates that adsorb silica [13-15]; however, these strategies may not be practical for desalination due to incomplete removal of silica and the production of large volumes of sludge, disposal of which is costly and labor intensive. Antiscalants may reduce scaling risk at silica concentrations exceeding saturation

by inhibiting polymer formation or preventing colloidal silica from attaching to surfaces [16], but may be expensive and are of limited effectiveness at very high silica concentrations [4]. Antiscalants can also contribute to fouling themselves and may increase the risk of organic fouling [17, 18].

Because both silica solubility and the kinetics of polymerization are highly influenced by pH, acidification or alkalization of feed water is a simple and potentially inexpensive technique to prevent silica scaling. Silica solubility increases dramatically above pH of 9 due to the deprotonation of silicic acid and formation of silicate anions, with all forms of solid silica converting to soluble silicates above pH 10.7 [1]. Operating with feed water above this point may eliminate any risk of silica scaling, although it may increase scaling risk of carbonate or silicate minerals for water containing calcium or magnesium [19]. On the other hand, polymerization rates are reduced at both high and low pHs, with the highest polymerization rates occurring at pH 7.5 [20]. Despite the low solubility of silica in acidic conditions, feed water acidification may also be an effective means to prevent silica scaling if polymerization rates are sufficiently low that colloids are unable to form during the residence time in the desalination process. Feed water acidification has been demonstrated using brackish water to allow sustainable operation of RO processes with silica concentrations up to 1,000 mg/L or more [7, 21].

Although pressure-driven membrane desalination processes such as RO may benefit from pH modification to reduce or prevent silica scaling in the treatment of impaired waters, recovery is still thermodynamically limited due to the increased osmotic pressure with high concentrations of dissolved solids [7, 22]. Development of technologies that are not limited by osmotic pressure and compatible with silica management strategies are crucial to achieve high-recovery desalination of water resources with high TDS and silica content. Membrane distillation (MD) is an emerging desalination technology that utilizes a temperature difference across a hydrophobic, microporous membrane to drive mass transport. The hydrophobicity of the membrane prevents liquid transfer through the pores, and mass transport occurs in the vapor phase only. Because it is an evaporative process, MD achieves almost complete rejection of dissolved solids and is very tolerant of extreme salinity, even at concentrations approaching or exceeding the solubility limit of NaCl [23-25]. Although MD has a high thermal energy demand, MD can operate at any temperature difference and energy costs may be alleviated through the use of inexpensive and

renewable heat sources such as solar thermal, geothermal, or waste heat from other industrial processes [26]. These unique characteristics make MD a promising strategy for high-recovery desalination and brine management, and several studies have explored the potential of MD for the desalination of natural hypersaline brines [27, 28] as well as concentrates from other membrane processes [29-33]. Investigation of scaling and fouling in MD has also been reported in the literature, mostly focusing on salt and mineral scaling caused by NaCl, carbonates, and sulfates [34, 35]. Comparatively few studies exist that specifically address the problem of silica; however, one study found that while silica scaling reduces performance in the MD process, it can be removed by dissolution using a high-pH solution of Na_2CO_3 [36].

The membranes used and operating conditions applied in MD are substantially different than those used in pressure-driven processes such as RO. MD membranes are hydrophobic, and thus are not receptive for deposition of monomeric silica [1], and fouling by colloidal silica is not subject to compaction because the pressure difference between the feed and distillate is very low. Also, the solubility of silica and the kinetics of silica polymerization are affected by temperature, and the influence of feed pH on scaling behavior in MD may be different than in isothermal processes due to the elevated temperatures and polarization phenomenon encountered in MD. The main objectives of this study were to investigate the influence of pH on silica polymerization and scaling behavior in the MD process at pH ranges from 4 to 11, and how feed water pH adjustment might be used as a strategy to prevent silica scaling in MD. Additionally, the influence of pH on dissolution behavior of silica scale on MD membranes was investigated using process modification with neutral and high pH solutions. The long-term effectiveness of an alkaline cleaning process for MD membranes scaled with silica and its viability as a practical tool for silica scale management was also explored.

3.3 Materials and methods

3.3.1 Membranes and modules

A hydrophobic, microporous polypropylene membrane manufactured by 3M (St. Paul, MN) was used in the study. The membrane is symmetric with a nominal pore size of 0.2 μm, a porosity of 85%, and a thickness of 110 μm. This membrane was chosen due to its high performance as an MD membrane, which has been characterized previously [37], and because its

isotropic nature allows the MD process to be reversed by swapping the feed and distillate channels.

Custom flow cells were fabricated using transparent acrylic and featured ten 18 cm (7") long, by 6.35 mm (0.25") wide, by 3.2 mm (0.0125") deep parallel flow channels on both the feed and distillate sides, providing a total membrane surface area of 125 cm^2. Spacers were not installed in the flow channels to ensure consistent hydrodynamic conditions near the membrane surface and to allow direct observation of scaling and fouling behavior on the membrane surface during experiments.

3.3.2 System description

An automated, closed-loop, bench-scale system was utilized for all experiments (Figure 3.1). Data collection and operating conditions were controlled using LabVIEW software (National Instruments) and a Labjack U6 (Labjack, Lakewood, CO) DAQ device. Both feed and distillate solutions were pumped continuously through the system using gear pumps (Micropump Integral Series, IDEX Corp. Vancouver, WA). Water flux across the membrane was calculated by measuring the change in height of the water column in a cylindrical distillate tank over time using a pressure transducer (Model PX309-001G5V, Omegadyne Inc., Sunbury, OH). The distillate tank was also fitted with an automated solenoid valve to allow collected distillate to drain by gravity back into the feed tank, allowing for extended operation within a specified feed concentration range. To reduce losses from evaporation, the distillate tank was covered and the feed tank was completely sealed except for a small opening on the top, which was fitted with a pressure-relief tube extending several feet above the tank to allow water vapor to condense and drain back into the tank.

The temperature of the feed solution was maintained constant using water heated with a 1500 W electric heater (Model 1019, Hotwatt, Danvers, MA) on the opposite side of a heat exchanger, and the temperature of the distillate was maintained constant using a chilled glycol solution circulated on the opposite side of a second heat exchanger. Temperature was monitored at the inlets and outlets of both feed and distillate channels of the flow cell using silicon-type temperature sensors (Model EI1034, Electronic Innovations Corp., Lakewood, CO) to enable measurement of thermal efficiency during experiments.

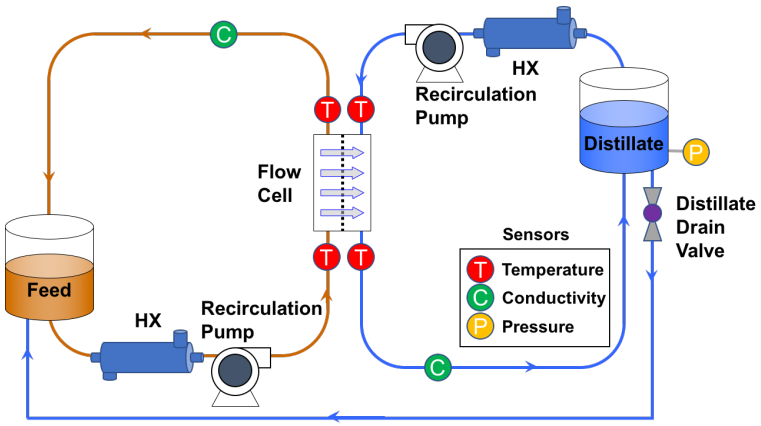

Figure 3.1. Schematic of the MD system. Feed and distillate temperatures were monitored at the inlet and outlet of the flow cell and controlled by heat exchangers (HX). Conductivity was monitored in both the feed and distillate streams between the flow cell and tanks. The volume of the collected distillate was measured using a pressure transducer installed on the bottom of the distillate tank. Feed concentration was controlled by periodically returning the collected distillate to feed tank using an automated solenoid valve.

Thermal efficiency (η_{th}) of the MD process is defined as the ratio of latent heat transferred by vapor to the total heat transfer, which includes both latent heat transfer and conductive heat transfer through the membrane:

$$\eta_{th} = \frac{Q_{vap}}{Q_{vap}+Q_{cond}} \tag{3.1}$$

where Q_{vap} is the latent heat transferred by vapor through the membrane, and Q_{cond} is the conductive heat transfer through the membrane. The vapor heat transfer can be related to the vapor mass transfer, and the conductive heat transfer can be related to the thermal conductivity of the membrane using Fourier's equation:

$$\eta_{th} = \frac{\dot{m}_m \Delta H_{vap}}{\dot{m}_m \Delta H_{vap}+\frac{k_m}{\delta}\Delta T_m} \tag{3.2}$$

where $\dot{m}_m$ is the mass flow rate of vapor through the membrane, ΔH_{vap} is the latent enthalpy of vaporization of water, k_m/δ is the thermal conductivity of the membrane, and ΔT_m is the temperature difference between the feed and distillate at the membrane surface. Thermal

conductivity of the membrane is difficult to measure and not commonly provided by membrane manufacturers, and temperature difference at the membrane surface cannot be explicitly measured, but will always be lower than the temperature difference betwwn the bulk feed and distillate streams because of temperature polarization in the flow channels [38]. However, because the temperature of the distillate is close to the ambient temperature, the heat transfer to the environment on the distillate side is negligible. Therefore, the total heat transfer through the membrane is almost equal to the change in enthalpy of the distillate between the inlet and outlet of the flow cell. Thus, in the present study the thermal efficiency was calculated using Eq. (3.3):

$$\eta_{\mathrm{th}} = \frac{\dot{m}_{\mathrm{m}} \Delta H_{\mathrm{vap}}}{(\dot{m}_{\mathrm{d}} + \dot{m}_{\mathrm{m}}) c_{\mathrm{p,out}} T_{\mathrm{d,out}} - \dot{m}_{\mathrm{d}} c_{\mathrm{p,in}} T_{\mathrm{d,in}}} \tag{3.3}$$

where $\dot{m}_{\mathrm{d}}$ is the mass flow rate of the distillate, $T_{\mathrm{d,in}}$ and $T_{\mathrm{d,out}}$ are the temperature of the distillate at the inlet and outlet of the flow cell, respectively, and $c_{\mathrm{p,in}}$ and $c_{\mathrm{p,out}}$ are the constant-pressure specific heat of pure water calculated at $T_{\mathrm{d,in}}$ and $T_{\mathrm{d,out}}$, respectively. Conductive heat transfer was calculated by subtracting the vapor heat transfer from the measured total heat transfer.

Conductivity was monitored continuously in both feed and distillate solutions using a toroidal type sensor (Model TCSMA, Sensorex, Garden Grove, CA) and a conductivity probe (Model T-35820-62, Cole-Parmer, Vernon Hills, IL), respectively. Salt rejection was calculated using Eq. (3.4):

$$\text{Salt rejection}(\%) = \left(1 - \frac{V_{\mathrm{d2}} \sigma_{\mathrm{d2}} - V_{\mathrm{d1}} \sigma_{\mathrm{d1}}}{(V_{\mathrm{d2}} - V_{\mathrm{d1}})\, \sigma_{\mathrm{f}}}\right) \times 100 \tag{3.4}$$

where σ_{f} and σ_{d} are the conductivities of the feed and distillate solutions, and V_{d1} and V_{d2} represent the total volume of the distillate system at times 1 and 2 across a time interval.

3.3.3 Analytical methods

Soluble silica concentration was determined using the Hach Silicomolybdate Method (Method 8185) and a Hach spectrophotometer (Model DR 5000, Hach Company, Loveland, CO) to measure absorbance at 452 nm. The silicomolybdate method is useful for molybdate-reactive silica in concentrations between 1 and 100 mg/L, which includes dissolved simple silicates,

monomeric silica, silicic acid, and an undetermined amount of polymeric silica [39]. Colloidal polymeric silica is not measured by the method due to its unreactive nature, effectively allowing this approach to provide a measurement of polymerization as soluble silica is transformed into colloidal silica. Samples were diluted before analysis using ultrapure water to ensure that soluble silica concentrations did not exceed the range of the analysis method.

3.3.4 Experimental procedures

This study investigated feed water pH modification as a potential strategy to mitigate silica scaling in the MD process. Batch experiments were first performed using heated solutions supersaturated with respect to silica to investigate silica polymerization rates for different pH conditions at a temperature typical of those used in MD. The influence of pH on silica scaling behavior and its impacts were investigated using solutions with initial silica concentrations approximately equal to the solubility limit then concentrated with MD. A series of experiments were also performed to test the reversibility of silica scaling on MD membranes and to investigate dissolution behavior of silica scale at high pH.

3.3.4.1 Batch silica polymerization tests

Experiments were conducted in beakers to investigate the influence of pH on silica solubility and polymerization rates at concentrations and temperature similar to those that will be used in the MD experiments. Solutions were prepared by dissolving 2120 mg of sodium silicate pentahydrate, $Na_2SiO_3 \cdot 5H_2O$, into 1 L of deionized water to achieve an initial concentration of 600 mg/L SiO_2, which is approximately the maximum concentration that will be reached in the MD experiments. The solutions were then adjusted to a desired pH between 4 and 11 using HCl and NaOH, placed in a water bath to maintain temperature of 60 °C, and stirred periodically. Silica solubility and polymerization rates were determined by collecting 1 mL samples, diluting them with 9 mL of HCl solution at pH 1 to halt any further polymerization, and analyzed for soluble silica concentration using Hach Method 8185. Samples were collected every minute for the first 10 minutes, with the interval between sampling time gradually increasing within the first hour to 20 minutes. Sampling continued over the next 5–7 hours until measured soluble silica concentration stabilized and silica concentration reached equilibrium. To correct for evaporation

in the test samples, the evaporation rate at the experimental conditions was measured using 1 L of deionized water maintained at 60 °C for a period of 8 hours.

3.3.4.2 MD performance and silica scaling tests at pH 4–11

Silica scaling behavior in the MD process was investigated using synthetic solutions prepared by dissolving 795 mg/L of $Na_2SiO_3 \cdot 5H_2O$ into deionized water to provide an initial concentration of 225 mg/L (3.74 mmol/L) as SiO_2, which is slightly less than twice the solubility limit of silica at neutral pH and 25 °C, and approximately equal to the solubility limit of silica at neutral pH and 60 °C, as calculated by OLI Stream Analyzer (OLI Systems, Inc., Cedar Knolls, NJ). Solutions were adjusted to a desired pH between 4–11 with concentrated HCl and NaOH.

For the silica scaling experiments, feed and distillate temperatures were maintained at 60 °C and 20 °C, respectively. Both feed and distillate were circulated through the system at a constant flow rate of 2.0 L/min in a countercurrent flow configuration, providing a flow velocity of 16.6 cm/s and Reynolds number of 1460 for the feed solution and 690 for the distillate. In each experiment, 4 L of feed solution was concentrated until a maximum of 2.5 L of distillate was collected. Then the solenoid valve on the distillate tank was opened momentarily, allowing 0.5 L of distillate to return to the feed tank while the MD process continues. After the initial concentration step the repeated collection of 0.5 L distillate and its return to the feed tank continued for the duration of the experiment, maintaining the concentration factor of the feed solution between 2 to 2.7, which corresponds to a SiO_2 concentration between 450 and 600 mg/L, based on the initial concentration of 225 mg/L.

3.3.4.3 Silica scale mitigation using MD reversal with deionized water

The membranes used in the study are isotropic and the performance of clean membranes is similar regardless of the direction of water flux. Temporarily reversing the MD process by circulating hot water through the distillate channel and chilled water through the feed channel has been demonstrated to be an effective method for mitigating the effects of scaling and fouling in the MD process [27, 28]. Although dissolution of polymeric silica proceeds slowly in solutions with low temperatures and ionic strength [40, 41], and because the scale layer is not subject to compaction in the MD process as in pressure-driven processes, the scale layer may not be strongly adhered to the hydrophobic membrane surface. Thus, temporarily reversing the

direction of water flux may facilitate efficient membrane cleaning. To investigate the effectiveness of MD reversal as a cleaning strategy for silica scaling, a new set of experiments was conducted using the same procedure as described in Section 2.4.2 with a new membrane and 225 mg/L SiO_2 solution at neutral pH. Following concentration and scaling, the collected distillate was drained into the feed tank, returning the feed to its initial concentration, and stored. Deionized water was circulated through both feed and distillate channels for 10 minutes to flush any silica solution and the system was drained. The feed and distillate circuits were then swapped, and the system was operated for one hour using deionized water maintained at 50 °C on the distillate side of the membrane and deionized water maintained at 20 °C on the original feed side of the membrane. The system was then drained, and the feed and distillate were reconnected in the standard configuration and operation resumed with the original silica solution maintained at 60 °C as feed and deionized water maintained at 20 °C on the distillate side. To further investigate silica scaling and dissolution behavior during MD reversal, the feed and distillate circuits were then swapped again and operation continued with the silica solution circulated through the original distillate channel and deionized water circulated through the original feed channel.

3.3.4.4 Silica scale dissolution using MD reversal with NaOH solution

Silica is highly soluble in water above pH 10.7, and depolymerization rates of amorphous silica increase with pH [1]. To investigate the potential of silica scale removal from MD membranes using a high pH solution, an experiment was conducted combining MD reversal followed by a cleaning procedure with a solution of NaOH maintained at a pH of 11. In this experiment, a new membrane and new feed solution with initial concentration of 225 mg/L SiO_2 and neutral pH was concentrated using the same procedure as described in Section 2.4.2. After initial scaling, the feed and distillate channels were swapped to reverse the direction of water flux and the MD process was resumed for an additional 40 hours. The system was then drained, and several cleaning cycles were conducted using a solution of NaOH maintained at pH of 11. During the first cycle, the NaOH solution was maintained at 50 °C and circulated through the original distillate channel (where feed solution was most recently flowing) and deionized water maintained at 30 °C was circulate through the original feed channel for 6 hours. During the second cleaning cycle, the NaOH solution was circulated through the original feed channel and

deionized water was circulated through the original distillate channel. The NaOH solution was maintained at 50 °C and the deionized water maintained at 30 °C for 3 hours, then the temperature of the NaOH solution was increased to 60 °C and the temperature of the deionized water reduced to 20 °C and circulated for an additional 3 hours. The pH of the NaOH solution was continuously monitored during the cleaning cycle, and additional NaOH was added as needed to maintain pH of 11. Membrane performance was then tested using a solution of 1 g/L NaCl maintained at 60 °C and deionized water maintained at 20 °C.

3.3.4.5 Alkaline cleaning as a silica scale management strategy in MD

The tenacity of silica scale has been noted in many investigations, and previous studies have reported remnant silica colloids on membrane surfaces and accelerated scaling rates following cleaning of membranes scaled with silica [12, 36]. To further investigate silica scale dissolution and the potential of an alkaline cleaning process as a silica scale management strategy for the membrane used in this investigation, a set of experiments was conducted with a more aggressive scaling and cleaning approach. Compared to pure water, the presence of up to 0.1 M NaCl has been shown to increase silica dissolution rates [40], and thus the addition of NaCl may be an inexpensive method to improve the effectiveness of membrane cleaning with NaOH. A solution was prepared with an initial concentration of 1000 mg/L SiO_2 and neutral pH and concentrated using a new membrane and similar operating conditions as described in Section 2.4.2 Following initial scaling, the system was drained, flushed with deionized water, and the membrane was tested using a 1 g/L NaCl feed solution to test performance after scaling. A cleaning cycle was then implemented using a solution containing 0.1 M NaCl (5.85 g/L NaCl) with added NaOH to maintain pH of 11. During the cleaning cycle, the cleaning solution was maintained at 60 °C and distillate maintained at 20 °C and both were circulated through the system until water flux was restored. A second scaling experiment was then conducted with a new solution with an initial concentration of 1000 mg/L SiO_2 and neutral pH using similar operating conditions as described in Section 3.3.4.2.

3.3.4.6 Membrane characterization

Membranes were air-dried following scaling experiments. Scale layer morphology and composition were analyzed using scanning electron microscopy (SEM) and energy dispersive x-

ray spectroscopy (EDS) (Quanta 600, FEI Corp., Hillsboro, OR). Membrane samples were prepared using an ethanol cryofracture technique to preserve the internal pore structure for analysis. The membrane samples were first submerged in ethanol until the pores were completely flooded, then submerged in liquid nitrogen and cut with a razor blade. The membranes were then air dried and gold sputtered before analysis.

3.4 Results and Discussion

3.4.1 Effect of pH on silica solubility and polymerization

Silica polymerization rates were determined at pH between 4 and 11 by measuring the change in soluble silica concentration over time using solutions with initial concentration of approximately 600 mg/L SiO_2. To correct for evaporation that occurred in the test samples, volume at each sampling time was determined using the measured evaporation rate of deionized water at similar conditions, which was found to be 0.4 mL/min. Total soluble silica for each solution is presented in Figure 3.2.

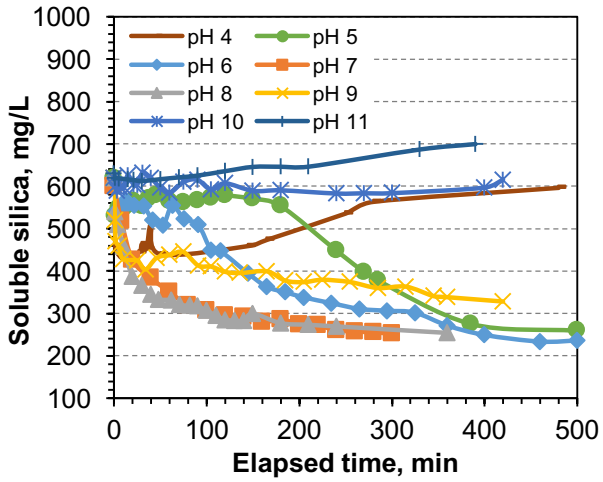

Figure 3.2. Measured total soluble silica concentration for test solutions with initial concentration of 600 mg/L SiO_2, initial pH of 4–11, and maintained at 60 °C.

Soluble silica concentration stabilized between 290 and 330 mg/L for solutions of pH 5–8, which is consistent with the solubility of silica at 60 °C and similar pH reported in the literature [1, 42]. Polymerization rates varied considerably with pH, and were highest for solutions of pH 7 and 8, as indicated by the rapid initial decline in total soluble silica

concentration for these solutions. The extent of polymerization for solutions at slightly acidic conditions were similar, but the rate of polymerization was lower compared to neutral and slightly alkaline solutions. Moreover, the induction time prior to the onset of silica concentration decline was longer for the solution of pH 6 and even longer for the solution of pH 5 compared to solutions of pH 7 and 8. These results are consistent with other observations that indicate similar silica solubility between pH 5–8, but reduced polymerization rates below pH 7 [7, 21, 43]. Polymerization rate for the solution of pH 9 was initially similar to that of the solutions of pH 7 and 8; however, the extent of polymerization was slightly lower due to the increase in silica solubility. Total soluble silica for solutions of pH 4, 10, and 11 were relatively constant and similar at the end of experiments to the initial concentration, indicating that negligible polymerization occurred at these pHs.

3.4.2 Effect of pH on silica scaling in MD

3.4.2.1 Scaling rates and impacts on performance

Baseline performance of the membrane for the experimental configuration used in the study was established by testing with a 1 g/L NaCl feed solution maintained at 60° and distillate maintained at 20 °C. Water flux and thermal efficiency for MD experiments conducted using solutions with initial concentration of 225 mg/L SiO_2 were similar to the measured baseline performance, although generally slightly higher than the water flux of 26.8 L/m^2/hr and thermal efficiency of 0.53 for the 1 g/L NaCl feed solution at similar operating conditions (Figure 3.3a–b). Both water flux and thermal efficiency were unaffected in the initial few hours of operation despite an increase of concentration above the solubility limit of silica. After sufficient induction time at supersaturated concentrations, a decline in water flux and thermal efficiency was observed for solutions with pH of 5–9 due to silica polymerization and subsequent scaling of the membrane surface (Figure 3.3c–d).

Impacts of silica scaling on thermal efficiency were less severe than water flux. For example, in the case of pH 7, water flux declined by 78% while the decline in thermal efficiency was only 55%. Also, the calculated conductive heat transfer over the course of the experiment performed at pH 7 declined from approximately 200 W to approximately 150 W. Decline in calculated conductive heat transfer occurred for other solutions with pH 5–9 and followed similar trends as water flux and thermal efficiency. This suggests that the silica scale layer

increases overall thermal resistance; however, the thermal conductivity of hydrated solid silica gel is in the range of 0.9–1.2 W/m/K [44, 45]. Taking into consideration the fact that the scale layer may be porous and the thermal conductivity of water between 20° C and 60° C is in the range of 0.6–0.65 W/m/K [46], it can be estimated that the effective thermal conductivity of the scale layer including water-filled pores is between 0.6–1.2 W/m/K. Using an average thickness of 10 µm (based on SEM cross section images) the estimated heat transfer coefficient of the silica scale layer is between 60000 and 120000 W/m^2/K, which is orders of magnitude higher than the total heat transfer coefficient of the membrane [37]. Thus, the reduced conductive heat transfer is more likely related to the adsorbent properties of silica gel, which will be discussed further in Section 3.4.3.1.

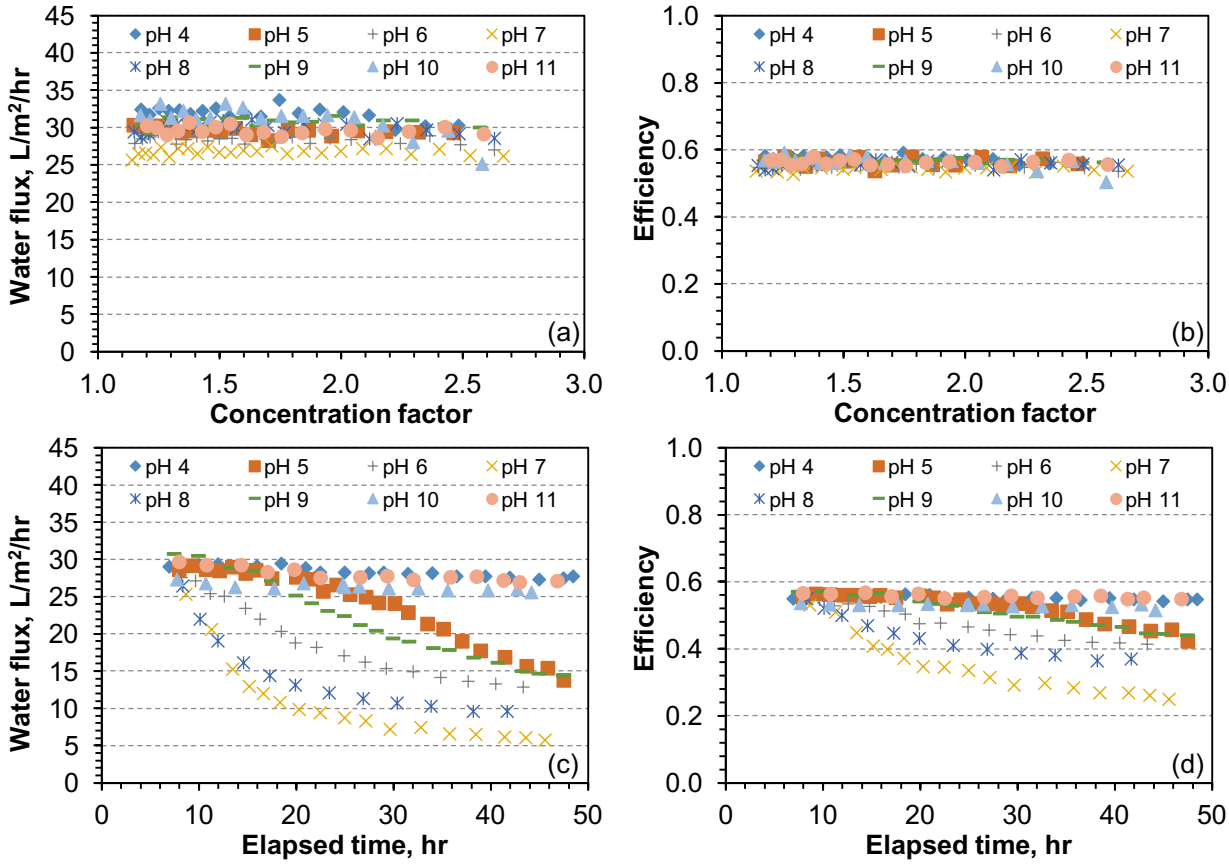

Figure 3.3. Measured water flux (a) and thermal efficiency (b) for MD experiments during the initial concentration of 225 mg/L SiO_2 solutions with pH 4–11, plotted by concentration factor. Measured water flux (c) and thermal efficiency (d) for MD experiments using solutions with initial concentration of 225 mg/L SiO_2 and pH 4–11 during distillate cycling phase with concentration factor maintained between 2 and 2.67. All solutions were tested with feed temperature of 60 °C, distillate temperature of 20 °C, and countercurrent flow with velocity of 16.6 cm/s for both feed and distillate.

Based on initial concentration of 225 mg/L SiO_2 and the maximum concentration factor of 2.67, silica concentration reached as high as 600 mg/L before scaling substantially impacted performance. The highest rates of flux decline were observed for solutions of pH 6–8 between 10 and 15 hours of experimental time (Figure 3.4). After 15 hours, rates of flux decline decreased for pH 6–8 and stabilized near 40 hours. In contrast, rates of flux decline were highest between 25 and 40 hours of experimental time for pH 5, and 15 and 30 hours for pH 9. Rates of decline were generally lower for both pH 5 and 9 and did not begin to stabilize until approximately 60 hours of experimental time. Negligible flux decline was observed for pH of 4, 10, and 11. These observations regarding the influence of pH on performance decline due to silica scaling in MD are consistent with the behavior observed during the batch polymerization tests with solutions containing 600 mg/L SiO_2 at 60 °C, indicating that the timing of polymerization and rate of polymerization are closely tied to silica scaling behavior in the MD process. Distillate conductivity was not affected in any of the experiments despite feed conductivities in a range of 1500–3000 μS/cm, indicating no loss of rejection or wetting of the membrane pores due to scaling or pH effects.

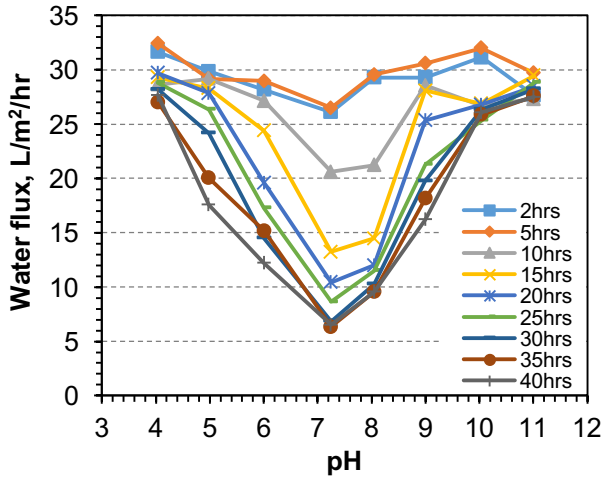

Figure 3.4. Water flux for MD experiments with initial concentration of 225 mg/L SiO_2 and maximum concentration of 600 mg/L SiO_2 and pH 4–11. All solutions were tested with feed temperature of 60 °C, distillate temperature of 20 °C, and countercurrent flow with velocity of 16.6 cm/s for both feed and distillate.

3.4.2.2 Scale morphology

At the end of the experiments the membranes were covered with an opaque scale layer that was beige to light-brown in color. The scale layer was highly hydrophilic—the contact angle of the scaled membranes was impossible to measure and practically zero. SEM analysis of membrane scaling at neutral pH indicated the presence of an amorphous scale layer that completely covered the membrane surface, obscuring the membrane structure and pores (Figure 3.5a and Figure 3.5b vs. Figure 3.5c and Figure 3.5d). EDS analysis detected only silicon and oxygen in the scale layer, confirming its composition to be polymerized silica. Some gaps were observed in the scale layer; however, the gaps were typically only a few microns in thickness and may have resulted from the cracking of the scale layer as it dried (Figure 3.5c and Figure 3.5d).

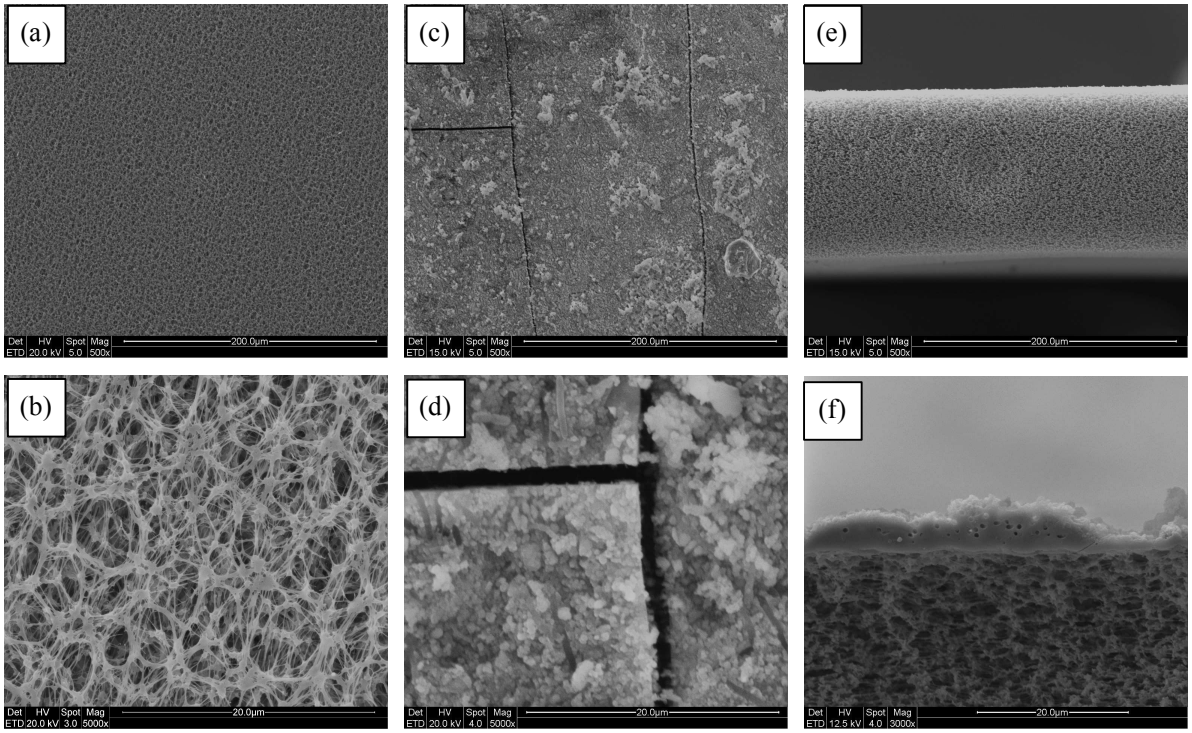

Figure 3.5. SEM micrographs of (a, b) new MD membrane surface, (c, d) scaled MD membrane surface, (e) new membrane cross-section, and (f) scaled MD membrane cross-section after >40 hours of MD operation with maximum concentration of 600 mg/L SiO_2 and neutral pH.

Scale morphology appeared as aggregates of spherical and cylindrical particles approximately 1 micron in size, suggesting that scale layer growth occurred at least in part by deposition of colloidal silica that polymerized in the bulk solution. Cross-section analysis

indicated a more uniform scale layer beneath the surface structures except for scattered circular gaps; however, it is not clear whether this is due to more uniform scale growth early in the experiment or because of later polymerization that filled in the gaps between deposited colloidal silica (Figure 3.5f). The scale layer did not appear to penetrate the membrane pores and was confined to the membrane surface.

3.4.3 Dissolution of silica scale from MD membranes at high pH

3.4.3.1 MD reversal with deionized water

The silica scale layer was observed to form as an amorphous deposit on only the surface of the membranes. An experiment using a new membrane and silica solution was conducted using the MD reversal process described in Section 2.4.3 to determine if reversing the direction of vapor flux would promote separation and removal of the scale layer from the membrane surface at neutral pH. Water flux was slightly improved following one hour of MD reversal operation, with an increase from ~7 L/m^2/hr at the end of the first scaling cycle to ~11 L/m^2/hr at the beginning of normal operation with the silica solution maintained at 60 °C and distillate maintained at 20 °C (Figure 3.6).

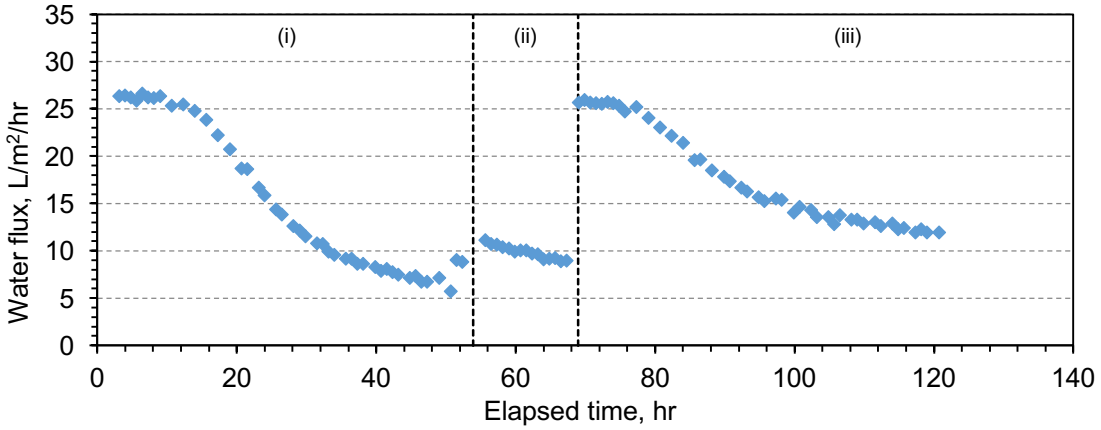

Figure 3.6. Water flux and as a function of time for MD tested with maximum concentration of 600 mg/L SiO_2 and neutral pH. (i) Initial scaling cycle with new solution and new membrane and standard MD configuration. (ii) Operation with original concentration silica solution in standard MD configuration after one hour of MD reversal cycle using deionized water in both feed and distillate channels. (iii) Operation with original concentrated silica solution in reverse MD configuration.

No noticeable changes in the appearance of the scale layer on the membrane surface were observed, and water flux declined to ~9 L/m^2/hr over the next 15 hours (phase ii). Surprisingly, the reverse water flux during MD reversal using deionized water (not shown) was ~18 L/m^2/hr—much higher than the observed water flux in standard configuration before or after the MD reversal process. Also, despite the low flux observed in normal operation and silica scaling still present on the membrane surface, water flux was completely restored when MD reversal was applied to the original silica solution (phase iii). Additional scaling subsequently occurred on the original distillate side of the membrane (now feed side), resulting in a pattern of flux decline similar to that of a new membrane, albeit slightly less severe.

At the conclusion of the experiment, SEM analysis confirmed the presence of silica scale completely covering both the feed and distillate sides of the membrane (Figure 3.7). The scale layer on the original feed side was similar in thickness to the scale layer formed without MD reversal, indicating that the MD reversal process using deionized water was ineffective at removing the scale. Thus, the restored water flux observed during MD reversal indicates that the silica layer is porous and does not impact MD performance by reducing permeability or blocking the membrane pores, otherwise lower flux would be observed regardless of the direction of mass transfer. This phenomenon can be explained by considering the driving force in MD and possible mechanisms by which silica impacts the MD process. Evaporation from porous media occurs more slowly than evaporation from free surfaces due to the effects of confined spaces, and stronger intermolecular forces between the molecules of a liquid and the surfaces of the pore walls lead to lower evaporation rates [47]. Silica gel is hydrophilic, its adsorbent characteristics with respect to water have been extensively investigated for use in applications such as air dehumidification [48], adsorbent refrigeration [49-53], and adsorbent desalination [54]. Evaporation rates of water from narrow pores of silica gel can be orders of magnitude lower than evaporation rates from a free water surface [47]. Thus, while the silica scale layer does not substantially impede water flow to and from the membrane surface, reduced water flux is observed when the scale layer is present on the feed side because a substantial amount of evaporation is confined to the silica pores.

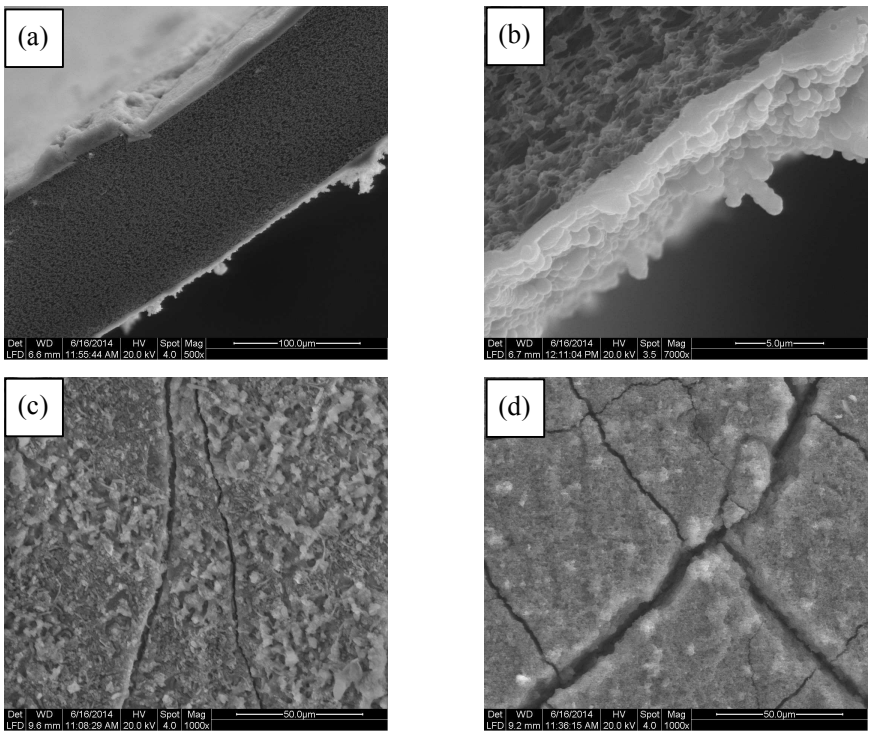

Figure 3.7. SEM micrographs of (a) cross-section, (b) cross-section of distillate surface, (c) feed surface, and (d) distillate surface of MD membrane used in MD reversal mode with deionized water experiment. Maximum silica concentration was 600 mg/L SiO_2.

Additionally, adsorption is an exothermic process, and an important parameter of an adsorption pair is the latent heat of adsorption, which is the energy exchanged during adsorption or desorption of a unit mass of sorbate [55]. The latent heat of adsorption is generally higher than the heat of vaporization of the adsorbate and approximately 2800 kJ/kg for the silica gel/water pair, but values from 2500 to 3500 kJ/kg have been reported for commercially available silica gels [56-58]. Thus, the energy required to desorb water from silica gel is higher than the energy required to evaporate pure water. When the feed side of the membrane is covered in silica scale, this results in reduced temperatures at the membrane surface because some fraction of the total vapor transport is a result of desorption, which may explain why a decline in both water flux and conductive heat transfer are observed. In the opposite scenario, when the distillate side of the membrane is covered in silica scale, the adsorbent properties of the silica gel are negligible because it is already fully hydrated and porous enough that it does not impede condensation and transport of liquid water into the bulk distillate channel.

3.4.3.2 MD reversal with NaOH solution

During this experiment, both sides of a new membrane were exposed to concentrated silica solution and subject to scaling, followed by a cleaning cycle of both membrane surfaces using an NaOH solution maintained at a pH of 11 to promote dissolution of polymerized silica. Scaling and resulting decline in water flux followed a similar trend as in previous experiments at similar conditions (Figure 3.8a, phase i). Following initial scaling, performance was tested using deionized water as both feed and distillate in both standard and MD reversal configuration (phase ii). Water flux improved slightly to 12–13 L/m^2/hr using deionized water in the first test at the standard configuration, returned to ~26 L/m^2/hr in MD reversal, then improved slightly again in standard configuration to ~15 L/m^2/hr in the second test of standard configuration, confirming the results of the previous experiment that silica scaling only impacts water flux when present on the feed side of the membrane. In the MD reversal configuration using silica solution as feed (phase iii) (same operating conditions as phase i except with feed flowing on the original distillate side of the membrane), water flux was initially comparable to clean membrane performance, but slowly declined to 20 L/m^2/hr as scaling occurred on the original distillate side of the membrane. Performance was then tested again using deionized water as feed and distillate (phase iv). Compared to the end of phase i, water flux increased slightly to 10 L/m^2/hr when the silica solution was returned as feed and the system was operated in standard MD configuration (phase v), which is similar to the performance increase after one hour of MD reversal discussed in Section 3.3.1 (Figure 3.6, phase i–ii). A similar phenomenon was also observed when the silica solution was used as feed in MD reversal configuration (phase vi, feed on the original distillate side of the membrane), and water flux increased slightly to about 23 L/m^2/hr compared to the 20 L/m^2/hr observed at the end of phase iii. Thus, while MD reversal does not remove the scale layer, it may cause some changes in structure or its interface with the membrane surface that slightly reduce its impact on performance.

Following the standard and MD reversal silica scaling cycles (phases i–vi), the system was drained and flushed with deionized water and the cleaning cycle using NaOH solution described in Section 3.3.4.4 was performed (phase vii). Membrane performance was then tested using a 1 g/L NaCl solution, both in standard MD (phase viii) and MD reversal (phase ix) configuration to test performance after cleaning. Water flux was fully restored to 25–27 L/m^2/hr for both configurations. Although distillate conductivity increased slightly during the cleaning

cycle due to the swapping of the feed and distillate channels, calculated salt rejection during both performance tests with NaCl solution was very high, greater than 99.99%.

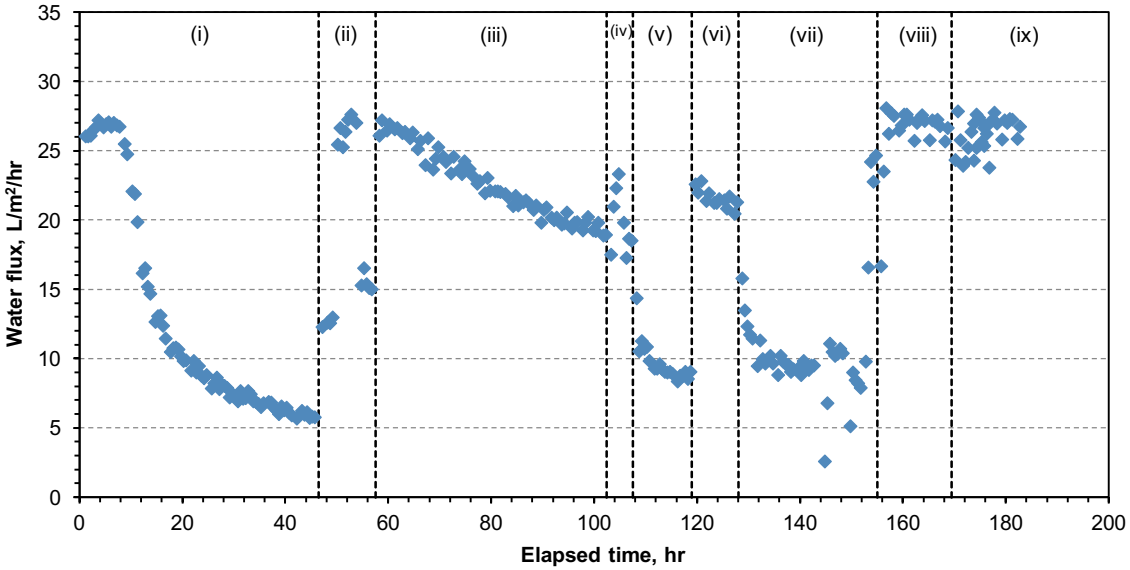

Figure 3.8. Water flux and for MD tested with maximum feed concentration of 600 mg/L SiO_2 and neutral pH. (i) Initial scaling cycle with new solution and new membrane and standard MD configuration. (ii) Standard configuration and MD reversal test with deionized water. (iii) Operation with original concentration silica solution in MD reversal configuration after performance test using deionized water. (iv) Standard configuration and MD reversal test with deionized water. (v) Operation with original concentrated silica solution in standard MD configuration after performance test using deionized water. (vi) Operation with original concentrated silica solution in MD reversal configuration. (vii) Cleaning cycle using NaOH solution maintained at a pH of 11. (viii) Performance test in standard MD configuration using 1 g/L NaCl solution. (ix) Performance test in MD reversal configuration using 1 g/L NaCl solution.

Following the scaling testing and cleaning cycles, the membrane was removed from the flow cell, air dried, and analyzed using SEM. Scaling on the surface of the membrane was noticeably more fractured than the membrane tested using only MD reversal with deionized water, and the surface of the membrane was visible between scale plates (Figure 3.9). Scaling on both sides of the membrane was also thinner and surface structures composed of spherical colloidal silica were absent. EDS analysis confirmed the scale layers as composed primarily of silicon and oxygen. The results suggest that the application of cleaning cycles using NaOH solution maintained at high pH may indeed promote dissolution of silica scaling on MD membranes, but complete removal of silica scale may require impractically long cleaning cycles

due to the low rate of dissolution. Also, membrane performance using pure water or dilute salt solutions is not sufficient as an indicator that complete cleaning has occurred, and silica scale may remain on membrane surfaces despite restored performance.

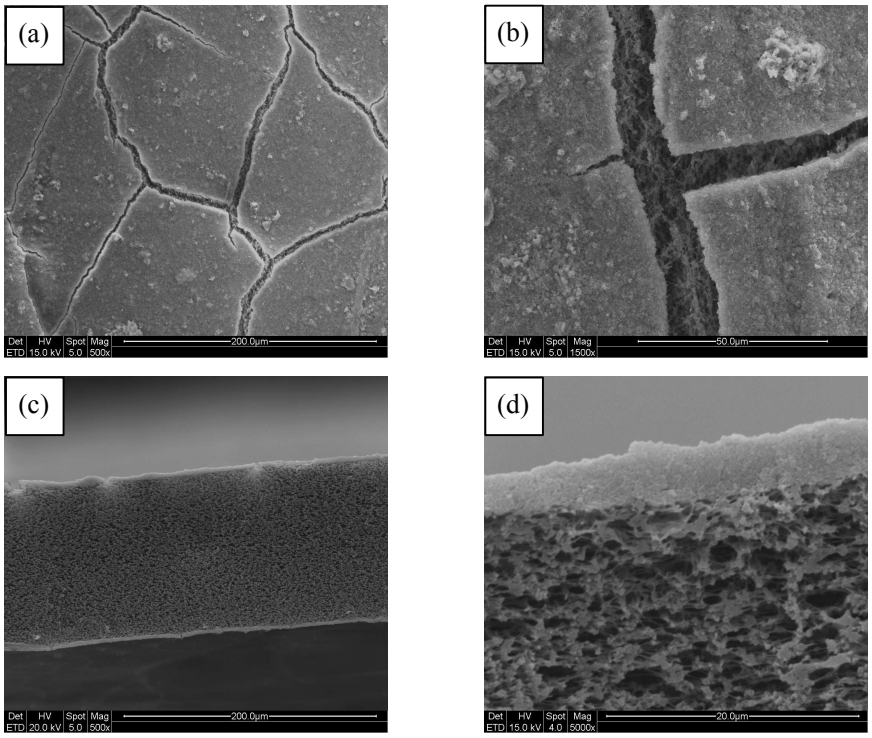

Figure 3.9. SEM micrographs of (a, b) feed surface, (c) cross-section, and (d) cross-section of feed surface of MD membrane used in MD reversal with NaOH cleaning experiment. Maximum silica concentration was 600 mg/L SiO_2.

3.4.3.3 Silica scaling with NaOH and NaCl cleaning with repeated scaling cycles

A third experiment was conducted using a more aggressive scaling and cleaning approach using NaOH cleaning solution maintained at pH 11, which also contained 0.1 M NaCl. Not surprisingly, scaling began sooner and completed in less time than for solutions with initial concentration of 225 mg/L SiO_2. In the first scaling cycle using solution with initial concentration of 1000 mg/L SiO_2 and pH of 7.95, water flux and thermal efficiency were similar to the measured baseline performance in the first few hours of the experiment (Figure 3.10). Impacts of scaling were first observed after 5 hours of experimental time, when the concentration was 1.68 times the initial concentration, or about 1,680 mg/L SiO_2 based on initial concentration. Water flux and thermal efficiency both declined rapidly for the next 7 hours, then stabilized

somewhat. This pattern of decline is similar to what was observed in experiments with initial concentration of 225 mg/L, but occurred much faster. Water flux declined to ~5 L/m^2/hr after only 20 hours, and the scaling cycle was stopped shortly afterwards. After the initial scaling cycle, water flux and thermal efficiency were slightly higher at 9–11 L/m^2/hr and 0.36–0.4, respectively, when tested using a solution of 1 g/L NaCl. Similar performance was observed at the beginning of the cleaning cycle using a solution of 0.1 M NaCl and NaOH maintained at pH 11; however, both water flux and thermal efficiency increased rapidly and was almost completely restored to measured baseline performance after about 10 hours. To determine if the silica scale could be thoroughly removed, the cleaning cycle was continued for a total of 24 hours before beginning the second scaling cycle using a new solution of 1000 mg/L SiO_2 and pH 8.01. Initial water flux of the second scaling cycle was slightly lower than that of the first scaling cycle, but still similar to baseline conditions. Water flux was stable for the first couple hours of the experiment, but induction time was less than during the first scaling cycle, and impacts of scaling began after only 2 hours of experimental time. Water flux then declined at a similar rate and followed a similar pattern of decline as the first scaling cycle. The early onset of scaling impacts on water flux indicates incomplete scale removal despite the long duration of the cleaning cycle, and residual silica on the membrane surface acting as seeds for silica polymerization.

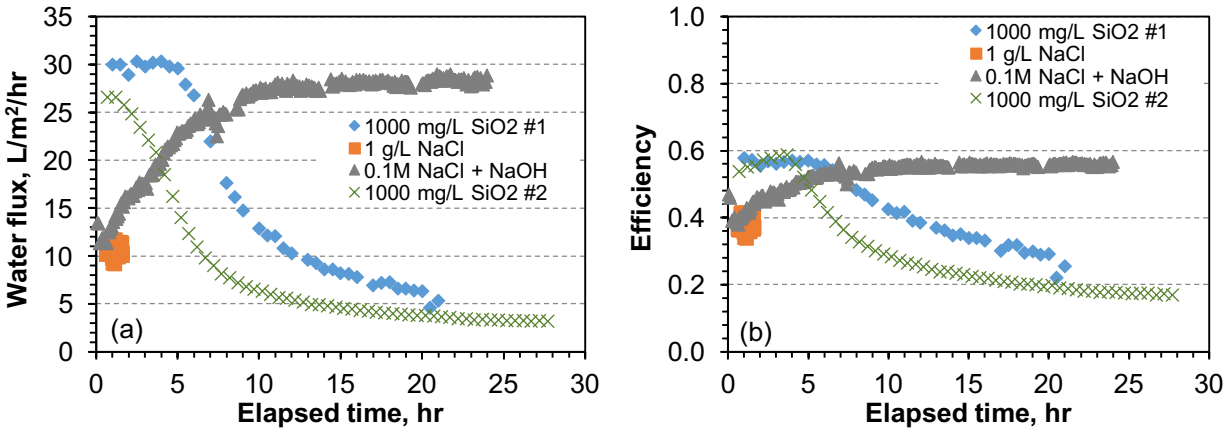

Figure 3.10. (a) Water flux and (b) thermal efficiency for MD tested with maximum concentration of 2667 mg/L SiO_2 and neutral pH. First scaling cycle used new silica solution with initial concentration 1000 mg/L SiO_2 and pH 7.95. Performance test using 1 g/L NaCl followed first scaling cycle, followed by cleaning cycle using solution of 0.1 M NaCl and NaOH maintained at pH >11. Second scaling cycle used new silica solution with initial concentration of 1000 mg/L SiO_2 and pH 8.01.

Despite slightly lower water flux and total heat transfer, thermal efficiency at the beginning of the second scaling cycle was approximately equal to the efficiency of the new membrane and remained stable for slightly longer than water flux. This may be related to the residual silica scale leftover from the first scaling cycle and suggests that the scale layer may contribute to a slight increase in total thermal resistance. Trends in calculated conductive heat transfer were similar for both scaling cycles, declining from approximately 200 W to 140 W in the first cycle, then increasing to 200 W during the cleaning cycle, and declining again to 140 W by the end of the second scaling cycle.

3.4.4 Some aspects on the practical application of pH adjustment to natural water resources

Experimental results suggest that pretreatment of feed water by pH adjustment is more effective as a silica scale management strategy than scale removal with a high pH cleaning solution. Silica polymerization and scaling risk in MD was substantially reduced at pH of below 5 or above 10, but once scale formed, it was difficult to completely remove with deionized water or an NaOH solution of pH 11. However, pH adjustment of natural water resources may be costly and may lead to increased scaling risk of other minerals involving ions such as calcium and magnesium, which are commonly present in groundwater resources. Also, carbonate alkalinity acts as a buffer, and water with high alkalinity may require more acid or base to adjust pH. Thus, the total chemical composition of a natural water resource must be carefully considered to determine if acidification or alkalization is an appropriate strategy to reduce risk of silica scaling. Also, implications of pH adjustment on post-treatment requirements of the brines should be considered.

To address some of these concerns, the potential costs of pH adjustment and its impacts on mineral scaling tendencies were considered using data obtained from the cooling tower makeup water of a geothermal power plant. The original water resource was close to saturation with respect to silica, but relatively low in salinity, hardness, and alkalinity, and thus an ideal candidate for potential treatment using MD with pH adjustment. The major constituents in the synthetic solution are summarized in Table 3.1.

Table 3.1. Composition of real cooling tower makeup water from the Tuscarora geothermal power plant (Nevada, USA) and synthetic solution with similar chemistry

Composition	Concentration (mg/L)	
	Real Tuscarora makeup (T-MU) cooling water	Synthetic T-MU solution
Sodium, Na^{+}	23.5	74.8
Potassium, K^{+}	8.94	8.94
Magnesium, Mg^{+2}	2.54	2.54
Calcium, Ca^{+2}	9.59	9.59
Barium, Ba^{+2}	0.22	0.22
Aluminum, Al^{+3}	0.23	0.23
Iron, Fe^{+3}	0.24	0.24
Chloride, Cl^{-}	8.33	33.8
Sulfate, SO_4^{-2}	12.4	12.4
Silica, SiO_2	90	90
Alkalinity (as mg/L $CaCO_3$)	84	84
pH	7.0	7.0

Synthetic solutions were prepared with similar chemical composition as the real water sample. Two experiments were conducted using 100 mL of synthetic T-MU solution to determine how much HCl or NaOH is required to adjust pH to outside the range where silica polymerization and scaling is a substantial risk. Concentrated HCl (32% by volume) was added to one sample to lower the pH to 5. In the other sample, a 0.2 g/L NaOH solution was added until pH reached 11. NaOH required progressively higher dosing per cubic meter as pH increased (Figure 3.11a). This is not surprising due to the buffering effect of silica with increased pH as silicic acids and monomeric silica are converted into soluble silicates. Assuming a cost of $300 per metric ton for industrial-grade concentrated HCl, and $400 per metric ton for 99% pure NaOH, the amount of HCl and NaOH required to reach the desired pH was used to calculate the approximate cost for pretreatment of the Tuscarora T-MU water. The cost of pH adjustment was relatively low at about $0.025 per m^3 using HCl and just over $0.04 per m^3 using NaOH (Figure 3.11b).

Scaling tendencies were calculated using OLI Stream Analyzer, and found that the original T-MU water exceeded saturation with respect to $CaCO_3$ above pH 9, which is not high enough to substantially reduce silica scaling risk. Considering the lower cost of pH adjustment with HCl, feed water acidification may be a viable pretreatment strategy in this particular case. This analysis did not consider the potential costs of neutralization of brine following treatment

with MD. However, it should be noted that in some cases brine neutralization may not be required. For example, well injection is the most common method of brine disposal for inland desalination, and it may be preferable to inject brine at low pH to reduce mineral scaling during the injection process. Also, because it is not limited by the osmotic pressure difference between the feed and permeate, the successful application of scale prevention strategies with MD may allow sufficiently high water recoveries that a zero-liquid-discharge process could be considered.

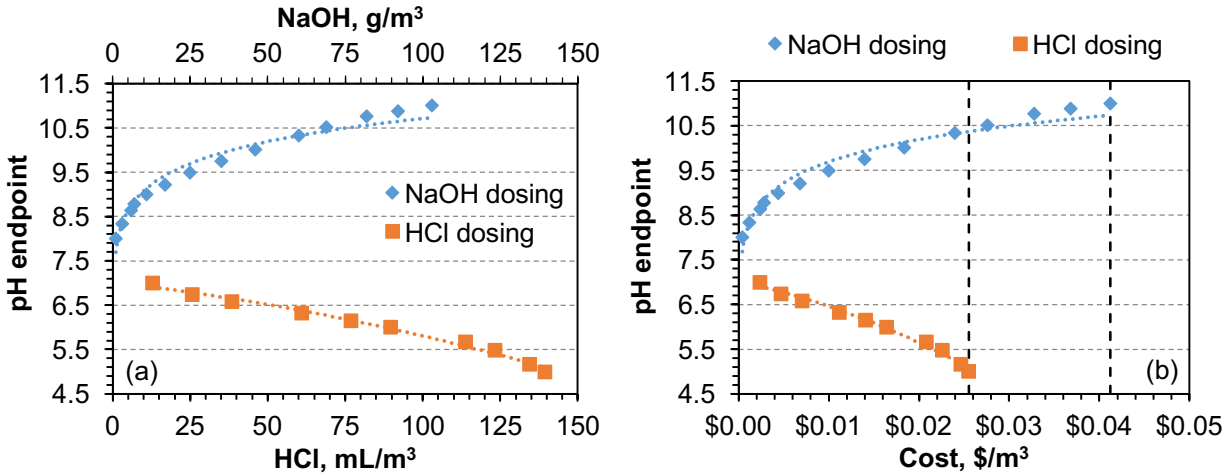

Figure 3.11. (a) HCl and NaOH dosing required to adjust synthetic Tuscarora T-MU solution to pH 5 and 11, respectively. (b) Estimated cost of pH adjustment of Tuscarora T-MU water based on results of experimental results from adjustment of synthetic solution.

3.5 Conclusion

This study investigated the application of pH adjustment as a pretreatment strategy for the prevention of silica scaling in the MD process applied to water supersaturated with respect to silica, and the effectiveness of various cleaning strategies for MD membranes scaled with silica. It was determined that both acidification and alkalization are effective pretreatment strategies to prevent silica scaling if pH can be adjusted outside the range where silica polymerization occurs, i.e. lower than 5 or higher than 10. Outside of this pH range, the MD process was capable of producing high quality distillate with silica concentrations as high as 600 mg/L for more than 40 hours and negligible decline in performance. For water resources containing high silica but relatively low in carbonate alkalinity or hardness, pretreatment using HCl or NaOH may be an inexpensive pretreatment strategy for water resources with no adverse effects on performance characteristics including water flux, thermal efficiency, or rejection.

Removing silica scale once it occurs proved to be much more difficult. Simply flushing the membrane using deionized water by reversing the temperature difference between the feed and distillate had no substantial effect on removing silica scale. Despite increased silica solubility and complete lack of polymerization at high pH, the application of a cleaning solution maintained at pH >11 was only partially effective at dissolving polymerized silica from membrane surfaces. Although cleaning cycles were successful at restoring water flux even after operation using silica concentrations exceeding 2500 mg/L, scaling occurred more rapidly on cleaned membranes when exposed to new silica solutions compared to new membranes. If complete cleaning of silica-scaled MD membranes is possible at all, it would likely require very long and impractical cleaning cycles based on the results of this investigation. Therefore, pretreatment and careful monitoring of performance for indications of scaling is imperative for long-term implementation of MD as a treatment strategy for silica-laden water resources.

Silica scaling on MD membranes was found to adversely affect water flux and thermal efficiency, although the impacts on thermal efficiency were less severe due in part to the insulating effect of the scale layer. Surprisingly, silica scaling was found to adversely affect MD performance only when present on the feed side of the membrane. Even with silica scale completely covering the membrane surface, performance was almost identical to that of a new membrane when the direction of water flux was reversed, indicating that silica scaling does not impede mass transport in the MD process by reducing overall permeability of the scale layer and membrane. Rather, it is proposed that the pore structure and adsorption properties of silica gel lead to reduced evaporation rates at the interface between the scale layer and membrane surface.

3.6 References

[1] R.K. Iler, The chemistry of silica: solubility, polymerization, colloid and surface properties, and biochemistry, Wiley, 1979.

[2] P. Sahachaiyunta, T. Koo, R. Sheikholeslami, Effect of several inorganic species on silica fouling in RO membranes, Desalination, 144 (2002) 373-378.

[3] R. Sheikholeslami, S. Zhou, Performance of RO membranes in silica bearing waters, Desalination, 132 (2000) 337-344.

[4] R. Semiat, I. Sutzkover, D. Hasson, Scaling of RO membranes from silica supersaturated solutions, Desalination, 157 (2003) 169-191.

[5] T. Koo, Y.J. Lee, R. Sheikholeslami, Silica fouling and cleaning of reverse osmosis membranes, Desalination, 139 (2001) 43-56.

[6] N.A. Milne, T. O'Reilly, P. Sanciolo, E. Ostarcevic, M. Beighton, K. Taylor, M. Mullett, A.J. Tarquin, S.R. Gray, Chemistry of silica scale mitigation for RO desalination with particular reference to remote operations, Water Research, 65 (2014) 107-133.

[7] R.Y. Ning, A.J. Tarquin, J.E. Balliew, Seawater RO treatment of RO concentrate to extreme silica concentrations, Desalin Water Treat, 22 (2010) 286-291.

[8] N. Ghaffour, T.M. Missimer, G.L. Amy, Technical review and evaluation of the economics of water desalination: Current and future challenges for better water supply sustainability, Desalination, 309 (2013) 197-207.

[9] B. Hamrouni, M. Dhahbi, Analytical aspects of silica in saline water — application to desalination of brackish waters, Desalination, 136 (2001) 225-232.

[10] A.M. Al-Rehaili, Comparative chemical clarification for silica removal from RO groundwater feed, Desalination, 159 (2003) 21-31.

[11] Ş.G. Öner, N. Kabay, E. Güler, M. Kitiş, M. Yüksel, A comparative study for the removal of boron and silica from geothermal water by cross-flow flat sheet reverse osmosis method, Desalination, 283 (2011) 10-15.

[12] M. Badruzzaman, A. Subramani, J. DeCarolis, W. Pearce, J.G. Jacangelo, Impacts of silica on the sustainable productivity of reverse osmosis membranes treating low-salinity brackish groundwater, Desalination, 279 (2011) 210-218.

[13] F.K. Lindsay, J.W. Ryznar, Removal of Silica from Water by Sodium Aluminate, Industrial & Engineering Chemistry, 31 (1939) 859-861.

[14] L.D. Betz, C.A. Noll, J.J. Maguire, Removal of Silica from Water by Hot Process, Industrial & Engineering Chemistry, 32 (1940) 1323-1329.

[15] R. Sheikholeslami, I.S. Al-Mutaz, S. Tan, S.D. Tan, Some aspects of silica polymerization and fouling and its pretreatment by sodium aluminate, lime and soda ash, Desalination, 150 (2002) 85-92.

[16] E. Neofotistou, K.D. Demadis, Use of antiscalants for mitigation of silica (SiO2) fouling and deposition: fundamentals and applications in desalination systems, Desalination, 167 (2004) 257-272.

[17] A. Sweity, T.R. Zere, I. David, S. Bason, Y. Oren, Z. Ronen, M. Herzberg, Side effects of antiscalants on biofouling of reverse osmosis membranes in brackish water desalination, Journal of Membrane Science, 481 (2015) 172-187.

[18] A. Antony, J.H. Low, S. Gray, A.E. Childress, P. Le-Clech, G. Leslie, Scale formation and control in high pressure membrane water treatment systems: A review, Journal of Membrane Science, 383 (2011) 1-16.

[19] J.S. Gill, Inhibition of silica—silicate deposit in industrial waters, Colloids and Surfaces A: Physicochemical and Engineering Aspects, 74 (1993) 101-106.

[20] Precipitation of amorphous silica from high-temperature hypersaline geothermal brines, California Univ., Livermore (USA). Lawrence Livermore Lab.: 1975.

[21] P.V. Brady, S.J. Altman, L.K. McGrath, J.L. Krumhansl, H.L. Anderson, pH modification for silica control, Desalin Water Treat, 51 (2013) 5901-5908.

[22] L.F. Song, J.Y. Hu, S.L. Ong, W.J. Ng, M. Elimelech, M. Wilf, Performance limitation of the full-scale reverse osmosis process, Journal of Membrane Science, 214 (2003) 239-244.

[23] M. Gryta, Concentration of NaCl solution by membrane distillation integrated with crystallization, Separation Science and Technology, 37 (2002) 3535-3558.

[24] M. Gryta, Direct contact membrane distillation with crystallization applied to NaCl solutions, Chem Pap-Chem Zvesti, 56 (2002) 14-19.

[25] C.M. Tun, A.G. Fane, J.T. Matheickal, R. Sheikholeslami, Membrane distillation crystallization of concentrated salts - flux and crystal formation, Journal of Membrane Science, 257 (2005) 144-155.

[26] A. Al-Karaghouli, L.L. Kazmerski, Energy consumption and water production cost of conventional and renewable-energy-powered desalination processes, Renewable and Sustainable Energy Reviews, 24 (2013) 343-356.

[27] J.A. Bush, J. Vanneste, T.Y. Cath, Membrane distillation for concentration of hypersaline brines from the Great Salt Lake: Effects of scaling and fouling on performance, efficiency, and salt rejection, Separation and Purification Technology, 170 (2016) 78-91.

[28] K.L. Hickenbottom, T.Y. Cath, Sustainable operation of membrane distillation for enhancement of mineral recovery from hypersaline solutions, Journal of Membrane Science, 454 (2014) 426-435.

[29] M. Osman, J.J. Schoeman, L. Baratta, Desalination/concentration of reverse osmosis and electrodialysis brines with membrane distillation, Desalin Water Treat, 24 (2010) 293-301.

[30] C.R. Martinetti, A.E. Childress, T.Y. Cath, High recovery of concentrated RO brines using forward osmosis and membrane distillation, Journal of Membrane Science, 331 (2009) 31-39.

[31] X. Ji, E. Curcio, S. Al Obaidani, G. Di Profio, E. Fontananova, E. Drioli, Membrane distillation-crystallization of seawater reverse osmosis brines, Separation and Purification Technology, 71 (2010) 76-82.

[32] D. Qu, J. Wang, B. Fan, Z.K. Luan, D.Y. Hou, Study on concentrating primary reverse osmosis retentate by direct contact membrane distillation, Desalination, 247 (2009) 540-550.

[33] J.P. Mericq, S. Laborie, C. Cabassud, Vacuum membrane distillation of seawater reverse osmosis brines, Water Res, 44 (2010) 5260-5273.

[34] L.D. Tijing, Y.C. Woo, J.-S. Choi, S. Lee, S.-H. Kim, H.K. Shon, Fouling and its control in membrane distillation—A review, Journal of Membrane Science, 475 (2015) 215-244.

[35] D.M. Warsinger, J. Swaminathan, E. Guillen-Burrieza, H.A. Arafat, J.H. Lienhard V, Scaling and fouling in membrane distillation for desalination applications: A review, Desalination, 356 (2015) 294-313.

[36] J. Gilron, Y. Ladizansky, E. Korin, Silica Fouling in Direct Contact Membrane Distillation, Ind Eng Chem Res, 52 (2013) 10521-10529.

[37] J. Vanneste, J.A. Bush, K.L. Hickenbottom, C.A. Marks, D. Jassby, C.S. Turchi, T.Y. Cath, Novel thermal efficiency-based model for determination of thermal conductivity of membrane distillation membranes, Journal of Membrane Science, 548 (2018) 298-308.

[38] J. Vanneste, J.A. Bush, K.L. Hickenbottom, C.A. Marks, D. Jassby, C.S. Turchi, T.Y. Cath, Novel thermal efficiency-based model for determination of thermal conductivity of membrane distillation membranes, Journal of Membrane Science, Under Review (2017).

[39] ASTM D859-16, Standard Test Method for Silica in Water, in, ASTM International, West Conshohocken, PA, 2016.

[40] J.P. Icenhower, P.M. Dove, The dissolution kinetics of amorphous silica into sodium chloride solutions: effects of temperature and ionic strength, Geochimica et Cosmochimica Acta, 64 (2000) 4193-4203.

[41] K.B. Krauskopf, Dissolution and precipitation of silica at low temperatures, Geochimica et Cosmochimica Acta, 10 (1956) 1-26.

[42] G. Okamoto, T. Okura, K. Goto, Properties of silica in water, Geochimica et Cosmochimica Acta, 12 (1957) 123-132.

[43] H.P. Rothbaum, A.G. Rohde, Kinetics of silica polymerization and deposition from dilute solutions between 5 and 180°C, Journal of Colloid and Interface Science, 71 (1979) 533-559.

[44] J.M. Gurgel, R.P. Klüppel, Thermal conductivity of hydrated silica-gel, The Chemical Engineering Journal and the Biochemical Engineering Journal, 61 (1996) 133-138.

[45] H. Bjurström, E. Karawacki, B. Carlsson, Thermal conductivity of a microporous particulate medium: moist silica gel, International Journal of Heat and Mass Transfer, 27 (1984) 2025-2036.

[46] IAPWS, Revised Release on the IAPS Formulation 1985 for the Thermal Conductivity of Ordinary Water Substance, Internation Association for the Properties of Water and Steam, (1998).

[47] V.M. Gun'ko, O.V. Goncharuk, J. Goworek, Evaporation of polar and nonpolar liquids from silica gels and fumed silica, Colloids and Surfaces A: Physicochemical and Engineering Aspects, 474 (2015) 52-62.

[48] P. Finocchiaro, M. Beccali, V. Gentile, Experimental results on adsorption beds for air dehumidification, International Journal of Refrigeration, 63 (2016) 100-112.

[49] D. Wang, J. Zhang, Q. Yang, N. Li, K. Sumathy, Study of adsorption characteristics in silica gel–water adsorption refrigeration, Applied Energy, 113 (2014) 734-741.

[50] D. Wang, J. Zhang, X. Tian, D. Liu, K. Sumathy, Progress in silica gel–water adsorption refrigeration technology, Renewable and Sustainable Energy Reviews, 30 (2014) 85-104.

[51] D.C. Wang, Z.Z. Xia, J.Y. Wu, R.Z. Wang, H. Zhai, W.D. Dou, Study of a novel silica gel–water adsorption chiller. Part I. Design and performance prediction, International Journal of Refrigeration, 28 (2005) 1073-1083.

[52] D.C. Wang, J.Y. Wu, Z.Z. Xia, H. Zhai, R.Z. Wang, W.D. Dou, Study of a novel silica gel–water adsorption chiller. Part II. Experimental study, International Journal of Refrigeration, 28 (2005) 1084-1091.

[53] Y.L. Liu, R.Z. Wang, Z.Z. Xia, Experimental performance of a silica gel–water adsorption chiller, Applied Thermal Engineering, 25 (2005) 359-375.

[54] K. Thu, A. Chakraborty, B.B. Saha, K.C. Ng, Thermo-physical properties of silica gel for adsorption desalination cycle, Applied Thermal Engineering, 50 (2013) 1596-1602.

[55] Y. Teng, R.Z. Wang, J.Y. Wu, Study of the fundamentals of adsorption systems, Applied Thermal Engineering, 17 (1997) 327-338.

[56] L.W. Wang, R.Z. Wang, R.G. Oliveira, A review on adsorption working pairs for refrigeration, Renewable and Sustainable Energy Reviews, 13 (2009) 518-534.

[57] H.T. Chua, K.C. Ng, A. Chakraborty, N.M. Oo, M.A. Othman, Adsorption Characteristics of Silica Gel + Water Systems, Journal of Chemical & Engineering Data, 47 (2002) 1177-1181.

[58] N.C. Srivastava, I.W. Eames, A review of adsorbents and adsorbates in solid–vapour adsorption heat pump systems, Applied Thermal Engineering, 18 (1998) 707-714.

CHAPTER 4
DETERMINATION OF CRITICAL FEED TEMPERATURE AND CO-ION COMPOSITION TO MINIMIZE SILICA SCALING IN MEMBRANE DISTILLATION

Manuscript in preparation for submission and potential publication in
Environmental Science: Water Research & Technology

John A. Bush[1❖], Johan Vanneste[1], Tzahi Y. Cath[1*]

4.1 Abstract

Membrane distillation is a promising technology for high-recovery desalination because performance is not substantially impacted by salinity. However, desalination of inland brackish resources is often also limited by high potential for scaling by silica and other minerals. The presence of divalent cations such as calcium and magnesium are a complicating factor, as these can catalyze silica polymerization and accelerate membrane fouling. In this study, the influence of cation concentration, carbonate alkalinity, and pH on silica scaling behavior of MD membranes was investigated. Both calcium and magnesium were found to accelerate silica scaling rates, but did not incorporate into the scale layer or alter its impact on water flux and thermal efficiency. The effect of calcium was reduced with increased alkalinity, possibly due to calcium carbonate precipitation in the system or due to interactions between calcium and bicarbonate that reduced the catalytic effect of calcium on silica polymerization. Reducing the feed temperature dramatically reduced both the rate and severity of impacts caused by silica scaling, and optimization of feed temperature may be a promising strategy to minimize silica scaling while maintaining thermal efficiency in MD.

[1]Colorado School of Mines, Golden, Colorado, USA 80401
❖Primary researcher and author
*Corresponding author: email: tcath@mines.edu; phone: (303) 273-3402; fax: (303) 273-3413

4.2 Introduction

Desalination of inland brackish groundwater typically must achieve high water recovery due to the technical challenges and costs associated with brine management and disposal [1, 2]. Membrane desalination processes such as reverse osmosis (RO) and nanofiltration (NF) are presently the most economical technologies considered for brackish groundwater desalination [3, 4], but recovery is often limited in these processes due to membrane fouling and scaling [5-7]. In particular, silica scaling is a major challenge for inland brackish desalination [8-13]. Silica is present in most groundwater resources and can polymerize to form a hard scale on membrane surfaces if feed water silica concentrations exceed its solubility limit of approximately 120 mg/L at neutral pH [14]. Silica scale severely impacts performance of RO membranes and is extremely difficult to remove once formed [10, 13, 15]; thus, management strategies for desalination of water resources with high silica content are heavily dependent on preventative measures. While silica concentration may be reduced by removal during pretreatment, most strategies (i.e. lime/soda softening, coagulation) produce large amounts of sludge that can be costly and labor intensive to dispose of, especially for remote inland locations [9].

In situations where silica removal during pretreatment may be impractical, the effective solubility limit can be increased with the use of antiscalants that inhibit polymerization or disperse silica colloids in solution [16]. Modifying the feed water pH may also be an effective strategy, because polymerization proceeds slowly at low pH, and silica solubility increases at high pH [17, 18]. However, the mechanisms of silica polymerization are complex and difficult to predict, being influenced by many factors including temperature, pH, ionic strength, and interactions with other ions [14, 19]. In particular, multivalent ions such as calcium, magnesium, barium, iron, and aluminum common to groundwater resources catalyze silica polymerization, and have been shown to accelerate silica scaling in RO membranes [12, 15, 20, 21]. Thus, management of silica scaling in the desalination of brackish resources requires careful consideration of the overall water chemistry and accurate assessment of silica scaling risk as well as other types of scaling and fouling. For example, pH modification may not be practical for water with high alkalinity or other buffering capacity, and operating at high pH may increase scaling risk of carbonate and silicate minerals [22]. Also, pretreatment with antiscalants may be compromised depending on solution composition because they are typically designed to target

specific types of scaling, and incorrect dosing may contribute to fouling or increase the risk of biofouling [23, 24].

Development of new technologies that are more tolerant of high silica concentrations may also have potential to increase recovery in the desalination of inland brackish resources. Membrane distillation (MD) is a thermally-driven membrane separation process that has been explored in recent years for its potential as a high recovery desalination process [25-36] and to extract minerals from hypersaline brines [37-47]. MD utilizes a difference in vapor pressure across a porous, hydrophobic membrane as the driving force for mass transfer which is induced by continuously heating the feed water while simultaneously cooling the permeate water [48]. As a desalination process, MD has advantages over pressure-driven membrane processes because mass transport occurs in the vapor phase and is not limited by the osmotic pressure of the feed, and it is generally considered to be more resistant to fouling than RO [49, 50]. Additionally, the morphology of fouling and its impacts on the driving force in MD can be quite different than those of pressure-driven membrane processes [51]. Nevertheless, MD membranes are vulnerable to fouling by colloidal silica [52, 53], and the presence of soluble silica can also lead to scaling if solutions are concentrated above the solubility limit [54]. However, the hydrophobic membranes used in MD are not receptive to heterogeneous nucleation of silica polymers, and have been shown to be initially resistant to silica scaling at concentrations up to twice the solubility limit of silica at neutral pH, and even higher with pH adjustment [55]. Once scaling occurs, silica is difficult to remove from MD membranes, and accelerated fouling rates have been observed following chemical cleaning [55] and electrochemical cleaning of specially modified MD membranes [56] due to residual silica remaining on membrane surfaces.

The operating conditions and driving force in MD are quite different than in pressure-driven membrane processes, and the influence of factors such as temperature, pH, and ionic composition on silica polymerization may be different than pressure-driven processes. Because it is a thermally-driven separation process, MD experiences both concentration and temperature polarization, and the combined effects of these phenomena on silica polymerization rates are difficult to predict. While previous investigations have considered the influence of divalent ions on silica scaling of MD membranes [54], there is little research that directly compares silica polymerization and scaling behavior for different solution compositions and operating temperatures. In this study, scaling behavior and its impacts on MD performance were

investigated as solutions containing various combinations of silica, calcium, magnesium, and bicarbonate alkalinity were concentrated above the solubility limit of silica. The influence of feed temperature and driving force on silica polymerization and scaling behavior were also investigated for solutions containing both silica and calcium. Additionally, a cleaning procedure that involved flooding the membrane pores and flushing with a high pH solution was tested for its potential to remove silica from scaled membranes and restore performance.

4.3 Materials and Methods

4.3.1 Membranes and modules

The membrane used in the study was a hydrophobic, microporous polypropylene membrane manufactured by 3M (St. Paul, MN), and was isotropic with a nominal pore size of 0.2 μm, a porosity of 85% and a thickness of 110 μm. This membrane has been shown to perform well as an MD membrane, exhibiting high water flux and low variation in thermal efficiency over a wide range of temperature conditions [57]. Flow cells were fabricated using transparent acrylic, and designed using parallel narrow channels to support the flexible membranes without the need for spacers and ensure consistent hydrodynamic conditions near the membrane surface. Each channel was 18 cm (7") long, by 6.35 mm (0.25") wide, by 3.2 mm (0.0125") deep, and there were ten channels on opposite sides of the membrane for the feed solution and distillate, providing a total membrane surface area of 125 cm^2.

4.3.2 System description

An automated, closed-loop, bench-scale system was utilized for experimental testing, and is described elsewhere [55]. Briefly, data collection and operating conditions were controlled using LabVIEW software (National Instruments) and a Labjack U6 (Labjack, Lakewood, CO) DAQ device. Positive-displacement gear pumps were used to circulate feed and distillate continuously through the system at a constant flow rate. The distillate was stored in a cylindrical tank with a pressure transducer installed near the bottom of the tank, and water flux across the membrane was measured by calculating the change in height of the water column in the tank. A solenoid valve installed in the distillate tank enabled periodic draining of distillate back into the feed tank by gravity to keep the feed concentration within a specific range. The temperature of the feed solution was maintained constant using an electric heater and the distillate temperature

was maintained constant using a chiller. Temperature was monitored at the inlets and outlets of both the feed and distillate channels of the membrane test cell.

The temperature difference in the distillate between the inlet and outlet of the flow cell was used to calculate the enthalpy change of the distillate as it passed through the flow cell, which was used to calculate thermal efficiency of the process. Thermal efficiency (η_{th}) in MD is defined as the ratio of latent heat transfer with the vapor to the total heat transfer through the membrane, which includes both latent heat transfer and conduction heat transfer:

$$\eta_{\mathrm{th}} = \frac{Q_{\mathrm{vap}}}{Q_{\mathrm{tot}}} = \frac{Q_{\mathrm{vap}}}{Q_{\mathrm{vap}}+Q_{\mathrm{cond}}} \tag{4.1}$$

where Q_{vap} is the heat transfer resulting from the vapor transport across the membrane, Q_{tot} is the total heat transfer across the membrane, and Q_{cond} is the heat transfer due to conduction through the membrane. The vapor heat transfer is equal to the mass vapor transfer multiplied by the latent heat of vaporization of water (ΔH_{vap}). Conduction heat transfer is difficult to determine because it requires knowledge of the thermal conductivity of the membrane, which is difficult to measure and not commonly provided by membrane manufacturers [57]. Also, the temperature of the feed and distillate at the membrane surface typically cannot be measured directly and must be approximated, and are different than the bulk temperatures because of temperature polarization. However, because the temperature of the distillate is close to the ambient temperature, heat transfer through the flow cell is negligible, and the total heat transfer across the membrane may be approximated using the enthalpy change of the distillate. Using this approach, thermal efficiency was calculated using Eq. (4.2):

$$\eta_{\mathrm{th}} = \frac{\dot{m}_{\mathrm{m}}\Delta H_{\mathrm{vap}}}{(\dot{m}_{\mathrm{d}}+\dot{m}_{\mathrm{m}})c_{\mathrm{p,out}}T_{\mathrm{d,out}}-\dot{m}_{\mathrm{d}}c_{\mathrm{p,in}}T_{\mathrm{d,in}}} \tag{4.2}$$

where $\dot{m}_m$ is the mass flow rate of vapor across the membrane, $\dot{m}_d$ is the mass flow rate of the distillate, $T_{d,in}$ and $T_{d,out}$ are the temperature of the distillate at the inlet and outlet of the flow cell, respectively, and $c_{p,in}$ and $c_{p,out}$ are the constant-pressure specific heat of pure water calculated at $T_{d,in}$ and $T_{d,out}$, respectively. With total heat transfer and vapor heat transfer known, conduction heat transfer can be calculated as the difference between the two.

Salt rejection was calculated using a mass balance approach with the following equation:

$$\text{Salt rejection}(\%) = \left(1 - \frac{V_{d2}\sigma_{d2} - V_{d1}\sigma_{d1}}{(V_{d2} - V_{d1})\,\sigma_f}\right) \times 100 \quad (4.3)$$

where σ_f and σ_d are the conductivities of the feed and distillate solutions, and V_{d1} and V_{d2} represent the total volume of the distillate system at times 1 and 2 across a time interval. A toroidal sensor (Model TCSMA, Sensorex, Garden Grove, CA) was used to measure the conductivity of the feed, and a conductivity probe (Model T-35820-62, Cole-Parmer, Vernon Hills, IL) was used to measure the conductivity of the distillate.

4.3.3 Solution chemistry and analytical methods

Synthetic solutions were prepared for all experiments by dissolving sodium silicate pentahydrate, $Na_2SiO_3 \cdot 5H_2O$, into deionized water and adjusting the pH with concentrated HCl and NaOH. Most experiments were performed near pH 8 with an initial concentration of 225 mg/L SiO_2 (3.74 mmol/L) which is approximately equal to the saturation concentration with respect to silica at 60 °C [19]. The pH was chosen because the hydroxide ion is an important catalyst in silica polymerization, which is the result of reactions between two silanol (SiOH) groups to form Si–O–Si bonds [14]. Polymerization occurs most rapidly at slightly alkaline conditions and there is a high concentration of hydroxide, non-ionized SiOH groups, and ionized SiO^- groups. Experiments were also performed using solutions prepared with pH between 6 and 8 and initial concentrations from 170 mg/L and 1000 mg/L SiO_2 to establish scaling behavior and impacts of silica for the membrane and operating conditions at slightly acidic conditions and initial concentrations lower and greater than saturation.

The influence of calcium, magnesium, and bicarbonate on silica scaling behavior was investigated by adding reagents in quantities based on the molar concentration of silica (i.e., for a 225 mg/L SiO_2 solution, 150 mg/L Ca^{2+} is added to provide a 1:1 molar ratio of silica to calcium). Calcium and magnesium were provided by adding $CaCl_2 \cdot 2H_2O$ and $MgCl_2 \cdot 6H_2O$, respectively, and alkalinity was adjusted by adding $NaHCO_3$. When applicable, scaling tendencies of the solutions were predicted using OLI Stream Analyzer (OLI Systems, Inc., Cedar Knolls, NJ). To determine solution composition following experiments, samples were diluted

and filtered through a 0.45 micron filter and analyzed for anions with an ion chromatograph (Model ICS-90, Dionex, Sunnyvale, CA).

4.3.4 Membrane characterization

Membranes were air-dried following scaling experiments. Scale layer morphology and composition were analyzed using scanning electron microscopy (SEM) and energy dispersive x-ray spectroscopy (EDS) (Quanta 600, FEI Corp., Hillsboro, OR).

4.3.5 Experimental procedures

4.3.5.1 MD performance and silica scaling characterization

All experiments were executed with both feed and distillate solutions maintained at a constant flow rate of 2.0 L/min in a countercurrent flow configuration, providing a flow velocity of 16.6 cm/s and Reynolds number of 1056–1670 for the feed solution and 679–863 for the distillate, dependent on temperature. The baseline performance of the membrane was determined by measuring water flux, thermal efficiency, and salt rejection using a 1 g/L NaCl solution as feed at temperatures between 20 °C and 70 °C, and deionized water as distillate at temperatures of 20 °C and 30 °C. Scaling characterization experiments for different solution compositions were performed using prepared solutions with initial volume of 4 L and new membrane samples. A range of feed temperatures were tested between 40 °C and 60 °C, and all experiments were performed with distillate temperature maintained at 20 °C. In each scaling characterization experiment, the feed solution was concentrated until a maximum of 2.5 L of distillate was collected. Then the solenoid valve on the distillate tank was opened momentarily, allowing 0.5 L of distillate to return to the feed tank while the MD process continues. This cycling of the distillate was continued for the remainder of each experiment, maintaining the concentration factor of the feed solution between 2 and 2.67.

4.3.5.2 Silica scale cleaning

Silica scale is known for being difficult to remove from membrane surfaces. Previous investigations have reported some silica removal and performance recovery using cleaning solutions with high pH, but in some cases residual silica remained on the membrane surfaces [54] and led to increased fouling rates after cleaning [55]. A novel cleaning method was tested in

the present study, which involved flooding the membrane pores and reverse flushing the membrane with a heated NaOH solution maintained at 60 °C and pH 11. The membrane was first scaled using a solution with initial concentrations of 225 mg/L SiO_2 and 150 mg/L Ca^{2+} at neutral pH using the procedure described in Section 4.3.5.1. The membrane and flow cell was then removed from the experimental system, rinsed with deionized water, and filled with a surfactant solution to completely wet the membrane pores. The membrane and flow cell was then thoroughly rinsed with deionized water and reinstalled to the experimental system with the feed and distillate channels switched. Deionized water was then circulated through both feed and distillate circuits at constant 2.0 LPM, with the feed circuit heated to 60 °C. The feed circuit was then pressurized to approximately 50 kPa (7.25 psi) by partially closing a valve installed downstream of the flow cell outlet. Effectively, this mode of operation was similar to a microfiltration process, with the direction of water flux in the opposite direction as the previous MD process. The pH of the feed water was then adjusted to 11 using a concentrated NaOH solution. After 30 minutes, the system was flushed with deionized water and the membrane was dried by circulating air through the flow cell.

4.4 Results and Discussion

4.4.1 Baseline performance

Water flux of new membrane varied between 4.2 L/m^2/hr and 34.9 L/m^2/hr for the range of temperatures tested, increasing exponentially with increase in the temperature difference between the feed and distillate (ΔT) and mean membrane temperature ($T_m = (T_f + T_d)/2$) (Figure 4.1a). Thermal efficiency was similar for all conditions, only showing a slight increase at higher operating temperatures (Figure 4.1b). In all cases, salt rejection was 99.9% or higher.

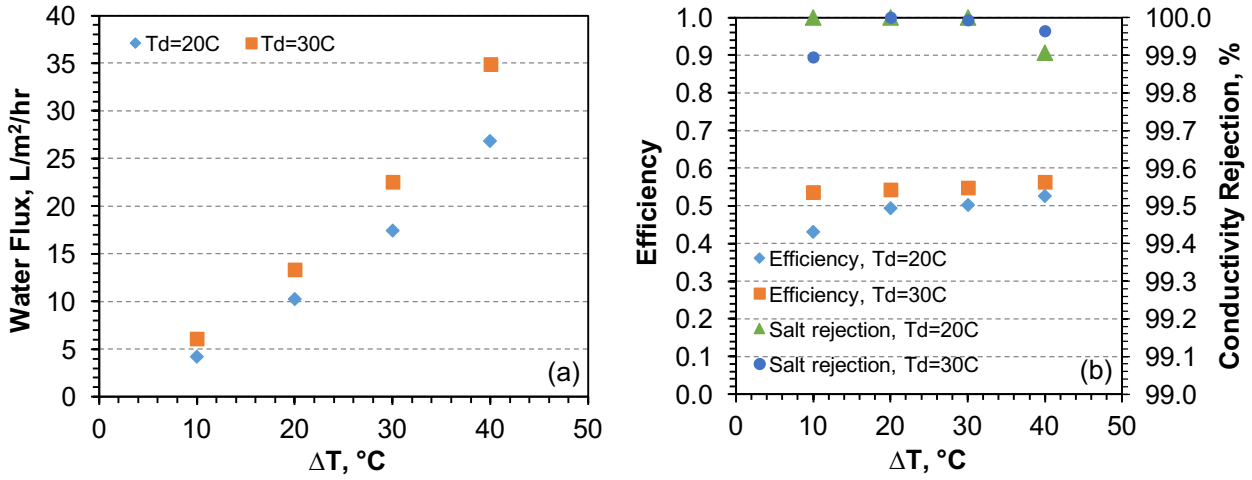

Figure 4.1. Measured (a) water flux and (b) thermal efficiency and conductivity rejection for 3M membrane tested with MD. Feed solution was 1 g/L NaCl and both feed and distillate were circulated at constant 2.0 L/min (16.6 cm/s). Influence of temperature was evaluated by testing ΔT between 10 °C and 40 °C with distillate temperature of 20 °C or 30 °C.

4.4.2 Effects of solution composition

4.4.2.1 Silica concentration

Experiments were performed using solutions prepared with pH of approximately 8 and initial concentrations from 170 mg/L to 1000 mg/L SiO_2 to investigate the influence of silica concentration on scaling behavior. In all cases, initial performance was very similar to that of pure water operating at similar conditions and was unaffected in the initial few hours of operation. After sufficient time at supersaturated concentrations, performance declined due to silica polymerization and scaling of the membrane surface.

Rates of flux decline were strongly affected by initial silica concentration and degree of supersaturation, which is not surprising due to its influence on polymerization rate and length of induction time for polymerization [19]. With an initial concentration of 225 mg/L SiO_2, water flux was stable for the first 8 hours of concentration at about 28 L/m^2/hr, slightly longer than the time required to reach the highest concentration factor of 2.67 (Figure 4.2a). Shortly afterwards, water flux began to rapidly decline, with the rate of decline steadily decreasing over the remainder of the experiment and approached a stable condition of about 10 L/m^2/hr. With initial silica concentration of 170 mg/L SiO_2, the induction time was much longer (12–14 hours) and the rate of flux decline was comparatively low and steady. Surprisingly, even with initial silica concentration of 1000 mg/L, water flux was stable for as much as 5 hours of experimental time

and did not begin to decline until reaching a concentration factor of more than 1.5, even though polymerization occurs rapidly with an induction time for polymerization of only minutes at such conditions [19]. Consequently, the induction time for scaling may be related to the operating conditions and time required for silica colloids to aggregate and attach to the membrane surface.

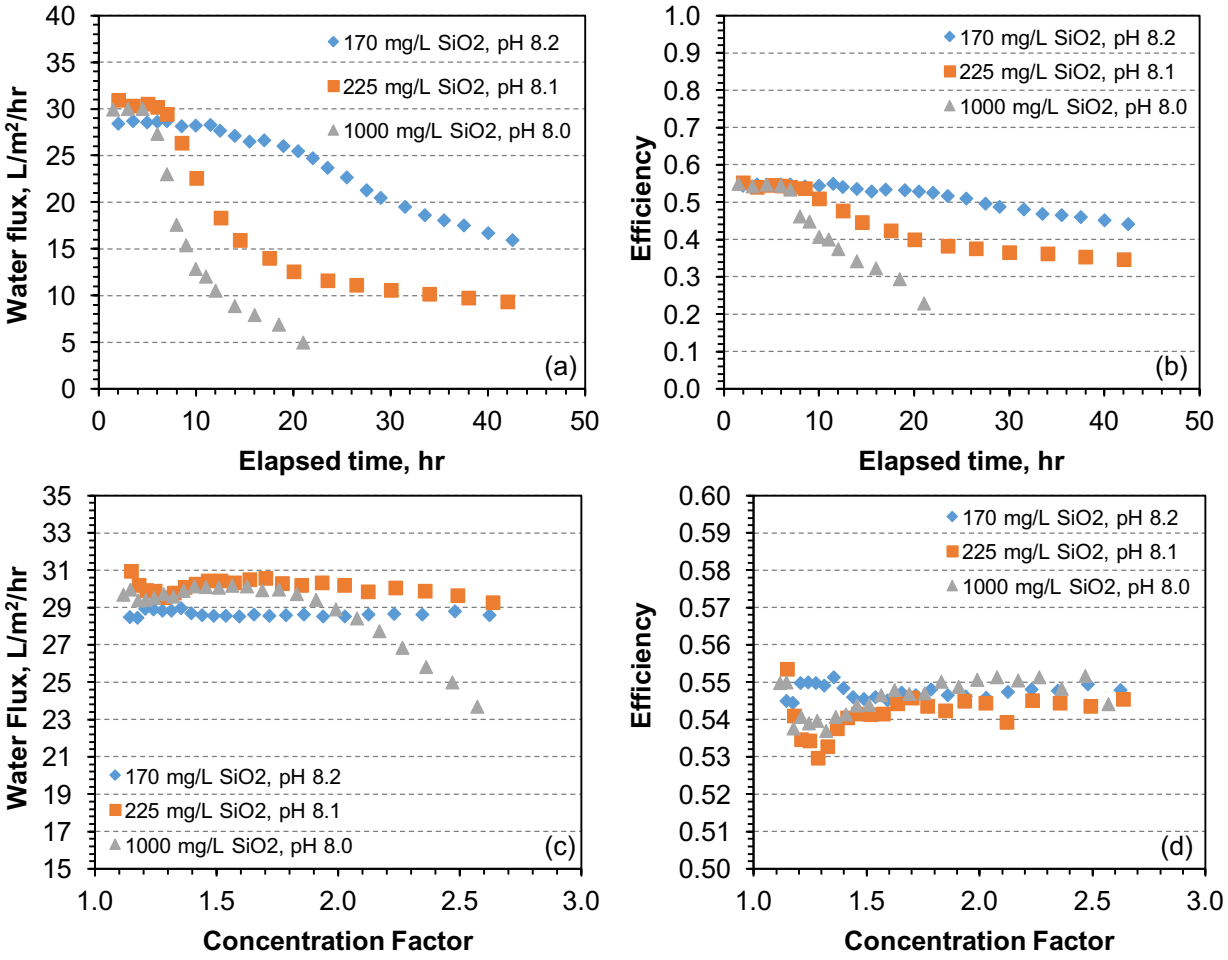

Figure 4.2. Influence of initial soluble silica concentration on scaling behavior of MD membranes. Measured (a) water flux and (b) thermal efficiency over time, and measured (c) water flux and (d) thermal efficiency versus concentration factor during initial concentration of solutions prepared with initial soluble silica concentrations of 170 mg/L to 1000 mg/L. Feed temperature was maintained at constant 60 °C and distillate temperature was maintained at constant 20 °C.

Thermal efficiency closely followed water flux for all conditions tested and also declined as a result of scaling (Figure 4.2b). However, decline in efficiency started later and was proportionally lower than decline in water flux. For example, in the most severe case, the

solution with initial concentration of 1000 mg/L SiO_2, water flux reduced by almost 80% between the beginning of the experiment and the end, after 20 hours of concentration. Over the same time period, the decline in thermal efficiency was less than 50%. Also, decline in water flux was observed when the concentration factor reached 2.0 (Figure 4.2c), whereas thermal efficiency was stable until reaching the maximum concentration factor of 2.67 (Figure 4.2d). Latent heat transfer scales proportionally with water flux, and thermal efficiency is primarily affected by conduction heat transfer. In the early stages of silica scaling, it was found that both latent heat transfer and conduction heat transfer declined at similar rates, resulting in negligible changes in thermal efficiency. As scaling continued, thermal efficiency began to decline because conduction heat transfer stabilized while water flux (and therefore latent heat transfer) continued to decline. Reduced conduction heat transfer with silica scaling was observed in a previous investigation and may be related to increased thermal resistance due to silica scaling coupled with increased temperature polarization because the heat of adsorption of the silica gel/water pair is higher than the latent heat of vaporization of water [55]. Overall, conduction heat transfer rates followed trends in water flux, declining from an initial value of between 200 and 220 W to approximately 170, 150, and 140 W for solutions with initial concentration of 170, 225, and 1000 mg/L SiO_2, respectively.

4.4.2.2 Calcium effects

Divalent cations are known to catalyze silica polymerization and accelerate scaling in membrane desalination processes. To investigate the influence of calcium concentration on silica scaling in MD, experiments were performed using solutions with initial concentration of 225 mg/L SiO_2 and $CaCl_2 \cdot 2H_2O$ added to reach 150 and 300 mg/L Ca^{2+} for a SiO_2:Ca^{2+} ratio of 1:1 and 1:2, respectively, on a molar concentration basis. Water flux as a function of time and feed concentration factor and efficiency as a function of water flux are shown in Figure 4.3. Increased rates of flux decline were observed for all solutions containing calcium compared to the solutions prepared using only sodium silicate, regardless of calcium concentration or pH (Figure 4.3a and Figure 4.3b). Total flux decline was also increased with the addition of calcium, but in all cases water flux stabilized to a minimum between 5 and 8 L/m^2/hr after about 30 hours of experimental time or less.

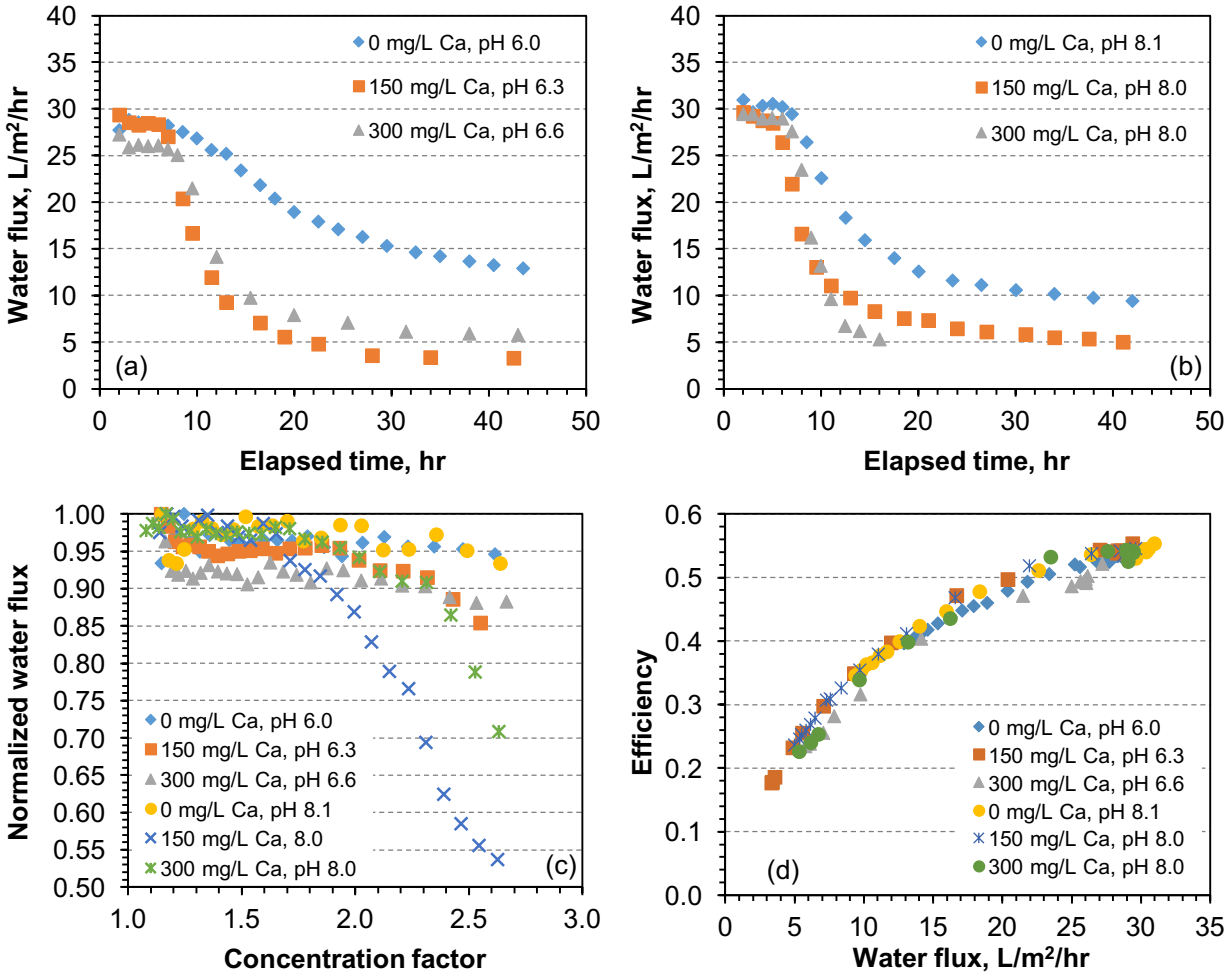

Figure 4.3. Measured water flux for solutions prepared with initial soluble silica concentration of 225 mg/L and calcium concentration between 0 and 300 mg/L for (a) slightly acidic solutions and (b) slightly alkaline solutions. Normalized water flux (c) during initial concentration of all solutions. Relationship between water flux and thermal efficiency (d) for all solutions. Feed temperature was maintained at constant 60 °C and distillate temperature was maintained at constant 20 °C.

In a previous study, the impacts of silica scaling on MD performance were found to be strongly affected by pH due to reduced rates of polymerization of soluble silica at low pH, resulting in lower rates of flux decline near pH 6 [55]. In comparison, rates of water flux decline were similar for silica solutions prepared with added calcium for solutions above and below pH 7. However, induction times were slightly lower for slightly alkaline solutions, and substantial decline in water flux was observed for both solutions with added calcium and pH 8.0 before reaching the maximum concentration of 2.67 (Figure 4.3c). The presence of calcium ions did not

affect trends in thermal efficiency, and the relationship between water flux and thermal efficiency was similar for all solutions regardless of pH and composition (Figure 4.3d). This indicates that while calcium concentration and pH influence the scaling rate, they do not alter the fundamental impacts of silica scaling in MD in terms of its effect on water flux or total thermal conductivity of the membrane and scale layer.

4.4.2.3 Carbonate alkalinity effects

The presence of calcium in groundwater is often associated with carbonate alkalinity due to the weathering of minerals such as limestone. To investigate the influence of carbonate alkalinity on silica scaling in MD, experiments were conducted with solutions containing different concentrations of silica, calcium, and bicarbonate. The initial concentration and molar ratio of each species for the solutions tested are summarized in Table 4.1.

Table 4.1. Molar concentration ratios and initial species concentration for silica-calcium-bicarbonate solutions.

Molar concentration ratio SiO_2:Ca^{2+}:HCO_3^-	Initial species concentration (mg/L)		
	SiO_2	Ca^{2+}	HCO_3^-
0:1:1	0	150	225
0.75:1:0	170	150	0
0.75:1:0.5	170	150	113
0.75:1:1	170	150	225
1:0:1	225	0	225
1:1:0	225	150	0
1:1:0.5	225	150	113
1:1:1	225	150	225

The inclusion of bicarbonate in the presence of calcium introduces a potential scaling risk due to the low solubility of $CaCO_3$ that is highly dependent on temperature and pH. Unlike most minerals, the solubility of $CaCO_3$ decreases with temperature, thus its degree of saturation increases exponentially with both temperature and pH. At the concentrations of calcium and bicarbonate investigated in the present study, predicted initial scaling tendencies based on solubility for calcite and aragonite were substantial at slightly alkaline conditions and negligible at slightly acidic conditions, increasing proportionally with bicarbonate concentration (Figure 4.4).

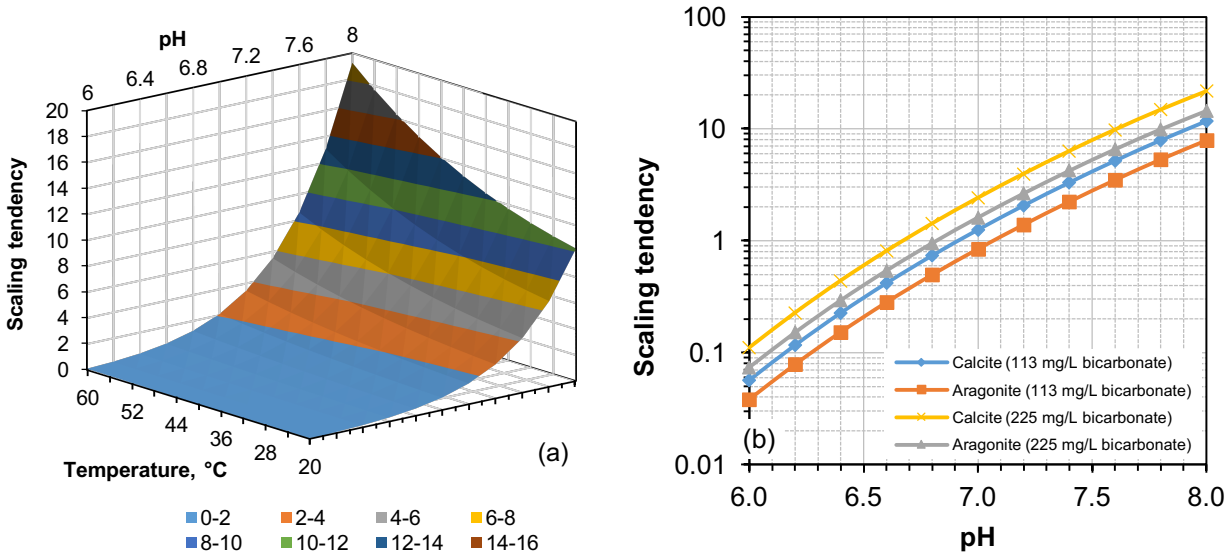

Figure 4.4. Predicted scaling tendency (a) of calcite at temperatures between 20 °C and 60 °C and pH between 6 and 8 for solution of 150 mg/L Ca^{2+} and 225 mg/L HCO_3^-. Numbers in legend indicate scaling tendency at corresponding temperature and pH in the plot. Predicted scaling tendency (b) of calcite and aragonite at 60 °C and pH between 6 and 8 for solution of 150 mg/L Ca^{2+} and HCO_3^- concentrations of 113 mg/L and 225 mg/L.

However, these scaling tendency calculations do not consider the kinetics of crystallization. Therefore, to assess the actual scaling risk and potential impacts of $CaCO_3$ scaling on the membrane at the tested conditions, experiments were also performed using a solution with initial concentrations of 150 mg/L Ca^{2+} and 225 mg/L HCO_3^-. This solution had a pH of 7.6, and despite a high scaling potential negligible performance decline was observed (Figure 4.5a), suggesting that $CaCO_3$ scaling was not a substantial factor for the conditions tested in this investigation. The lack of apparent scaling may be a result of the induction time for $CaCO_3$ crystallization exceeding the experimental time. Also, because of the temperature polarization phenomenon in MD, the temperature of the feed water is lower at the membrane surface than the bulk temperature in the channel. Therefore, the highest scaling potential may not be at the membrane surface because of the inverse solubility characteristics of $CaCO_3$ with respect to temperature.

Impacts of silica scaling were strongly affected by carbonate alkalinity, and tended to be less severe for solutions with high initial carbonate alkalinity. Solutions with an initial

concentration of 225 mg/L HCO_3^- had substantially lower rates of flux decline, regardless of initial silica and calcium concentration or pH (Figure 4.5a and Figure 4.5b).

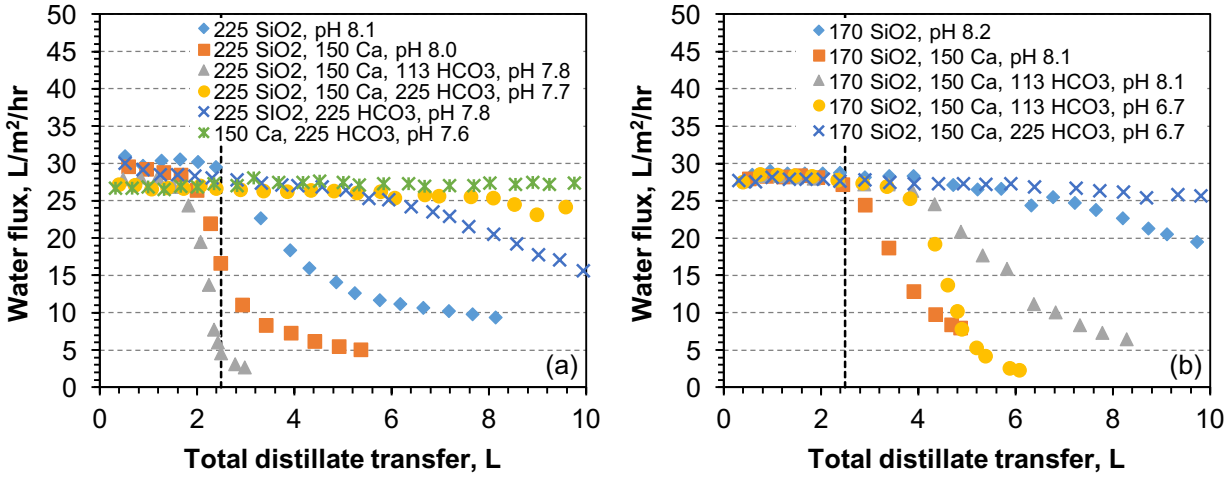

Figure 4.5. Water flux for solutions prepared with initial concentrations of (a) 225 mg/L SiO_2 and (b) 170 mg/L SiO_2 and various initial concentrations of calcium and bicarbonate. Feed temperature was maintained at constant 60 °C and distillate temperature was maintained at constant 20 °C. Vertical dashed line indicates the first time of maximum concentration (CF=2.67). After reaching maximum concentration permeate was periodically returned to feed tank to maintain concentration factor between 2 and 2.67 for the remainder of each experiment. Numbers in legend indicate initial solute concentration in mg/L.

However, results varied for solutions with lower initial bicarbonate concentration and suggest that the mitigating effect of carbonate alkalinity is influenced more by the ratio of calcium to bicarbonate than the ratio of silica to bicarbonate. For example, despite lower initial silica concentration, impacts of scaling were more severe for a solution with a SiO_2:Ca^{2+}:HCO_3^- molar ratio of 0.75:1:0.5 compared to a solution with a molar ratio of 1:1:1, and only slightly less severe than a solution with similar initial magnesium and calcium concentrations without added bicarbonate. Results also suggest that the influence of initial pH on silica scaling with solutions containing bicarbonate is the inverse of that observed with solutions prepared using only SiO_2 and calcium. In the case of similar initial concentrations of 170 mg/L SiO_2, 150 mg/L Ca^{2+}, and 113 mg/L HCO_3^-, decline in water flux was more severe for a solution with initial pH of 6.7 compared to 8.1.

Analysis of feed water composition after experiments found that the concentration of calcium tended to correspond with concentration factor for solutions prepared using only silica

and calcium. However, measured final calcium concentrations were lower than expected when solutions also contained bicarbonate, suggesting that precipitation of $CaCO_3$ does occur in the system and removes calcium ions from solution. The extent of calcium removal varied with initial bicarbonate and pH, and results suggest a correlation between final calcium concentration and impacts of scaling. For example, the final calcium concentrations for solutions prepared with initial concentrations of 170 mg/L SiO_2 and 150 mg/L Ca^{2+} are compared in Figure 4.6.

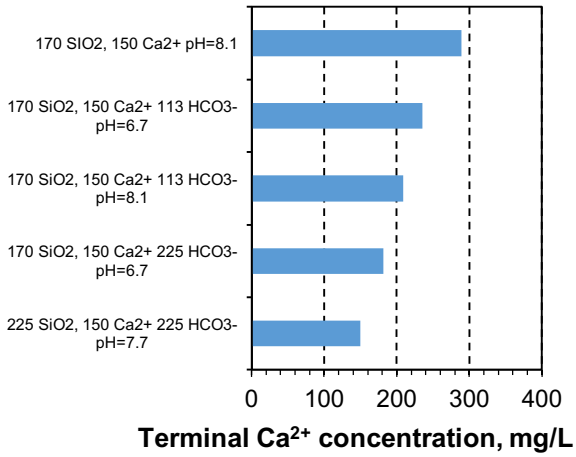

Figure 4.6. Measured final calcium concentration in feed water for MD experiments performed with initial concentration of 150 mg/L Ca^{2+}. Samples were collected at feed concentration factor of 2.0. Numbers in legend indicate initial solute concentration in mg/L.

In each case, the samples were taken at the end of the experiment after adjusting the concentration factor to exactly 2, thus the expected calcium concentration would be 300 mg/L if no precipitation occurred. Actual measured calcium concentrations were between 182 mg/L and 289 mg/L, with lower concentrations being associated with solutions that also had lower observed water flux decline during experiments. Using the trends in calcium removal as an indication of $CaCO_3$ precipitation, it is notable that they did not correlate with calculated scaling tendencies at the initial conditions, i.e. the lowest final calcium concentration was measured for the solution with initial concentration of 225 mg/L HCO_3^- despite a relatively low scaling tendency due to its low initial pH of 6.7. However, this can be explained by considering the influence of the equilibrium of carbon dioxide with water and the buffering effect of the carbonic acid system. The bicarbonate ion is the conjugate base of carbonic acid, H_2CO_3, and the conjugate acid of carbonate, carbonate. Because H_2CO_3 can dissociate into dissolved CO_2 and

H_2O, the equilibrium of these three species is dependent on the partial pressure of CO_2, pH, and temperature, with bicarbonate being dominant at pH near neutral. As concentration increases, $CaCO_3$ precipitation drives the equilibrium of bicarbonate ion towards carbonate, which releases H^+ and is thus inhibited at low pH. On the other hand, as the feed water is heated the solubility of CO_2 decreases and can pass through the membrane into the distillate and ultimately be released to the atmosphere, which drives the equilibrium of bicarbonate ion towards the protonated form of carbonic acid, which increases pH. Therefore, even with lower initial pH, as may be the case for some groundwater that can contain partial pressures of CO_2 higher than atmospheric, the equilibrium of the solution with higher alkalinity will tend towards $CaCO_3$ precipitation as CO_2 is released and pH increases. Accordingly, all the solutions compared in Figure 4.6 had similar pH between 7.6 and 7.8 and much lower alkalinity at the end of experiments compared to the initial conditions. Measured final alkalinity was primarily a function of initial bicarbonate concentration, and was 21 mg/L (as HCO_3^-) for both solutions prepared with 113 mg/L HCO_3^- and 28 mg/L (as HCO_3^-) for the solution prepared with 225 mg/L HCO_3^-.

4.4.2.4 Magnesium effects

The influence of magnesium on silica scaling was investigated by adding $MgCl_2 \cdot 6H_2O$ to provide 90 mg/L Mg^{2+}, which is approximately equal to the molar concentration of 225 mg/L SiO_2. Impacts of scaling were also accelerated in the presence of magnesium, but to a lesser degree than calcium. Induction times and initial rates of water flux decline were similar to those of the solution with initial concentration of 225 mg/L SiO_2; however, the rate of decline persisted longer than that solution and approached a lower stable condition than solutions prepared without added magnesium (Figure 4.7a). Rates of water flux decline were notably higher at slightly alkaline conditions compared to acidic conditions, which is similar to trends observed in silica solutions without added hardness ions and may be a result of the lower impact of magnesium on silica scaling compared to calcium.

In contrast to experiments performed with calcium, inclusion of bicarbonate in concentrations equal to the molar concentration of silica and magnesium tended to increase the rates and severity of scaling impacts compared to solutions without added bicarbonate. The contrasting effects of the two ions appeared to offset each other, as evidenced by the case of initial concentration of 225 mg/L SiO_2, 75 mg/L Ca^{2+}, 45 mg/L Mg^{2+}, and 225 mg/L HCO_3^-,

which had equimolar concentrations of silica, total hardness ions, and bicarbonate (Figure 4.7b). This phenomenon may be related to the fact that magnesium salts have slightly higher solubility than calcium salts and the addition of bicarbonate did not result in a substantial scaling risk of magnesium or carbonate minerals at the tested conditions. Thus, the inclusion of bicarbonate is less likely to induce precipitation and removal of magnesium compared to solutions containing calcium.

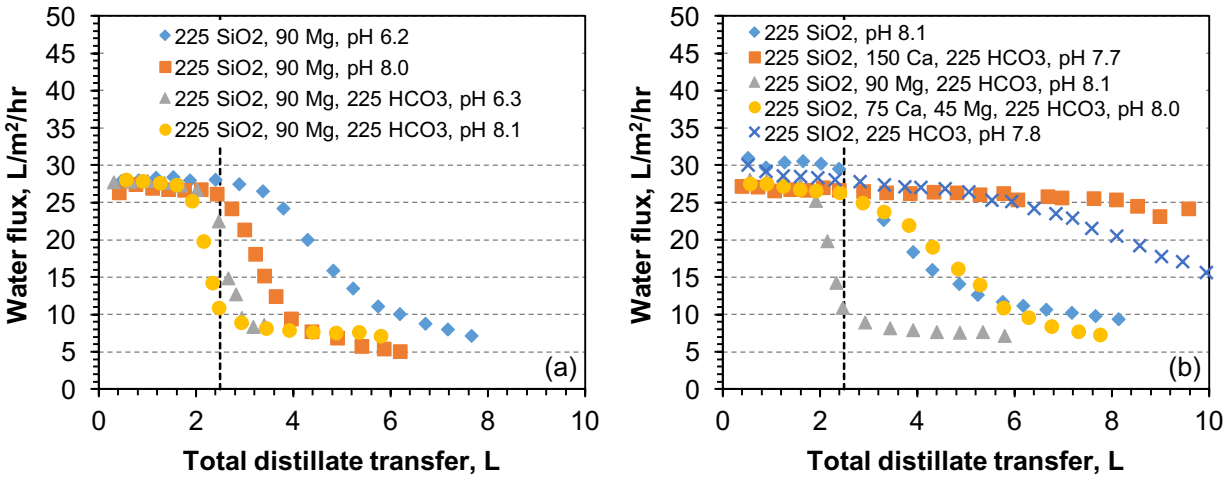

Figure 4.7. Measured water flux (a) for solutions prepared with initial concentrations of 225 mg/L SiO_2 and 90 mg/L Mg^{2+}, 225 mg/L HCO_3^- with initial pH of approximately 6 and 8, and (b) solutions prepared with initial concentrations of 225 mg/L SiO_2 with initial pH of 8 for different concentrations of calcium, magnesium, and bicarbonate. Feed temperature was maintained at constant 60 °C and distillate temperature was maintained at constant 20 °C. Vertical dashed line indicates the first time of maximum concentration (CF=2.67). After reaching maximum concentration permeate was periodically returned to feed tank to maintain concentration factor between 2 and 2.67 for the remainder of each experiment. Numbers in legend indicate initial solute concentration in mg/L.

Accordingly, the final magnesium concentration of the solution tested with magnesium and bicarbonate at slightly acidic initial conditions was similar to that of solutions tested without added bicarbonate (Figure 4.8); however, the solution tested with similar initial concentrations at slightly alkaline conditions contained lower magnesium at the conclusion of the experiment. As with $CaCO_3$, the solubility of $MgCO_3$ decreased with increased pH and temperature, and these results suggest that some precipitation may have occurred in the system. However, considering the final calcium and magnesium concentrations of the SiO_2–Ca^{2+}–Mg^{2+}–HCO_3^- solution, the

removal of magnesium is generally less extensive than removal of calcium with the addition of bicarbonate. Also, it is worth noting that the final total hardness of this solution, including both calcium and magnesium, was slightly lower on a molar concentration basis than the final total hardness for a solution with similar initial silica and bicarbonate concentrations and hardness consisting exclusively of calcium. The fact that the impacts of scaling were slightly more severe with the solution prepared with both calcium and magnesium suggests that the mitigating effect of bicarbonate may not be limited just to the extent of calcium removal, but also the interactions of calcium and bicarbonate still in solution that may inhibit the influence calcium on silica polymerization.

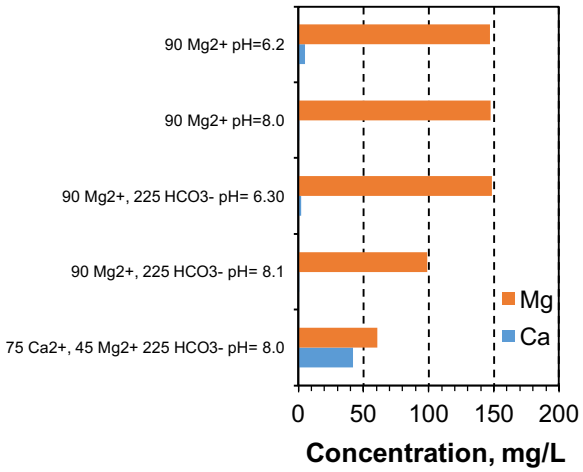

Figure 4.8. Measured final magnesium and calcium concentration in feed water for MD experiments performed with initial concentration of 225 mg/L SiO_2 and different combinations of magnesium, calcium, and bicarbonate. Samples were collected at feed concentration factor of 2.0. Numbers in legend indicate initial solute concentration in mg/L.

4.4.3 Scale morphology and composition

SEM analysis of membrane surfaces after experiments found similar scale morphology for membranes tested with only SiO_2 and calcium, typical examples are illustrated in Figure 4.9. In each case, the membrane surface was completely covered with an amorphous scale layer containing primarily silicon and oxygen. As reported by others, calcium was not detected in the scale layer, which supports the hypothesis that calcium acts as a catalyst for silica polymerization but does not incorporate into the scale structure. Trace amounts of calcium were detected on the membrane tested with a solution of 225 mg/L SiO_2, 150 mg/L Ca^{2+}, and 113 mg/L HCO_3^-, along

with additional deposits of a possible crystalline nature. These may be indicative of $CaCO_3$ scaling; however, the amount of calcium detected was much smaller than silicon and oxygen and were only a minor component of the scale layer compared to silica.

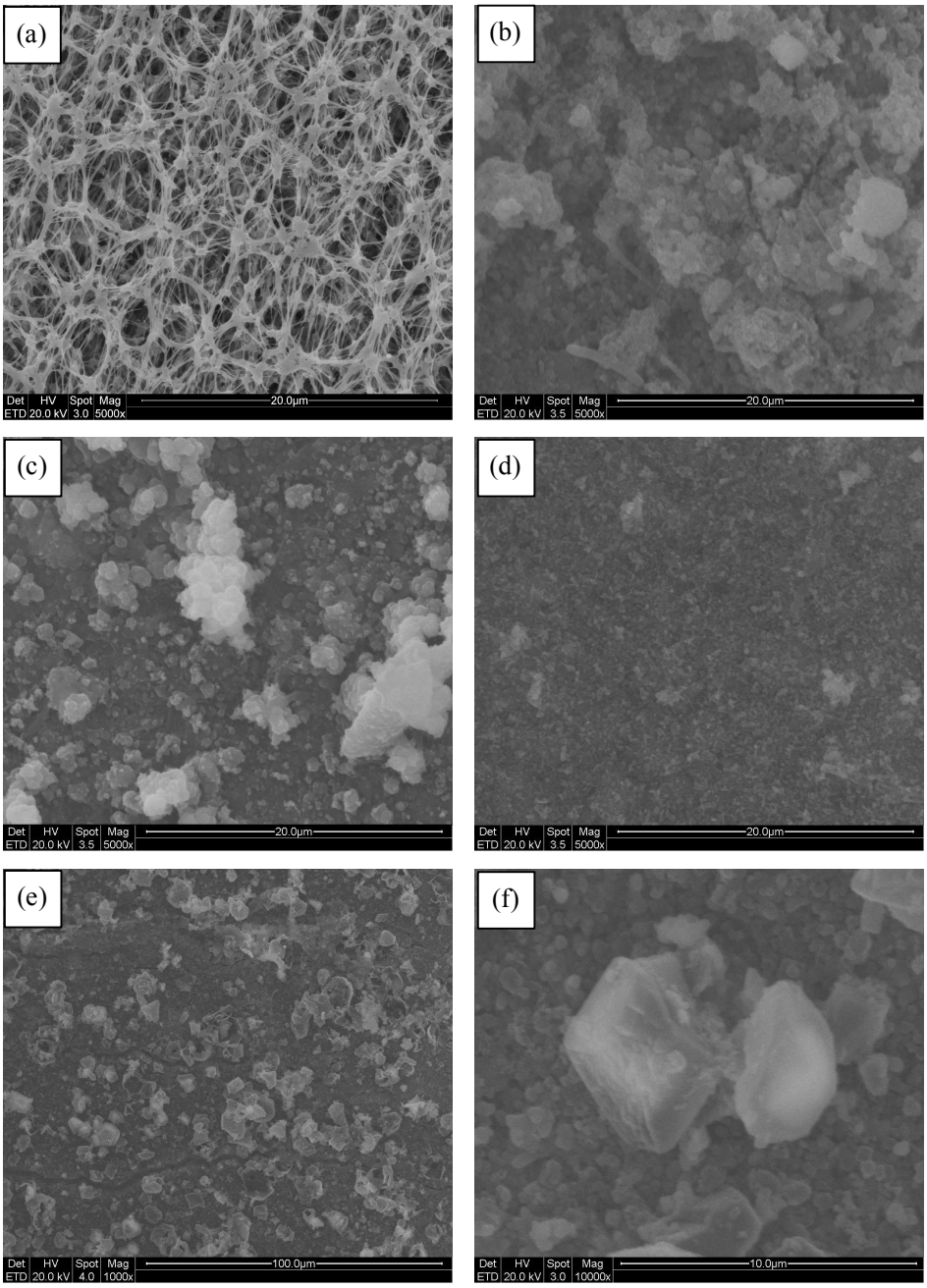

Figure 4.9. SEM images of (a) new membrane, (b) membrane after scaling with 225 mg/L SiO_2 solution, (c) membrane after scaling with 225 mg/L SiO_2 and 150 mg/L Ca^{2+} solution, (d) membrane after scaling with 225 mg/L SiO_2 and 300 mg/L Ca^{2+} solution, (e, f) membrane after scaling with 225 mg/L SiO_2, 150 mg/L Ca^{2+}, and 113 mg/L HCO_3^- solution.

4.4.4 Silica scale mitigation

4.4.4.1 Determination of critical flux

The effect of feed temperature and driving force on silica scaling in the presence of calcium was investigated with solutions containing initial concentrations of 225 mg/L SiO_2 and 150 mg/L Ca^{2+} at pH of 8. Additional experiments were performed using feed temperatures maintained at 40 °C and 50 °C, and the temperature of the distillate maintained at 20 °C. Initial performance closely matched the results of the 1 g/L NaCl tests for similar operating temperatures (Figure 4.1). Thus, initial water flux corresponded with the differences in temperature, but differences in initial thermal efficiency were negligible. Considering the strong influence that the degree of supersaturation has on silica polymerization, it might be expected that scaling would be more severe at lower feed temperatures because of the lower solubility of silica. However, results indicate that the opposite was true, and impacts of scaling on performance were substantially reduced by operating at lower feed temperatures (Figure 4.10a). Induction times were longer, and in the case of T_f=40 °C negligible decline in water flux occurred until after reaching the maximum concentration factor, whereas measurable drop in water flux was observed in the experiment performed with T_f=60 °C when the concentration factor was about 1.5. The rates and extent of flux decline also decreased with feed temperature, and the water flux after fouling was actually higher for experiments performed with lower feed temperatures, despite the initial flux being lower.

The longer induction times and lower initial rates of flux decline at reduced feed temperatures are not surprising. Though silica solubility decreases with temperature, concentration polarization also decreases with water flux and this may lead to lower degrees of supersaturation at the membrane surface compared to those at higher feed temperatures. Also, silica polymerization occurs more slowly at lower temperatures at constant supersaturation; however, for a given concentration the effect of reduced temperature on the kinetics of polymerization may be offset by the decrease in degree of supersaturation, which has a greater impact on polymerization rates [19]. Finally, colloidal fouling in cross-flow membrane processes is highly influenced by the different drag forces acting on suspended particles. Water flux induces movement towards the membrane surface, which tends to promote growth of the fouling layer, while bulk flow of water through the flow cell induces movement parallel to the membrane surface and tends to inhibit growth of the fouling layer [58, 59]. A critical flux point often exists

when these drag forces reach equilibrium. Thus, very little fouling is expected if the initial water flux is close to the critical flux.

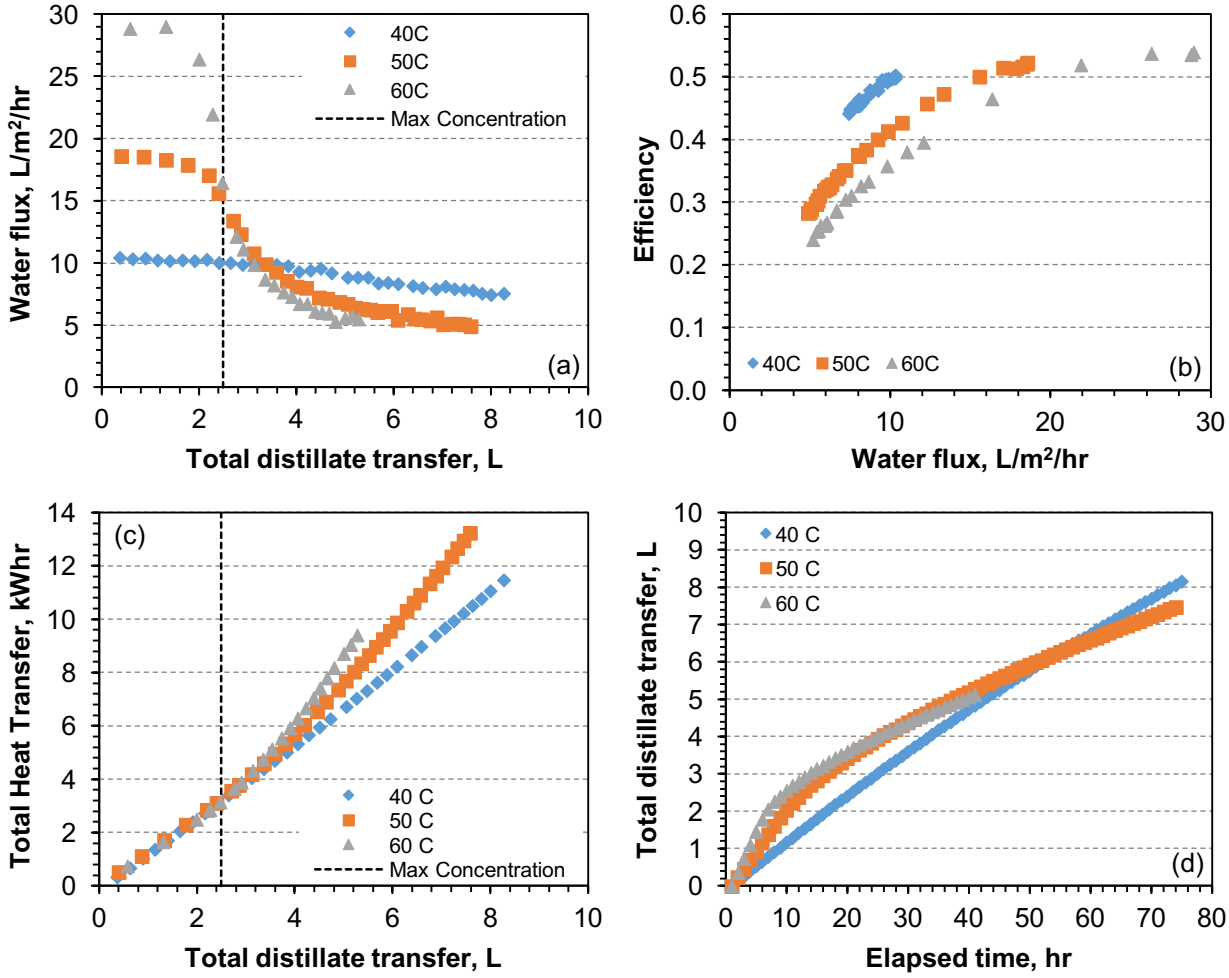

Figure 4.10. Measure water flux (a) as a function of total distillate transfer, thermal efficiency (b) as a function of water flux, cumulative total heat transfer (c) as a function of total distillate transfer, and (d) total distillate transfer over time for solutions prepared with 225 mg/L SiO_2 and 150 mg/L Ca^{2+} and pH of approximately 8 using feed temperatures between 40 °C and 60 °C and distillate temperature of 20 °C.

Thermal efficiency followed similar trends as other experiments, and declined with water flux as a result of scaling. An important distinction relates to the fact the thermal efficiency of new membranes is only slightly affected by feed temperature in MD, because both latent heat transfer and conductive heat transfer are driven by the temperature difference (ΔT) between the feed and distillate. However, latent heat transfer scales proportionally with water flux, which was

severely reduced as a result of fouling, while the overall thermal conductivity of the fouling layer and membrane was not substantially different than the thermal conductivity of the clean membrane. Thus, for a particular water flux the thermal efficiency of fouled membranes was much lower at higher ΔT because the conductive heat transfer is higher but the latent heat transfer is the same. For example, at a water flux of 10 L/m^2/hr, the thermal efficiencies for the experiments performed with T_f of 40, 50, and 60 °C were 0.49, 0.42, and 0.36, respectively (Figure 4.10b). As a result, reducing the feed temperature led to better long-term performance in terms of both total energy consumption (Figure 4.10c) and overall rate of water production (Figure 4.10d).

These results suggest that operation with low feed temperatures might be an attractive strategy to reduce silica scaling risk and maintain sustainable operation for longer periods of time with negligible impacts on efficiency. This is particularly important for the potential economic use of MD as a desalination strategy because the total energy demand of MD is generally higher than commercially available pressure-driven membrane processes such as RO or NF. However, most of the energy required for MD is thermal energy, and its electrical energy requirements can be much lower than pressure-driven membrane processes or other thermal desalination processes such as MED or MSF. Low operating temperatures offer the potential to use of inexpensive low-grade heat sources to provide the energy for the driving force, which could substantially reduce the operating costs of the process.

4.4.4.2 Temperature reversal

To further investigate the effect of feed temperature on silica scaling behavior in MD, a scaled membrane was tested using a range of temperatures, which included reversing the temperature difference between the feed and distillate solutions. Theoretical water flux (including reverse water flux) of an un-fouled membrane was predicted using the thermal efficiency-based model described in a previous work [57]. The parameters used in the model for the membrane and flow cell configuration of the present study were established using the baseline performance data of 1 g/L NaCl solutions (Figure 4.1).

After the initial scaling experiment using the solution with initial concentration of 225 mg/L SiO_2 and 150 mg/L Ca^{2+} at pH 6.3, the experiment was restarted with the feed temperature at 60 °C and the distillate temperature at 20 °C (Figure 4.11a, phase i). After about 10 hours,

water flux stabilized to ~3 L/m^2/hr, which is approximately equal to the water flux at the end of the initial scaling experiment. The feed solution was then cooled to 20 °C, and the distillate was heated to 40 °C (phase ii). The reverse water flux was constant during this phase at about 10 L/m^2/hr, which is approximately equal to the measured water flux for new membranes using 1 g/L NaCl as well as the predicted water flux. The feed water was then heated to 40 °C and the distillate cooled to 20 °C (phase iii). Water flux recovered slightly and was higher than the end of phase (i), but still about 40% lower than the predicted water flux for a clean membrane at these operating conditions. Incrementally increasing the feed temperature to 50 °C (phase iv) and then 60 °C (phase v) while maintaining the distillate at 20 °C resulted in slight increases in water flux, but the difference between the predicted water flux and measured water flux also increased with feed temperature. After a few hours with feed temperature of 60 °C, water flux began to decline again and eventually returned to approximately 3 L/m^2/hr. The feed solution was then cooled to 20 °C, and the distillate heated to 50 °C (phase vi). Reverse water flux during this phase was about 16 L/m^2/hr, which is slightly less than the predicted water flux, but the difference was much lower compared to the water flux with the feed temperature at 50 °C and distillate temperature at 20 °C (phase iv). Reverse water flux was also slightly less than predicted after cooling the distillate to 40 °C (phase vii), but the difference was smaller compared to phase (vi). Finally, the feed solution was heated to 40 °C and the distillate cooled to 20 °C (phase viii). Water flux was initially approximately equal to the predicted water flux, but quickly declined and ultimately stabilized at about 5 L/m^2/hr.

These results are consistent with a previous investigation that determined the impacts of silica scaling on MD are primarily a result of reduced evaporation rates at the membrane surface due to the adsorbent properties of the porous scale layer, and silica scaling has little to no effect on performance when present on the membrane surface undergoing condensation [55]. In that study, it was found that reversing the direction of water flux did not remove or reduce the thickness of the scale layer, but a slight performance improvement was observed after restoring the initial operating conditions, possibly as a result of changes that occurred in the structure of the scale layer or its interaction with the membrane. Similar behavior was observed in the present study, with both water flux and thermal efficiency being approximately equal to those of clean

membranes when the temperature difference across the membrane was reversed, and low performance observed again when the original temperature regime was restored.

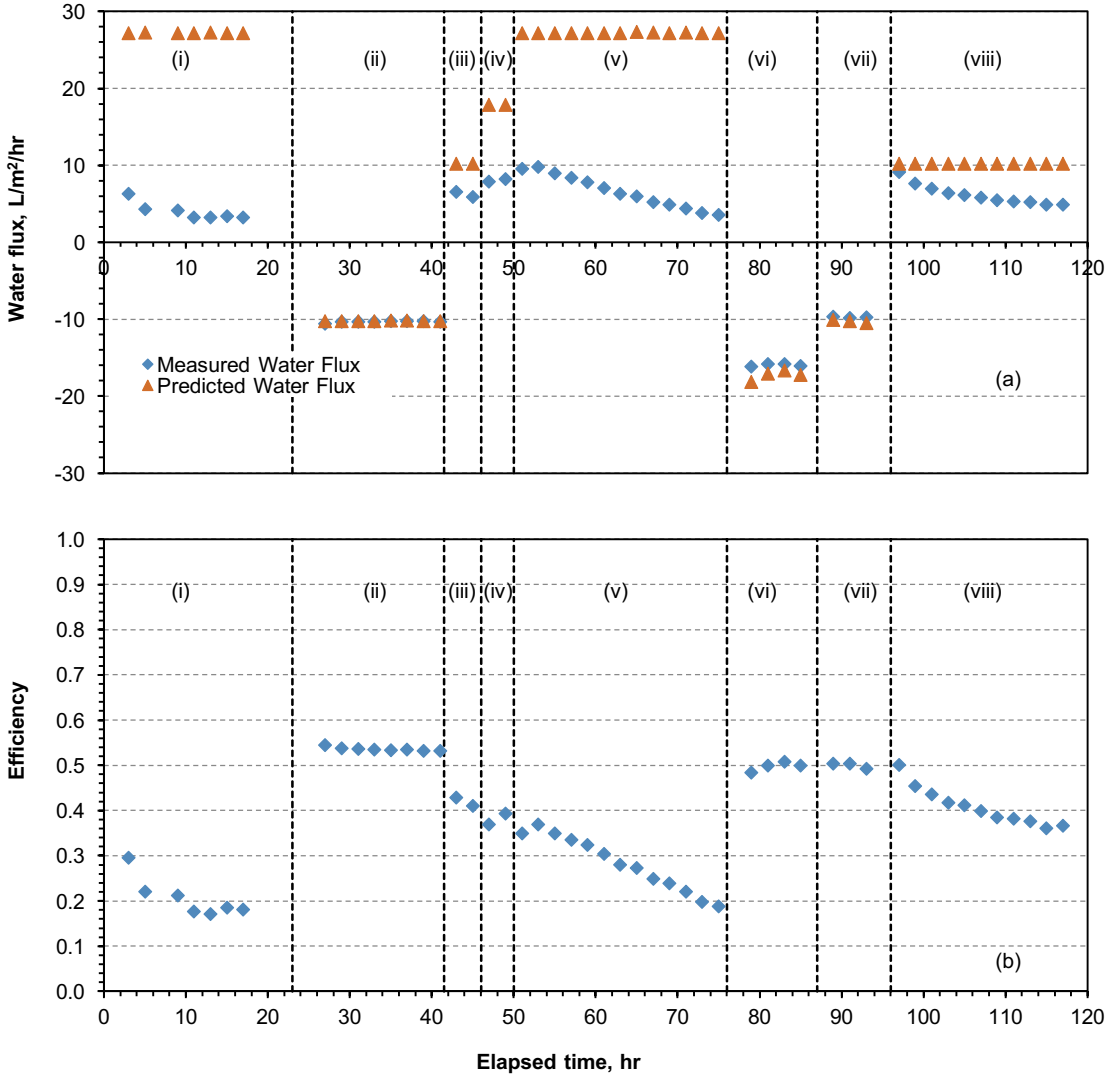

Figure 4.11. Measured and predicted water flux (a) and measured thermal efficiency (b) for membrane previously scaled with solution of 225 mg/L SiO_2 and 150 mg/L Ca^{2+} tested using the original solution over a range of feed and distillate temperatures.

Interestingly, thermal efficiency was consistently higher at lower temperature differences using the original temperature regime (Figure 4.11b, phases iii, iv, and viii), even at the end of the experiment when the membrane was fully scaled. If it is assumed that the silica scale reduces water flux by blocking the membrane pores, this would reduce the effective surface area

available for mass transport without affecting the surface area for heat transport, leading to reduced water flux and thermal efficiency. However, if this were the principle cause of flux decline, it would be expected that similar impacts on both water flux and thermal efficiency would be observed when the direction of water flux is reversed, considering that negligible dissolution and scale removal occurs with this method. Thus, the reduced impacts of silica scale associated with lower feed temperatures observed in Section 4.4.4.1 may not be solely due to reduced scaling rates and propensity, but may also be related to fundamental differences in how silica scale impacts the driving force in MD at different temperatures.

4.4.4.3 Scale cleaning

Previous investigations have reported some removal of silica scaling on MD membranes by applying a high-pH cleaning solution to dissolve the scale [54, 55], but complete removal and restored performance remains elusive. In this study, a different cleaning method is proposed which involved flooding the membrane pores and converting to a MF process. A solution of NaOH maintained at pH 11 was then applied with the direction of water flux through the membrane reversed to promote dissolution at the membrane surface and separation of the scale layer.

Performance during the initial scaling cycle using a solution with initial concentration of 225 mg/L SiO_2, 150 mg/L Ca^{2+}, and pH 7.0 followed similar trends as previous experiments with similar composition (Figure 4.12). After the membrane pores were wetted, water flux was initially almost 1500 L/m^2/hr with a pressure of 50 kPa in reverse MF operation, then steadily declined to 1166 L/m^2/hr after 30 minutes. MD testing using a 1 g/L NaCl solution after the membrane was dried indicated almost complete recovery of water flux and thermal efficiency. Conductivity rejection was unaffected, and was at least 99.9% before and after the reverse MF cleaning process. However, after cleaning and the membrane was tested using a new solution with 225 mg/L SiO_2, 150 mg/L Ca^{2+}, and pH 7.2, initial water flux was substantially lower than that of the new membrane, and both water flux and thermal efficiency rapidly declined with no induction time. Similar to results reported previously, this was likely due to incomplete removal of the scale layer by the reverse MF procedure, and residual silica on the membrane surface provided sites for polymerization. Thus, pore flooding does not appear to improve the efficacy of silica scale cleaning using high-pH solutions.

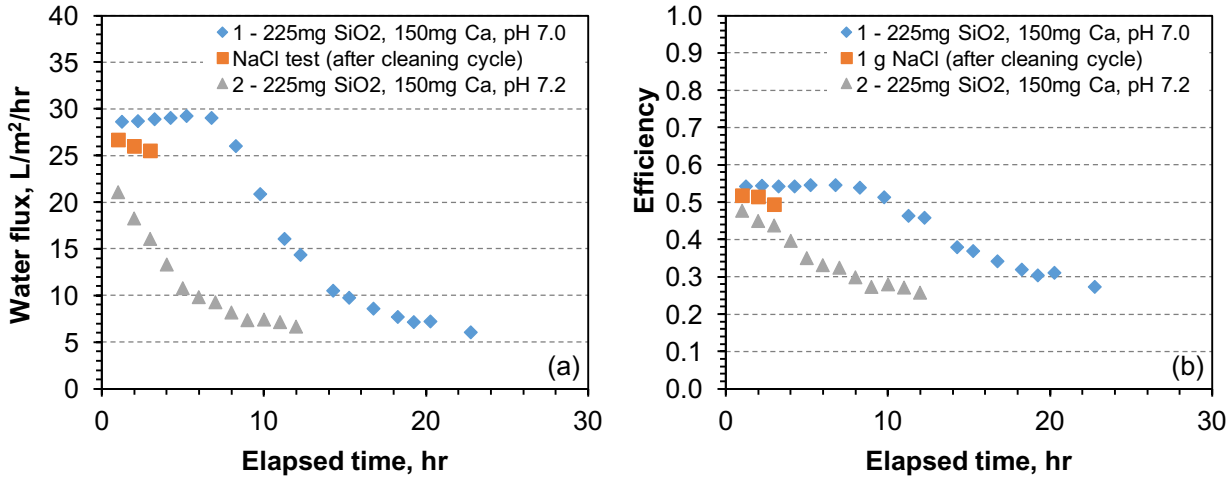

Figure 4.12. Measured water flux (a) and thermal efficiency (b) during initial scaling using solution of 225 mg/L SiO_2 and 150 mg/L Ca^{2+}, integrity test with 1 g/L NaCl solution following reverse MF cleaning, and second scaling cycle of cleaned membranes with new solution prepared with similar solution chemistry as initial scaling cycle. Feed temperature was maintained at constant 60 °C and distillate temperature was maintained at constant 20 °C.

4.5 Conclusion

In this study, the influence of divalent ion concentration, carbonate alkalinity, and pH on scaling behavior of MD membranes was investigated for solutions concentrated above the solubility limit of silica. The presence of calcium and magnesium were both found to shorten induction times of scaling and increased scaling rates, though the effects of calcium were slightly higher than those of magnesium for similar molar concentrations. The effect of calcium on scaling rates was determined to be due to its ability to catalyze and accelerate silica polymerization, and was relatively independent of calcium concentration or degree of silica supersaturation. However, increased carbonate alkalinity tended to mitigate the effects of calcium on scaling rates, likely due to some calcium carbonate precipitation in the system which reduced the concentration of calcium ions, but may also be related to interactions between calcium and bicarbonate and carbonate inhibiting the catalytic effect of calcium on silica polymerization. In contrast, the solubility of magnesium carbonates is higher than the solubility of calcium carbonates, thus carbonate alkalinity did not mitigate the influence of magnesium on silica scaling rates at the concentrations tested in this study.

Operating with reduced feed temperature (and therefore reduced initial water flux) was found to substantially reduce silica scaling rates even at high degrees of silica supersaturation

and presence of calcium. Several factors are proposed to explain this phenomenon, including reduced degree of supersaturation at the membrane surface due to reduced concentration polarization, reduced drag forces drawing silica colloids toward the membrane surface, and the effect of temperature on the kinetics of silica polymerization. Thus, similar to the concept of critical flux that is observed with pressure-driven membrane separation processes, a critical temperature may exist in MD that could be utilized as a strategy to mitigate silica scaling at high concentrations.

4.6 References

[1] A.M.O. Mohamed, M. Maraqa, J. Al Handhaly, Impact of land disposal of reject brine from desalination plants on soil and groundwater, Desalination, 182 (2005) 411-433.

[2] M. Ahmed, W.H. Shayya, D. Hoey, J. Al-Handaly, Brine disposal from reverse osmosis desalination plants in Oman and the United Arab Emirates, Desalination, 133 (2001) 135-147.

[3] J. Zhou, V.W.C. Chang, A.G. Fane, Environmental life cycle assessment of brackish water reverse osmosis desalination for different electricity production models, Energ Environ Sci, 4 (2011) 2267-2278.

[4] M.S. Mohsen, J.O. Jaber, M.D. Afonso, Desalination of brackish water by nanofiltration and reverse osmosis, Desalination, 157 (2003) 167.

[5] M. Uchymiak, A.R. Bartman, N. Daltrophe, M. Weissman, J. Gilron, P.D. Christofides, W.J. Kaiser, Y. Cohen, Brackish water reverse osmosis (BWRO) operation in feed flow reversal mode using an ex situ scale observation detector (EXSOD), Journal of Membrane Science, 341 (2009) 60-66.

[6] L.F. Greenlee, D.F. Lawler, B.D. Freeman, B. Marrot, P. Moulin, Reverse osmosis desalination: Water sources, technology, and today's challenges, Water Research, 43 (2009) 2317-2348.

[7] M. Uchymiak, A. Rahardianto, E. Lyster, J. Glater, Y. Cohen, A novel RO ex situ scale observation detector (EXSOD) for mineral scale characterization and early detection, Journal of Membrane Science, 291 (2007) 86-95.

[8] P. Sanciolo, N. Milne, K. Taylor, M. Mullet, S. Gray, Silica scale mitigation for high recovery reverse osmosis of groundwater for a mining process, Desalination, 340 (2014) 49-58.

[9] N.A. Milne, T. O'Reilly, P. Sanciolo, E. Ostarcevic, M. Beighton, K. Taylor, M. Mullett, A.J. Tarquin, S.R. Gray, Chemistry of silica scale mitigation for RO desalination with particular reference to remote operations, Water Research, 65 (2014) 107-133.

[10] M. Badruzzaman, A. Subramani, J. DeCarolis, W. Pearce, J.G. Jacangelo, Impacts of silica on the sustainable productivity of reverse osmosis membranes treating low-salinity brackish groundwater, Desalination, 279 (2011) 210-218.

[11] W. Den, C.-J. Wang, Removal of silica from brackish water by electrocoagulation pretreatment to prevent fouling of reverse osmosis membranes, Separation and Purification Technology, 59 (2008) 318-325.

[12] R. Sheikholeslami, I.S. Al-Mutaz, S. Tan, S.D. Tan, Some aspects of silica polymerization and fouling and its pretreatment by sodium aluminate, lime and soda ash, Desalination, 150 (2002) 85-92.

[13] T. Koo, Y.J. Lee, R. Sheikholeslami, Silica fouling and cleaning of reverse osmosis membranes, Desalination, 139 (2001) 43-56.

[14] R.K. Iler, The chemistry of silica: solubility, polymerization, colloid and surface properties, and biochemistry, Wiley, 1979.

[15] R. Sheikholeslami, S. Zhou, Performance of RO membranes in silica bearing waters, Desalination, 132 (2000) 337-344.

[16] E. Neofotistou, K.D. Demadis, Use of antiscalants for mitigation of silica (SiO2) fouling and deposition: fundamentals and applications in desalination systems, Desalination, 167 (2004) 257-272.

[17] P.V. Brady, S.J. Altman, L.K. McGrath, J.L. Krumhansl, H.L. Anderson, pH modification for silica control, Desalin Water Treat, 51 (2013) 5901-5908.

[18] R.Y. Ning, A.J. Tarquin, J.E. Balliew, Seawater RO treatment of RO concentrate to extreme silica concentrations, Desalin Water Treat, 22 (2010) 286-291.

[19] H.P. Rothbaum, A.G. Rohde, Kinetics of silica polymerization and deposition from dilute solutions between 5 and 180°C, Journal of Colloid and Interface Science, 71 (1979) 533-559.

[20] R. Sheikholeslami, I.S. Al-Mutaz, T. Koo, A. Young, Pretreatment and the effect of cations and anions on prevention of silica fouling, Desalination, 139 (2001) 83-95.

[21] R. Sheikholeslami, S. Tan, Effects of water quality on silica fouling of desalination plants, Desalination, 126 (1999) 267-280.

[22] J.S. Gill, Inhibition of silica—silicate deposit in industrial waters, Colloids and Surfaces A: Physicochemical and Engineering Aspects, 74 (1993) 101-106.

[23] A. Antony, J.H. Low, S. Gray, A.E. Childress, P. Le-Clech, G. Leslie, Scale formation and control in high pressure membrane water treatment systems: A review, Journal of Membrane Science, 383 (2011) 1-16.

[24] A. Sweity, T.R. Zere, I. David, S. Bason, Y. Oren, Z. Ronen, M. Herzberg, Side effects of antiscalants on biofouling of reverse osmosis membranes in brackish water desalination, Journal of Membrane Science, 481 (2015) 172-187.

[25] J. Minier-Matar, A. Hussain, A. Janson, F. Benyahia, S. Adham, Field evaluation of membrane distillation technologies for desalination of highly saline brines, Desalination, 351 (2014) 101-108.

[26] J.A. Bush, J. Vanneste, T.Y. Cath, Membrane distillation for concentration of hypersaline brines from the Great Salt Lake: Effects of scaling and fouling on performance, efficiency, and salt rejection, Separation and Purification Technology, 170 (2016) 78-91.

[27] K.L. Hickenbottom, T.Y. Cath, Sustainable operation of membrane distillation for enhancement of mineral recovery from hypersaline solutions, Journal of Membrane Science, 454 (2014) 426-435.

[28] G. Chen, X. Yang, Y. Lu, R. Wang, A.G. Fane, Heat transfer intensification and scaling mitigation in bubbling-enhanced membrane distillation for brine concentration, Journal of Membrane Science, 470 (2014) 60-69.

[29] F. He, J. Gilron, K.K. Sirkar, High water recovery in direct contact membrane distillation using a series of cascades, Desalination, 323 (2013) 48-54.

[30] M. Osman, J.J. Schoeman, L. Baratta, Desalination/concentration of reverse osmosis and electrodialysis brines with membrane distillation, Desalin Water Treat, 24 (2010) 293-301.

[31] J.P. Mericq, S. Laborie, C. Cabassud, Vacuum membrane distillation of seawater reverse osmosis brines, Water Res, 44 (2010) 5260-5273.

[32] E. Curcio, X.S. Ji, G. Di Profio, A. Sulaiman, E. Fontananova, E. Drioli, Membrane distillation operated at high seawater concentration factors: Role of the membrane on CaCO3 scaling in presence of humic acid, Journal of Membrane Science, 346 (2010) 263-269.

[33] M. Safavi, T. Mohammadi, High-salinity water desalination using VMD, Chemical Engineering Journal, 149 (2009) 191-195.

[34] D. Qu, J. Wang, B. Fan, Z.K. Luan, D.Y. Hou, Study on concentrating primary reverse osmosis retentate by direct contact membrane distillation, Desalination, 247 (2009) 540-550.

[35] C.R. Martinetti, A.E. Childress, T.Y. Cath, High recovery of concentrated RO brines using forward osmosis and membrane distillation, Journal of Membrane Science, 331 (2009) 31-39.

[36] Y.B. Yun, R.Y. Ma, W.Z. Zhang, A.G. Fane, J.D. Li, Direct contact membrane distillation mechanism for high concentration NaCl solutions, Desalination, 188 (2006) 251-262.

[37] G.Z. Chen, Y.H. Lu, W.B. Krantz, R. Wang, A.G. Fane, Optimization of operating conditions for a continuous membrane distillation crystallization process with zero salty water discharge, Journal of Membrane Science, 450 (2014) 1-11.

[38] F. Edwie, T.-S. Chung, Development of simultaneous membrane distillation–crystallization (SMDC) technology for treatment of saturated brine, Chemical Engineering Science, 98 (2013) 160-172.

[39] G.Q. Guan, R. Wang, F. Wicaksana, X. Yang, A.G. Fane, Analysis of Membrane Distillation Crystallization System for High Salinity Brine Treatment with Zero Discharge Using Aspen Flowsheet Simulation, Ind Eng Chem Res, 51 (2012) 13405-13413.

[40] F. Edwie, T.S. Chung, Development of hollow fiber membranes for water and salt recovery from highly concentrated brine via direct contact membrane distillation and crystallization, Journal of Membrane Science, 421 (2012) 111-123.

[41] C.M. Tun, A.M. Groth, Sustainable integrated membrane contactor process for water reclamation, sodium sulfate salt and energy recovery from industrial effluent, Desalination, 283 (2011) 187-192.

[42] X. Ji, E. Curcio, S. Al Obaidani, G. Di Profio, E. Fontananova, E. Drioli, Membrane distillation-crystallization of seawater reverse osmosis brines, Separation and Purification Technology, 71 (2010) 76-82.

[43] L. Mariah, C.A. Buckley, C.J. Brouckaert, E. Curcio, E. Drioli, D. Jaganyi, D. Ramjugernath, Membrane distillation of concentrated brines - Role of water activities in the evaluation of driving force, Journal of Membrane Science, 280 (2006) 937-947.

[44] C.M. Tun, A.G. Fane, J.T. Matheickal, R. Sheikholeslami, Membrane distillation crystallization of concentrated salts - flux and crystal formation, Journal of Membrane Science, 257 (2005) 144-155.

[45] M. Gryta, Direct contact membrane distillation with crystallization applied to NaCl solutions, Chem Pap-Chem Zvesti, 56 (2002) 14-19.

[46] M. Gryta, Concentration of NaCl solution by membrane distillation integrated with crystallization, Separation Science and Technology, 37 (2002) 3535-3558.

[47] E. Curcio, A. Criscuoli, E. Drioli, Membrane crystallizers, Ind Eng Chem Res, 40 (2001) 2679-2684.

[48] K.W. Lawson, D.R. Lloyd, Membrane distillation, Journal of Membrane Science, 124 (1997) 1-25.

[49] D.M. Warsinger, J. Swaminathan, E. Guillen-Burrieza, H.A. Arafat, J.H. Lienhard V, Scaling and fouling in membrane distillation for desalination applications: A review, Desalination, 356 (2015) 294-313.

[50] L.D. Tijing, Y.C. Woo, J.-S. Choi, S. Lee, S.-H. Kim, H.K. Shon, Fouling and its control in membrane distillation—A review, Journal of Membrane Science, 475 (2015) 215-244.

[51] Y. Ko, Y. Choi, H. Cho, Y. Shin, S. Lee, Comparison of fouling behaviors of hydrophobic microporous membranes in pressure- and temperature-driven separation processes, Desalination, 428 (2018) 264-271.

[52] W. Qin, Z. Xie, D. Ng, Y. Ye, X. Ji, S. Gray, J. Zhang, Comparison of colloidal silica involved fouling behavior in three membrane distillation configurations using PTFE membrane, Water Research, 130 (2018) 343-352.

[53] W. Qin, J. Zhang, Z. Xie, D. Ng, Y. Ye, S.R. Gray, M. Xie, Synergistic effect of combined colloidal and organic fouling in membrane distillation: Measurements and mechanisms, Environmental Science: Water Research & Technology, 3 (2017) 119-127.

[54] J. Gilron, Y. Ladizansky, E. Korin, Silica Fouling in Direct Contact Membrane Distillation, Ind Eng Chem Res, 52 (2013) 10521-10529.

[55] J.A. Bush, J. Vanneste, E.M. Gustafson, C.A. Waechter, D. Jassby, C.S. Turchi, T.Y. Cath, Prevention and management of silica scaling in membrane distillation using pH adjustment, Journal of Membrane Science, 554 (2018) 366-377.

[56] L. Tang, A. Iddya, X. Zhu, A.V. Dudchenko, W. Duan, C. Turchi, J. Vanneste, T.Y. Cath, D. Jassby, Enhanced Flux and Electrochemical Cleaning of Silicate Scaling on Carbon Nanotube-Coated Membrane Distillation Membranes Treating Geothermal Brines, ACS Applied Materials & Interfaces, 9 (2017) 38594-38605.

[57] J. Vanneste, J.A. Bush, K.L. Hickenbottom, C.A. Marks, D. Jassby, C.S. Turchi, T.Y. Cath, Novel thermal efficiency-based model for determination of thermal conductivity of membrane distillation membranes, Journal of Membrane Science, 548 (2018) 298-308.

[58] Y.-N. Wang, C.Y. Tang, Protein fouling of nanofiltration, reverse osmosis, and ultrafiltration membranes—The role of hydrodynamic conditions, solution chemistry, and membrane properties, Journal of Membrane Science, 376 (2011) 275-282.

[59] C.Y. Tang, T.H. Chong, A.G. Fane, Colloidal interactions and fouling of NF and RO membranes: A review, Advances in colloid and interface science, 164 (2011) 126-143.

CHAPTER 5

MEMBRANE DISTILLATION FOR CONCENTRATION OF HYPERSALINE BRINES FROM THE GREAT SALT LAKE: EFFECTS OF SCALING AND FOULING ON PERFORMANCE, EFFICIENCY, AND SALT REJECTION

Modified from an article published in *Separation and Purification Technology*[1]

John A. Bush[2❖], Johan Vanneste[2], Tzahi Y. Cath[2*]

5.1 Abstract

Membrane distillation (MD) is a thermally-driven separation process that utilizes a difference in vapor pressure across a porous, hydrophobic membrane as the driving force. MD may be applied to aqueous systems at concentrations up to and exceeding saturation of both sparingly soluble salts and soluble salts such as sodium chloride (NaCl), leading to potential application in high-recovery desalination processes that approach Zero Liquid Discharge (ZLD) operation, or as a concentration strategy for mineral recovery. Scaling and fouling is a significant risk for such processes, and knowledge of the effects of these phenomena on performance is essential to the evaluation of MD as a viable technology for these applications. The present study investigated the scaling and fouling behavior of a hypersaline brine collected from the North Arm of the Great Salt Lake (GSL), which was nearly saturated with respect to NaCl, and also contained high concentrations of dissolved minerals and organic carbon. Effects on water flux, thermal efficiency, and salt rejection were measured, and membranes used were analyzed before and after testing to evaluate potential causes of these effects. Scaling by NaCl crystallization on the membrane surface limited water recovery to approximately 10%, and also caused damage to the internal pore structure of the membrane when the temperature difference (ΔT) between the feed and distillate was greater than 20 °C. Analysis of the solution chemistry of the GSL water was effective in predicting the scaling tendency of NaCl, but inadequate in predicting the scaling tendency of other salts. Amorphous scaling structures on the membrane surfaces containing

[1]Reprinted with permission of *Separation and Purification Technology*, 170 (2016) 78-91.
[2]Colorado School of Mines, Golden, CO, USA
❖Primary researcher and author
*Corresponding author: email: tcath@mines.edu; phone: (303) 273-3402; fax: (303) 273-3413

magnesium and oxygen were implied as the dominant factors contributing to performance decline at concentrations below NaCl saturation, and the result of fouling due to interactions between organic matter and magnesium. Operation at a maximum water recovery of 8% combined with intermittent reversal of the temperature gradient were effective strategies to prevent both scaling and fouling and maintain long-term performance.

5.2 Introduction

Desalination technologies are increasingly becoming important for the treatment of impaired water for drinking, agriculture, diverse industries, and for environmental protection. Due to increased water demand, technological advancements, and improvements in the cost-competitiveness of desalination, it is currently in a period of rapid growth and is expected to reach a global capacity of 100 million m^3/day in 2015 [1]. Although desalination may be a promising means of meeting fresh water demands in water scarce regions, it is rather energy intensive and produces a hypersaline reject brine that presents an environmental disposal challenge. Concentrated brines from seawater desalination are typically returned to the sea. In the case of inland brackish water desalination, where disposal to seawater is not an option, the brine must be disposed of by other means, including land application, which may adversely impact soil and groundwater [2].

Strategies to reduce the volume of brine generated during desalination could greatly reduce the environmental impact of desalination, particularly if they include mineral recovery from brine and approach a zero liquid discharge (ZLD) operation. These brines may contain minerals of economic importance, which could offset the increased cost of desalination. Naturally occurring hypersaline brines such as the Great Salt Lake (GSL) and the Dead Sea [3] are already utilized commercially for recovery of minerals composed of the most concentrated ions, including sodium, potassium, calcium, magnesium, sulfate, and chloride. Mineral extraction from lower salinity brines has also been explored, including from some geothermal brines [4-6] and desalination brines [7]. Some brines have also attracted interest as a source of higher value minerals such as lithium [8-11]. However, most brines are composed primarily of common salts such as sodium chloride (NaCl), and concentration combined with salt removal is needed before the more valuable minerals can be recovered. This initial concentration is often accomplished using evaporation ponds that require large amounts of land area and time for

evaporation, lose large amounts of water to the atmosphere, and experience seasonal variation in performance due to local climate conditions.

Separation processes that can desalinate water containing very high total dissolved solids (TDS) could potentially increase water recovery while serving as the primary concentration process for mineral recovery, which may improve overall process efficiency and reduce the footprint of combined desalination and mineral recovery operations. However, due to both inherent thermodynamic and physical limitations and high mineral scaling potential, high recovery desalination is difficult to achieve with existing technologies. Thermal desalination such as multi-stage flash distillation (MSF) and multiple-effect distillation (MED) are prone to mineral scaling of heat exchanger surfaces due to the high temperatures involved, and therefore they typically operate in the range of 10-30% water recovery for seawater desalination [12]. Reverse osmosis (RO) may achieve higher recovery, typically about 50% for seawater; however, it is also susceptible to organic and biological fouling [13, 14] and experiences increasing energy demand with recovery due to the increased osmotic pressure of the feed solution as it is concentrated. Moreover, as concentration increases, the hydraulic pressure required to overcome the osmotic pressure eventually exceeds the mechanical limitations of the membranes and modules used, effectively restricting the maximum operating concentration.

Membrane distillation (MD) is a unique membrane process that utilizes a partial vapor pressure difference across a hydrophobic, microporous membrane to induce vapor transport through the membrane pores [15]. The most common configuration, known as direct contact membrane distillation (DCMD), involves both the feed solution and distillate in direct contact with the two membrane surfaces, and vapor pressure difference is established by maintaining the feed solution at a higher temperature than the distillate. In principle, mass transport occurs in the vapor phase only, allowing for the separation of highly purified water from brines containing primarily nonvolatile solutes such as those present in seawater, brackish groundwater, or saline lake water. Because the feed solution and distillate are separated by a vapor phase, the difference in osmotic pressure between the feed and permeate streams does not affect the process; and because the partial vapor pressure of water is only slightly affected by the presence of dissolve ions, very high salinity streams can be desalinated with MD. Only minimal flux decline is observed when using MD to desalinate water having high NaCl concentrations [16-19], and because of this, MD is believed to have great potential as a desalination process for brines,

including concentrates from RO [20-24] and nanofiltration (NF) [25-27], and hypersaline streams such as water from the GSL [28].

The unique capabilities of MD at high salt concentrations have led to interest in its potential for integration with crystallization and mineral recovery in a combined membrane distillation crystallization (MDC) process, and has been effectively demonstrated at the laboratory scale for the recovery of various salts commonly found in natural and industrial brines, including NaCl [25, 29-32], $CaCO_3$ and $MgSO_4$ [25], and Na_2SO_4 [26, 32]. For the most part, efforts to date have used synthetic solutions, which may perform quite differently than natural brines. For example, in an MDC study using RO concentrate from natural seawater, Ji et al. [20] reported reduced transmembrane flux, a 20% reduction of salts crystallized, and a 15-23% reduction in crystal growth rate (compared to artificial concentrates) due to dissolved organic matter.

As in other desalination processes, mineral scaling and organic fouling may be significant problems for MD, and the potential for MDC to become established as a viable treatment strategy is in part dependent on a more comprehensive understanding of crystallization behavior of natural hypersaline brines concentrated with MD. Scaling by sparingly soluble salts such as $CaCO_3$, $CaSO_4$, and silica [33-38] are known to cause substantial flux decline. However, in some cases it has been shown that the scale layer formed on the feed side of MD membranes is relatively porous and does not completely prevent water flux [37] and may be removed with simple cleaning processes [28, 35, 39]. Also, employing management strategies such as periodic flushing of the membrane with DI water [36] or periodic reversal of the driving force, which reverses the direction of water transport [28], can interrupt the crystallization process before sufficient induction time has passed and may mitigate scale formation. While scaling by sparingly soluble salts typically forms on the membrane surface only and does not affect salt rejection, scaling by NaCl on the membrane surface itself has been shown to aggravate pore wetting [29, 39], which reduces water flux due to the loss of driving force and can also reduce salt rejection, and may lead to crystallization inside the pores themselves [30]. Crystallization on membrane surfaces may also affect membrane properties such as surface hydrophobicity and mechanical strength [40].

In this study we investigated scaling and fouling behavior of the MD process applied to the concentration of hypersaline brine obtained from the North Arm of the GSL, which is nearly

saturated with respect to NaCl and contains high concentrations of calcium, magnesium, potassium, sulfate, silica, and natural organic matter. Experiments and analyses were performed to isolate the effects of scaling by the different salts at high concentration factors, to identify dominant scaling and fouling mechanisms, and to characterize the short-term and long-term effects on membrane performance. Strategies for preventing and mitigating these effects were also investigated.

5.3 Mass and heat transfer in MD

Water flux (J) in the MD process is proportional to the vapor pressure difference between the feed and distillate streams [41]:

$$J = C_{\mathrm{m}}\left(p_{\mathrm{f,m}} - p_{\mathrm{d,m}}\right) \tag{5.1}$$

where $p_{\mathrm{f,m}}$ and $p_{\mathrm{d,m}}$ are the vapor pressures of the feed and distillate streams at the membrane surface, respectively, and C_{m} is a mass transfer coefficient that is characteristic of the system. C_{m} is a function of the membrane physical properties (i.e., thickness, porosity, pore size, and pore tortuosity), and the temperature and pressure of the gaseous phase within the pores. In the DCMD configuration, vapor pressure differential is accomplished by maintaining a higher feed stream temperature (T_{f}) than distillate stream temperature (T_{d}). For pure water or very dilute solutions, vapor pressure of water at the membrane surface is a function of the mean membrane temperature (T_{m}) in accordance to the Antoine equation:

$$p = \exp\left(23.238 - \frac{3841}{T_{\mathrm{m}} - 45}\right) \tag{5.2}$$

where $T_{\mathrm{m}} = (T_{\mathrm{f}} + T_{\mathrm{d}})/2$. At relatively low temperature difference between the feed and distillate streams, water flux may be expressed as a function of temperature:

$$J = C_{\mathrm{m}}\,\frac{dp}{dT}\,\Delta T \tag{5.3}$$

where $\Delta T = T_f - T_d$ and with dp/dT approximated using the Clausius-Claperyon relation evaluated at T_m:

$$\left.\frac{dp}{dT}\right|_{T_m} = \frac{p\Delta H_{vap} M}{RT_m^2} \tag{5.4}$$

where ΔH_{vap} is the latent enthalpy of vaporization evaluated at T_m, M is the molecular weight of water, and R is the universal gas constant. From equations (5.2) and (5.4) it can be seen that dp/dT increases with T_m, leading to an exponential relationship between water flux and ΔT.

The driving force in MD is negatively affected by salinity due to the reduction of vapor pressure caused by the presence of dissolved ions, which reduce the water activity of the solution. The associated reduction of water flux can be substantial; theoretical water flux in pure NaCl solutions approaching saturation concentration may be as little as 50% compared to pure water flux for similar operating conditions [42, 43].

Mass transfer in MD is a function of the vapor pressure, and hence the temperature and concentration, at the membrane surface and not the bulk fluid. Heat transfer in the MD process occurs primarily by conduction and by bulk transport as the water vapor carries the energy associated with latent enthalpy of vaporization through the membrane. Both mechanisms of heat transfer contribute to temperature polarization due to the development of a thermal boundary layer between both membrane surfaces and the bulk fluid in each flow channel, resulting in a lower ΔT between the membrane surfaces than the bulk ΔT.

The heat transport associated with mass transport is a necessary consequence of the process; however, the conductive heat transfer does not serve a useful purpose and is considered a loss. Thermal efficiency (η_{th}) of the MD process is defined as the ratio of heat transfer associated with mass transfer to the total heat transfer [44]:

$$\eta_{th} = \frac{Q_{vap}}{Q_{vap} + Q_{cond}} \tag{5.5}$$

where Q_{vap} is the heat transfer resulting from the vapor transport across the membrane and Q_{cond} is the heat transfer due to conduction through the membrane.

Thermal efficiency is primarily considered a property of the membrane; however, increasing ΔT increases thermal efficiency [42], as does increasing T_m for similar ΔT. This is because the driving force and water flux increase exponentially with ΔT whereas the conduction heat transfer rate increases linearly with ΔT. Experimentally, thermal efficiency may be measured if temperature of the water and the flow rates at the inlets and outlets of the flow channels are known. Because energy is conserved, the total heat transfer across the membrane is equal to the enthalpy change between the inlet and outlet of either the feed or distillate stream. To minimize the error due to heat loss through the flow cell, thermal efficiency in this study was calculated using the enthalpy change of the distillate stream, as expressed in the following:

$$\eta_{th} = \frac{\dot{m}_m \Delta H_{vap}}{c_p[(\dot{m}_d + \dot{m}_m)T_{d,out} - \dot{m}_d T_{d,in}]} \tag{5.6}$$

where $\dot{m}_m$ is the mass flow rate of water vapor through the membrane, $\dot{m}_d$ is the mass flow rate of the distillate stream, $T_{d,in}$ and $T_{d,out}$ are the distillate temperature at the inlet and outlet of the channel, respectively, and c_p is the constant-pressure specific heat of pure water.

Because mass transfer occurs in the vapor phase, MD provides very high rejection of nonvolatile solutes; however, solute transport can and does still occur if liquid water floods the membrane pores. In this case, it is assumed that the membrane does not selectively reject dissolved solids due to the large pore size; therefore, solute rejection may be calculated using the change in volume and conductivity of the distillate and feed streams over time:

$$\text{Salt rejection}(\%) = \left(1 - \frac{V_{d2}\sigma_{d2} - V_{d1}\sigma_{d1}}{(V_{d2} - V_{d1})\,\sigma_f}\right) \times 100 \tag{5.7}$$

where σ_f and σ_d are the conductivities of the feed and distillate solutions, and V_{d1} and V_{d2} represent the total volume of the distillate system at times 1 and 2 across a time interval.

5.4 Materials and Methods

5.4.1 Solution chemistry and analytical methods

Concentration and scaling experiments were performed primarily with brine collected from the North Arm of the GSL as the feed solution, and deionized water as the distillate stream.

Additional experiments were performed with synthetic solutions of ACS grade NaCl for comparison with the results from the GSL brine experiments. The raw GSL brine was pre-filtered through a 0.5 micron cartridge filter to remove suspended solids, and analyzed for dissolved solids according to Standard Methods [45]. Alkalinity was determined with a digital titrator test kit (Model 16900-01, Hach Co., Loveland, CO) using 1.6 N H_2SO_4 as titrant. Total organic carbon was determined using the combustion catalytic oxidation method (Model TOC-L, Shimadzu Corp., Kyoto, Japan). Water samples were diluted and filtered through a 0.45 micron filter and analyzed for anions with an ion chromatograph (Model ICS-90, Dionex, Sunnyvale, CA) and for cations with an inductively coupled plasma atomic emission spectrometer (ICS-AES) (Optima 5300 DV, PerkinElmer Inc., Waltham, MA).

OLI Stream Analyzer (OLI systems Inc., Cedar Knolls, NJ) was used to estimate the scaling tendency of the GSL brine at increased concentration. Stream Analyzer utilizes the OLI aqueous thermodynamic engine, and calculates scaling tendency as the ratio of the solution solubility product to the thermodynamic limit based on the thermodynamic equilibrium constant, also known as the saturation ratio.

5.4.2 Membranes and modules

Hydrophobic, microporous membrane acquired from GE Water (Minnetonka, MN) was tested in this study. The membrane used is a symmetric, isotropic membrane made from polypropylene, and have a nominal pore size of 0.22 μm, porosity of approximately 70%, thickness of approximately 150 μm, and a pure water contact angle of 122°. Two different flow cells were used in the investigation, both made of acrylic plastic. Cell 1 was a SEPA cell modified for DCMD operation, and Cell 2 was a custom-made flow cell fitted with a glass window on the feed side to allow observation of the membrane surface during experiments. Spacers were used in both the feed and distillate channels of the cell with a filament diameter of 2.3 mm, mesh length of 16 mm, mesh width of 10.8 mm, and hydrodynamic angle of 70°. Each flow cell was fitted with four Type-T thermocouples, located at the inlets and outlets of the feed and distillate channels.

The physical dimensions of the flow cell channels are summarized in Table 5.1, where membrane surface area, A_s is equal to the length l multiplied by the width w of the flow channel. Hydraulic diameter D_H for a spacer-filled channel is defined as [46]:

$$D_H = \frac{4\varepsilon}{\frac{2}{h}+(1-\varepsilon)S_{V,SP}} \tag{5.8}$$

where ε is the spacer porosity and $S_{V,SP}$ is the specific surface area of the spacer:

$$\varepsilon = 1 - V_{SP}/V_{\text{tot}} \tag{5.9}$$

$$S_{V,SP} = \frac{S_{SP}}{V_{SP}} = \frac{\pi[Dl]_{\text{filament}}}{\frac{\pi}{4}[D^2 l]_{\text{filament}}} = \frac{4}{D_{\text{filament}}} \tag{5.10}$$

Effective cross-section flow area of the channel is defined as:

$$A_{\text{c,eff}} = hw\varepsilon \tag{5.11}$$

Table 5.1. Physical dimensions of experimental flow cell channels. Cell 1 was a SEPA Cell modified for DCMD, Cell 2 was a custom-made flow cell fitted with a glass observation window on the feed side.

Cell	*Flow channel length* l (mm)	*Flow channel width* w (mm)	*Flow channel height* h (mm)	*Membrane surface area* A_s (cm^2)	*Channel cross section* $A_{\text{c,eff}}$ (cm^2)	*Channel hydraulic diameter* D_H (cm)
1	145	94	2.5	136	1.979	0.2758
2	212	40	3	85	1.042	0.3413

5.4.3 Bench-scale system description

An automated, closed-loop, bench-scale membrane testing system was used to evaluate the performance of the membranes in the DCMD process. Data acquisition and system controls were accomplished using LabVIEW (National Instruments, Austin, TX) software on a Windows PC using a DAC device (Model U6, LabJack Corporation, Lakewood, CO). A detailed schematic of the experimental system is presented in Figure 5.1.

The MD system provided heating and cooling to both feed and distillate streams, which were pumped continuously during operation using positive-displacement gear pumps (Micropump Integral Series, IDEX Corp. Vancouver, WA). The feed solution was heated directly using a 1500 W electric immersion heater (Model 1019, Hotwatt, Danvers, MA). Heat exchangers supplied with hot and cold glycol solutions were used to control the temperature of

the distillate. Feed solution temperature was maintained by intermittent operation of the electric heater and distillate temperature was maintained by adjusting the flow rates of the glycol solutions using proportional valves. Heater duty cycle and valve position were controlled using a PID algorithm in the LabVIEW code with the feed temperature (T_f) and distillate temperature (T_d) as process variables, both measured at the inlet of the flow cell. For experiments involving reversal of the temperature gradient, an additional heat exchanger installed in the feed loop was supplied with the cold glycol solution to maintain the desired temperature of the feed solution.

Conductivity of both the feed and distillate solutions were continuously monitored and recorded to estimate the concentration of the feed solution and to calculate salt rejection by the membrane. Feed conductivity was monitored using a toroidal sensor (Model TCSMA, Sensorex, Garden Grove, CA) and conductivity of the distillate was monitored using a dip style conductivity probe (Model T-35820-62, Cole-Parmer, Vernon Hills, IL) installed in the return line.

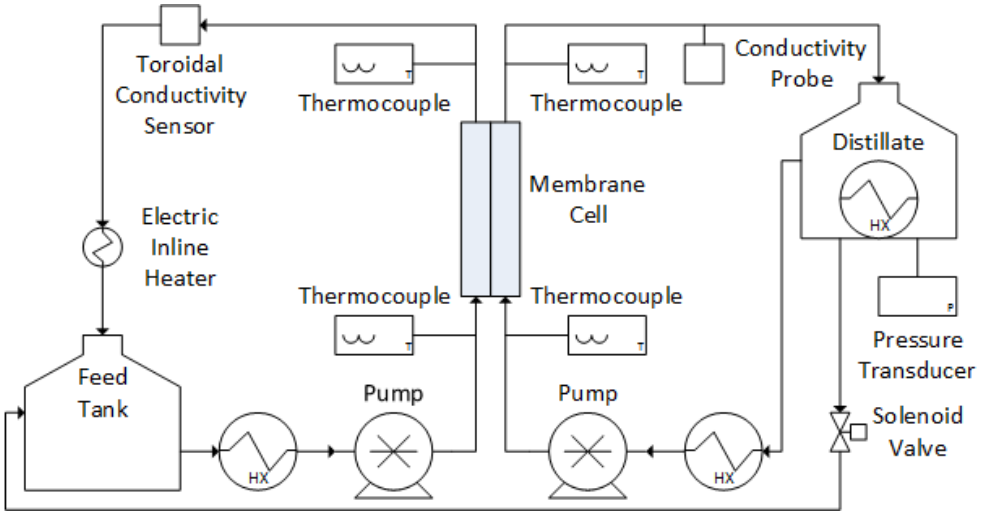

Figure 5.1. Flow schematic of the bench-scale MD system used in the study. Feed and distillate streams were recirculated on their respective closed loop at 1.6 L/min. Accumulated distillate was intermittently returned to the feed tank through a bypass line. Temperatures were measured at the inlets and outlets of the membrane test cell and were used to both monitor and control the streams temperatures.

Water flux was calculated using the measured change in mass of the distillate in a cylindrical acrylic tank, which was equipped with a pressure transducer installed near the bottom of the tank to measure the height of the water column. The distillate tank was also fitted with a

solenoid valve connected to a return line to the feed tank, allowing the collected distillate to be periodically drained back to the feed tank during operation.

5.4.4 Membrane performance experiments

For each set of experiments, a new membrane coupon was cut from dry flat sheets and installed into the membrane cell. The feed and distillate solutions were then pumped through the system at the desired flow rate and adjusted to the desired temperature. During the warm-up period the initial concentration was maintained constant by returning any collected distillate to the feed tank. All experiments were performed using co-current flow to minimize local pressure differential across the membrane at the channel entrances and exits due to pressure drop through the channels. For all experiments, both feed and distillate flow rates were kept constant at 1.6 L min^{-1}, corresponding to a bulk channel velocity of 13 cm s^{-1} for Cell 1 and 25 cm s^{-1} for Cell 2, based on the effective cross-section flow area, $A_{c,eff}$.

5.4.4.1 Baseline performance experiments

To establish a reference for comparison with brine concentration, experiments were performed using a dilute solution of NaCl. The NaCl was added at a low concentration to determine salt rejection without substantially affecting water flux. These experiments used 3 L of 1 g L^{-1} NaCl for the feed, and 3 L of deionized water for the initial distillate stream. Both flow cells were tested with T_f of 30 °C to 70 °C and T_d of 20 °C or 30 °C.

5.4.4.2 NaCl concentration and scaling experiments

Experiments were performed with synthetic solutions to characterize the effects of feed concentration and scaling by pure NaCl on the performance and durability of the membrane in the absence of other fouling agents. These experiments used Cell 1 and 4 L of a 200 g L^{-1} NaCl solution maintained at either 50 °C or 70 °C, concentrated with the distillate maintained at constant 30 °C until water flux ceased due to scaling of the membrane surface or the conductivity of the distillate exceeded 2000 μS cm^{-1} due to wetting of the membrane pores. Once either of these conditions occurred, the collected distillate was returned to the feed tank to dilute the solution to its initial concentration. This concentration and dilution cycle was repeated four times over the course of each experiment.

5.4.4.3 North Arm GSL concentration and scaling experiments

Performance and limitations of the MD process for the concentration of North Arm GSL brine were investigated with a series of experiments. Scaling behavior at high concentration, and the effects of scaling and fouling on long-term performance were also investigated. Initial concentration experiments were conducted with T_f of 50 °C and T_d of 30 °C until water flux ceased due to scaling to determine the practical limit of water recovery. These experiments were performed using Cell 2 to allow observation of scaling behavior using an optical microscope during the process.

Various scaling and fouling behaviors and long-term effects on performance were evaluated by repeated scaling and dilution cycles at different operating temperatures and water recovery. To investigate the effects of scaling of the membrane at high concentration factors, a series of experiments were performed using Cell 1 with constant T_f of 50 °C or 70 °C and constant T_d of 30 °C. Concentration was allowed to proceed until severe scaling reduced the water flux to below 50% of the initial rate before the collected distillate was returned to the feed tank to dilute the brine to its original concentration. Potential scaling and fouling behavior by contaminants other than NaCl were investigated by repeated concentration cycles with water recovery limited to 8%. These experiments were performed using Cell 2 with constant T_f of 50 °C and constant T_d of 30 °C.

A recent study found that intermittent reversal of the temperature gradient is an effective method to mitigate gradual flux decline in a DCMD process for the concentration of South Arm GSL brine [28], which has a similar composition as the North Arm GSL brine although at much lower concentrations. The effectiveness of this method was tested in the present study by first concentrating the North Arm GSL brine at T_f of 50 °C with T_d of 30 °C using Cell 2. Once 8% recovery was reached, the collected distillate was returned to the feed tank. However, before each subsequent concentration cycle the feed was temporarily changed to a separate feed source of GSL brine maintained at 20 °C while continuing to maintain the distillate temperature at 30 °C. Two different approaches to this method were tested: reverse temperature operation for a fixed time period of 5 minutes between each concentration cycle, and reverse temperature operation for a variable time period until stable reverse water flux was observed.

5.4.5 Membrane characterization

Upon completion of scaling experiments, the membranes were removed from the flow cells, air dried, and stored for further analysis. Characterization of the surface scale layer morphology and composition were accomplished using low-vacuum scanning electron microscopy (SEM) and energy dispersive x-ray spectroscopy (EDS) (Quanta 600, FEI Corp., Hillsboro, OR). The effects of the process on membrane structure and salt penetration were also investigated by observing the membrane cross-section at various locations. To ensure that the cutting process did not damage the internal structure of the membrane, an ethanol cryofracture procedure was utilized to produce the membrane samples for cross-section analysis. The membranes were first submerged in ethanol until the membrane and pores were completely flooded. The samples were then submerged in liquid nitrogen and cut with a razor blade, then removed from the liquid nitrogen and dried. All samples analyzed with the SEM were prepared with a gold sputtering using ionized argon gas.

Contact angle was measured after experiments were completed to investigate the effects on membrane hydrophobicity using the sessile drop method. Each membrane sample was prepared by taping flat to a microscope slide and analyzed using a Standard Goniometer (Model 200-00, Ramé-Hart Instrument, CO, Succasunna, NJ). Five 100 μL drops of pure water were then placed on different locations of the sample, and 10 measurements were taken of each drop to determine an overall contact angle for the sample.

5.5 Results and Discussion

5.5.1 Brine characterization

The water of the GSL is a concentrated brine containing primarily sodium, potassium, magnesium, chloride, and sulfate ions with low alkalinity [47]. The primary sources of the GSL, a terminal lake that has no outlet other than evaporation, are rivers, precipitation, and hydrothermal springs. Due to its large size, shallow depth, and location in an arid climate, its size and composition fluctuate considerably with changes in precipitation and inflow. The completion of the Southern Pacific Railroad (SPRR) causeway in 1959 effectively divided the lake into two distinct sections, referred to as the North Arm and the South Arm [48]. Because the causeway severely inhibits mixing between the two sections, and the fact that more than 90% of the total freshwater inflow is received by the South Arm, the North Arm is considerably more

concentrated than the South Arm, and has remained at or very close to saturation since 1960 [49]. The lake sediments contain substantial amounts of $CaCO_3$, and the concentration of calcium in the lake remains more or less constant despite fluctuations in the lake inflow due to precipitation and dissolution of carbonate species [50].

The water collected for use in the present study was found to contain dissolved inorganic constituents typical of North Arm GSL brine and was also high in organic matter (Table 5.2). At standard temperature of 25 °C and 1 atm pressure, the OLI simulation determined the GSL brine to be supersaturated with respect to silica and $CaCO_3$, and very close to saturation concentration of NaCl. The predicted concentration factor to reach NaCl saturation was 1.05 at 25 °C, increasing to 1.07 and 1.10 for 50 °C and 70 °C, respectively. Silica solubility increases with temperature and was found to exist below saturation at elevated temperature. Other salts with potential for scaling were $CaSO_4$ (anhydrite), gypsum, $Mg(OH)_2$, and $MgCO_3$, particularly at elevated temperatures.

Table 5.2. Composition of the brine from the North Arm of the Great Salt Lake.

Composition	Concentration (mg/L)
Lithium, Li^+	43.6
Sodium, Na^+	100,816
Potassium, K^+	5517
Calcium, Ca^{2+}	352
Magnesium, Mg^{2+}	9381
Strontium, Sr^{2+}	3.26
Chloride, Cl^-	181,940
Bromide, Br^-	127
Sulfate, SO_4^{2-}	19,727
Boron, B	25.3
Silica, SiO_2	102
Alkalinity (as $CaCO_3$)	278
Total dissolved solids	344,000
Total organic carbon (TOC)	87.1
pH	7.31

5.5.2 Baseline performance

Water flux and thermal efficiency as a function of the difference between the bulk feed and distillate temperature (ΔT) are shown in Figure 5.2 for the two different flow cells and distillate temperature (T_d) of 20 °C or 30 °C. For most of the operating conditions tested,

particularly at higher ΔT, measured flux was slightly higher for the Cell 1 than Cell 2 and thermal efficiency was slightly lower. In all cases, water flux increased exponentially with ΔT, and measured values were similar to those reported in a previous study using the same membrane in a similar configuration [28]. As expected per the discussion in Section 5.3 regarding the relationship between dP/dT and T_m, the exponential relationship between ΔT and water flux was more pronounced at T_d of 30 °C. Thermal efficiencies were also higher with T_d of 30 °C for similar ΔT. Calculated salt rejection was greater than 99.8% for all operating conditions.

The differences in performance between the two flow cells may be a result of reduced temperature polarization effects in Cell 2 at the experimental flow rate, due to its smaller flow area and increased crossflow velocity. Reynolds numbers were substantially larger at increased temperatures due to the reduced viscosity of the feed water, and were 600-1100 for Cell 1 and 1000-1800 for Cell 2. The lower thermal efficiencies in Cell 2 for similar conditions were unexpected because thermal efficiency generally increases with flow velocity [42].

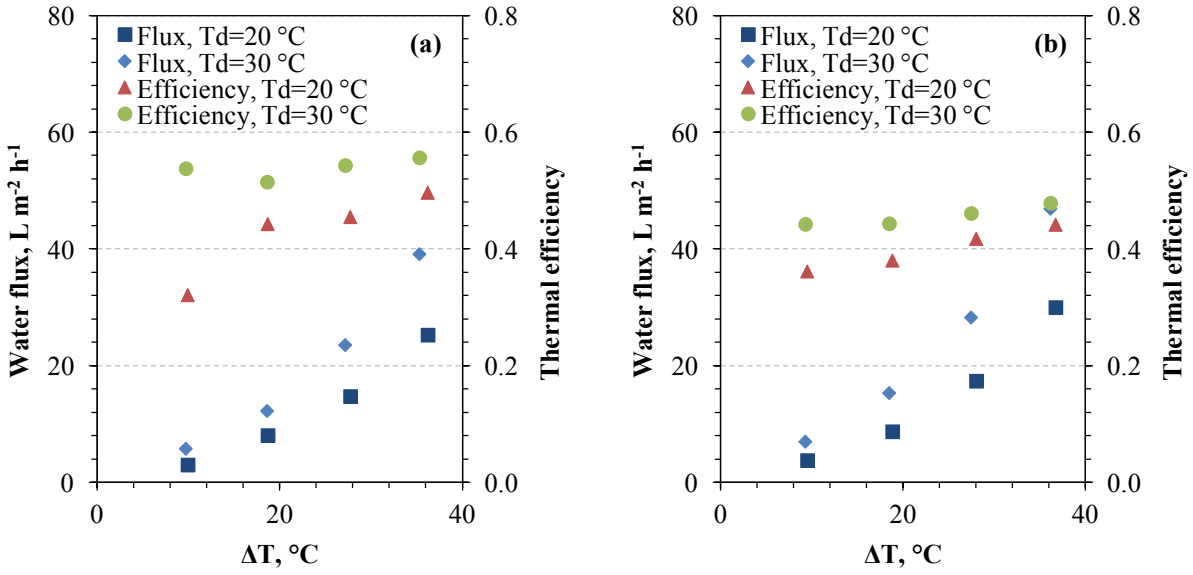

Figure 5.2. Measured water flux and thermal efficiency for (a) Cell 1 and (b) Cell 2 tested with 1 g/L NaCl feed solution and deionized water distillate stream. Feed temperatures (T_f) of 30-70 °C and distillate temperatures (T_d) of 20-30 °C were measured at the channel inlets. Flow rates for both feed and distillate were 1.6 L min^{-1} using co-current flow configuration, corresponding to cross-flow velocity of 13 cm s^{-1} for Cell 1 and 25 cm s^{-1} for Cell 2.

5.5.3 Effects of scaling with pure NaCl

To characterize the effects of NaCl scaling on the membrane used in this study, a solution of 200 g L^{-1} NaCl was concentrated using Cell 1 until water flux ceased due to scaling of the membrane surface, which was visible during testing due to the transparency of the acrylic flow cells used. Because thermal efficiency increases with overall temperature (Figure 5.2), the NaCl concentration experiments were performed with constant T_d of 30 °C and constant T_f of 50 °C or 70 °C. During these experiments, the solution was concentrated, then diluted by returning the collected distillate back to the feed tank, then concentrated again for a total of four concentration cycles.

Both water flux and thermal efficiency were very consistent over multiple concentration cycles for experiments performed with T_f of 50 °C, as depicted in Figure 5.3a. Water flux at feed concentration of 200 g L^{-1} NaCl was approximately 10 L m^{-2} h^{-1}, even after multiple scaling events—close to 82% of the water flux when operating with deionized water feed at similar conditions. Water flux declined steadily to ~7.5 L m^{-2} h^{-1} over the course of each cycle up to a feed concentration of approximately 330 g L^{-1}, or close to 62% of the water flux when operating with deionized water feed at similar conditions. No scaling was observed below a concentration of 330 g L^{-1} and salt rejection remained higher than 99.9% throughout all concentration cycles. Therefore, it can be concluded that the decline in water flux was due to the effects of reduced water activity at increased salinity. Above 330 g L^{-1} NaCl feed concentration the water flux declined rapidly to zero as a result of membrane scaling.

Curiously, thermal efficiency was not strongly affected by the increased concentration, and the measured thermal efficiency of ~54% at 200 g L^{-1} was similar to the measured efficiency during experiments with deionized water as feed, and declined to ~48% before rapidly declining to almost zero due to scaling (Figure 5.4a). The decline in efficiency observed in the present study is less than the theoretical efficiency decline from 50% to 40% over a similar concentration range predicted by Al-Obaidani et al. [42]; however, the membranes used in their study had lower thermal efficiency than the membranes used in the present study. Thermal efficiency is a function of the ratio between latent heat transfer and conduction heat transfer through the membrane; low thermal efficiency is a result of relatively high conduction heat transfer, which is independent of the properties of the water. On the other hand, the reduction in water flux due to reduced water activity at high salinity is independent of the membrane properties. For these

reasons, it can be seen from Equation (5.5) that the effect of concentration on thermal efficiency will always be proportionally lower than the effect on water flux, although the effect will be more pronounced for membranes with low efficiency compared to those with higher efficiency. These trends are similar for the drop in thermal efficiency due to scaling/fouling unless these processes also affect the thermal conductivity of the membrane.

Performance at increased ΔT was less consistent after multiple concentration and scaling cycles, as illustrated in Figure 5.3b. Initial water flux at 200 g L^{-1} NaCl feed concentration was approximately 35 L m^{-2} h^{-1}, which is close to 90% of the water flux when operating with deionized water as feed at similar conditions. No scaling or loss of salt rejection was observed during the first concentration cycle up to a concentration of 310 g L^{-1}, and steady flux decline was observed as concentration increased due to the reduced driving force. Above 310 g L^{-1} the water flux declined sharply as NaCl was observed to crystallize on the membrane surface. Water flux recovered with dilution to the initial feed concentration after scaling for the first three cycles, but the onset of rapid decline occurred at a lower feed concentration with each additional concentration cycle. Finally, water flux was noticeably reduced even with dilution during the fourth concentration cycle. This additional decline in water flux coincided with a more severe decline in thermal efficiency with each additional concentration cycle (Figure 5.4b). In addition, progressive decline in salt rejection occurred with each concentration cycle, with a minimum measured salt rejection of 99.4%, 96.9%, 92.4%, and 91.1% for cycles 1 through 4, occurring at the maximum concentration of each cycle. However, salt rejection recovered to 99.4% or higher when the solution was diluted back to its initial concentration of 200 g L^{-1}.

For both conditions tested the scale layer formed during concentration was observed to dissolve upon dilution of the feed solution to its original concentration. Cross-section SEM micrographs of both membranes revealed enlarged pores in the membrane structure (Figure 5.5), although the depth and extent of the damage was greater for the membrane tested with T_f of 70 °C (Figure 5.5c) than 50 °C (Figure 5.5b). Both membranes also experienced a loss of hydrophobicity, although much more so with T_f of 70 °C, which resulted in a contact angle of only 38.5° compared to 88.5° for the membranes tested with T_f of 50 °C. The membranes tested with the T_f of 70 °C also showed evidence of residual NaCl crystals embedded throughout the membrane, visible as bright spots in the SEM micrographs (Figure 5.5c).

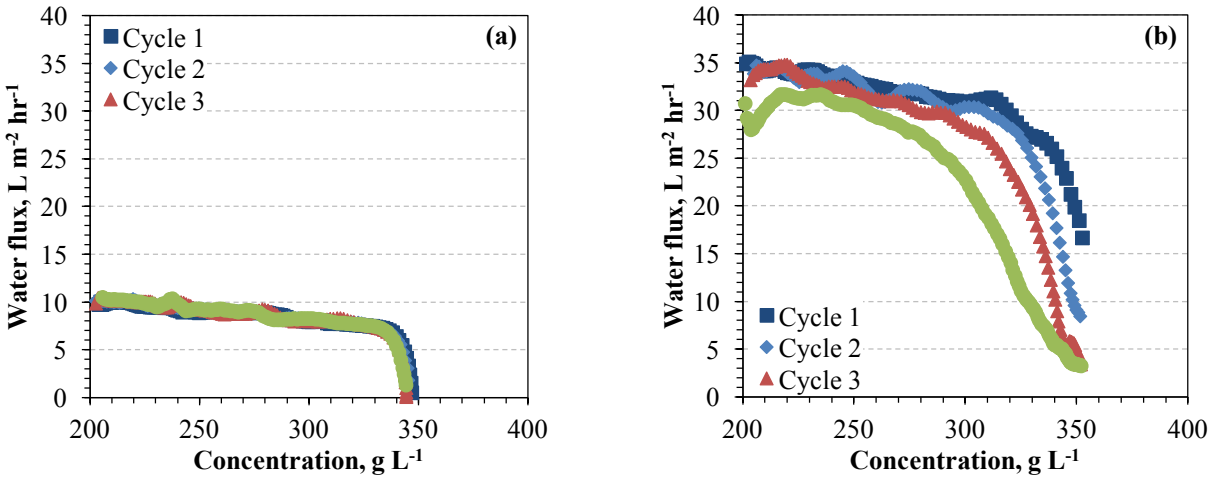

Figure 5.3. Water flux using feed solution with initial concentration of 200 g L^{-1} NaCl with constant T_d of 30 °C and constant T_f of (a) 50 °C and (b) 70 °C. Both feed and distillate flow rates were 1.6 L min^{-1} in co-current flow configuration, using Cell 1. Four concentration cycles were performed, during which the NaCl solution was concentrated until water flux ceased due to scaling, or the conductivity of distillate exceeded 2000 µS cm^{-1}. After each concentration cycle the solution was diluted to original concentration.

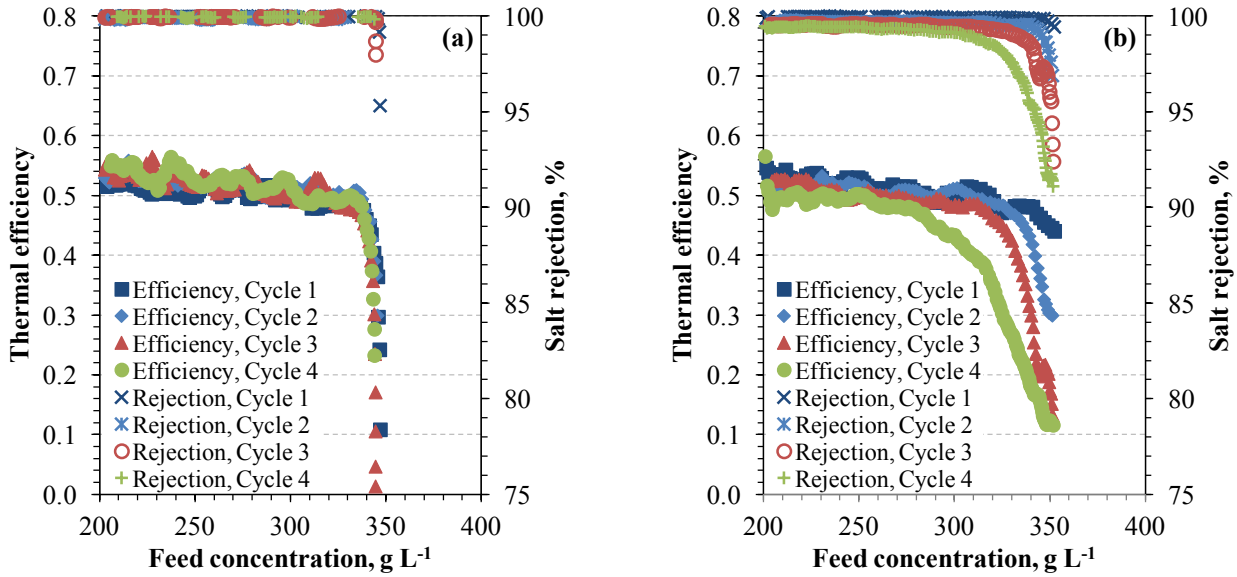

Figure 5.4. Thermal efficiency and salt rejection for the experimental results presented in Fig. 5.3. Feed solution with initial concentration of 200 g L^{-1} NaCl, constant T_d of 30 °C, and constant T_f of (a) 50 °C and (b) 70 °C.

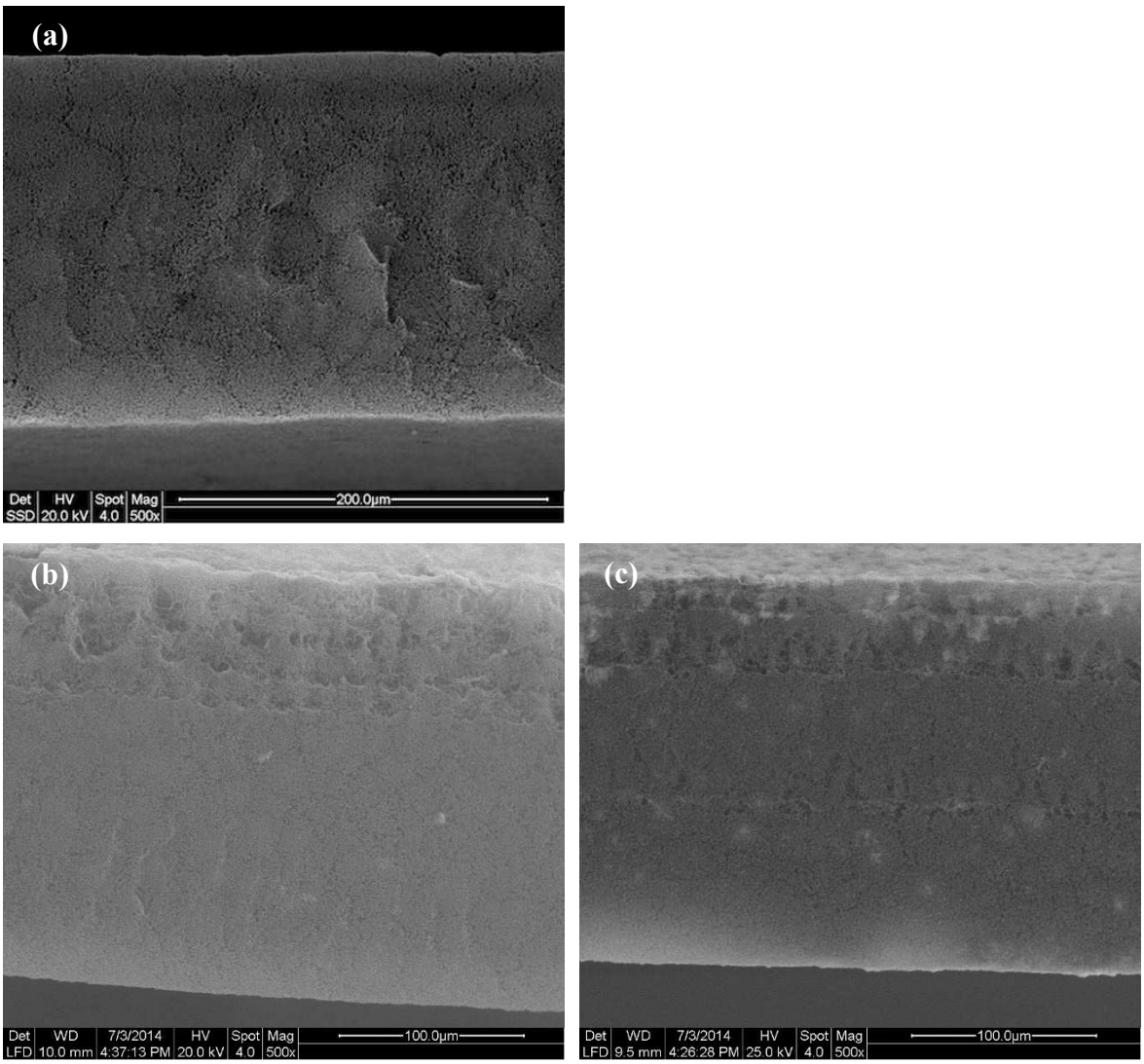

Figure 5.5. Cross-section SEM micrographs of (a) virgin membrane and (b, c) membranes used with 200 g L^{-1} NaCl solution concentrated to the point of scaling, then diluted to the original 200 g L^{-1}, then concentrated again for a total of four scaling cycles. Distillate temperature was constant at 30 °C and feed temperature was constant at (b) 50 °C and (b) 70 °C. Flow rates for both feed and distillate were 1.6 L min^{-1} in co-current configuration using Cell 1. The side of the membrane in contact with the feed solution during experiments is towards the top of the images, where enlarged pores due to damage by NaCl crystallization are seen. Bright spots inside the membrane structure were revealed by EDS analysis to be NaCl deposits.

These results suggest that the liquid-vapor interface likely penetrated the membrane in both cases, leading to salt crystallization inside the membrane itself, but that the resulting changes in surface hydrophobicity or membrane pore structure does not necessarily affect performance. Complete pore flooding was only a significant factor for experiments conducted with T_f of 70 °C. Increased NaCl scaling tendency and pore flooding at high ΔT has been reported in previous MD studies [30, 32], and results from the increase in concentration polarization that occurs with increased water flux. Because NaCl dissolves easily at concentrations below saturation, and performance was completely restored with each dilution cycle for experiments performed with T_f of 50 °C, the loss of effective membrane surface area due to wetting is likely the cause of performance decline below bulk concentration of 320 g L^{-1} for experiments conducted with T_f of 70 °C.

5.5.4 Effects of scaling with North Arm GSL water

5.5.4.1 Single batch concentration

The performance and limitations of the MD process applied to the GSL brine was initially determined by concentrating the brine at T_f of 50 °C and T_f of 30 °C. Water flux and concentration factor of the feed as a function of time are shown in Figure 5.6a. Initial water flux was 8.3 L m^{-2} h^{-1}, or 55% of the water flux when operating with deionized water as feed at similar conditions. Water flux declined by an additional 3% as the concentration factor increased to approximately 1.08, which is slightly higher than the NaCl saturation concentration factor of 1.07. As concentration increased the water flux sharply declined over a period of almost 3 hours. This rapid decline and ultimate termination of water flux coincided with a visible scale layer that formed on the membrane surface once the concentration factor exceeded 1.11. No increase in conductivity in the distillate was observed over the duration of the experiment, indicating complete rejection of dissolved salts.

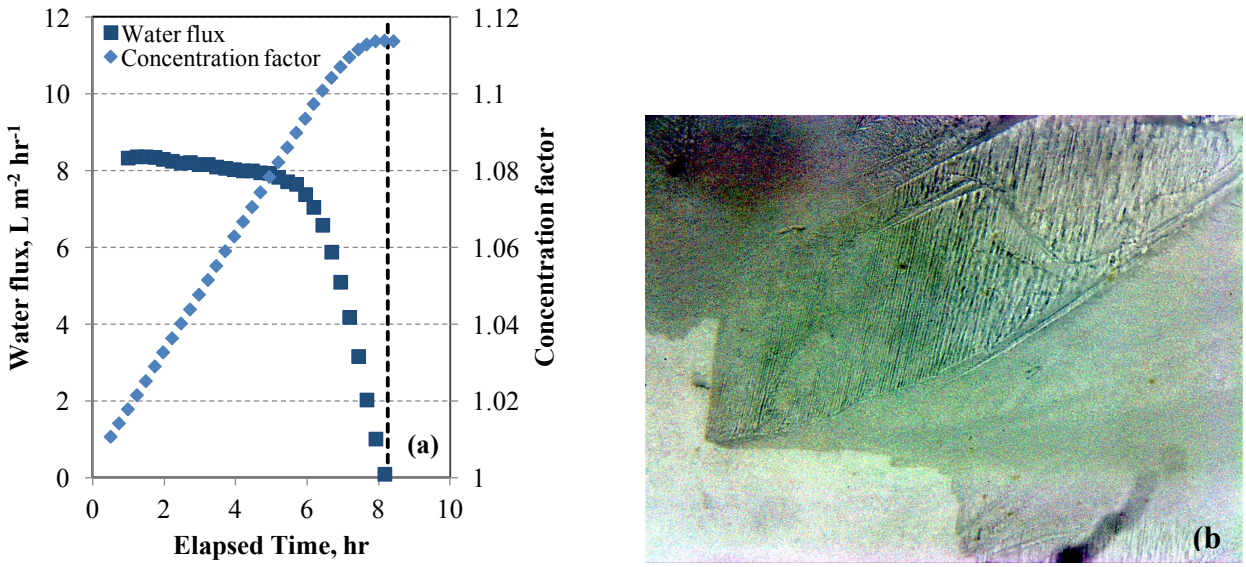

Figure 5.6. (a) Water flux and concentration factor as a function of time for the experiment conducted with GSL brine feed at a constant temperature of 50 °C and with distillate temperature of 30 °C. Flow rates for both feed and distillate were 1.6 L min^{-1} in co-current configuration using Cell 2. (b) Optical micrograph showing scale layer on membrane surface taken at the point of maximum concentration. Vertical dashed line on plot (a) indicates the time during experiment that image (b) was recorded.

The scale layer observed using optical microscopy appeared as a continuous sheet with cubic morphology characteristic of NaCl, and no additional nucleation sites on the membrane surface were visible within the field of view (Figure 5.6b). The morphology, timing of occurrence, and similar effect on performance as occurred during the pure NaCl experiments suggest that the observed scale layer was composed primarily of NaCl, which crystallizes readily despite the presence of impurities [51]. Also, because NaCl solubility increases with temperature [52], the scaling tendency is likely to be higher at the membrane surface than the bulk solution.

5.5.4.2 Effect of multiple scaling cycles with North Arm GSL brine

To investigate the effects of concentration and scaling on long term performance, repeated concentration and dilution cycles were performed using the GSL brine. Feed temperature for these experiments were constant at 50 °C or 70 °C, and the distillate temperature was constant 30 °C. Water flux results were quite different between the low and high ΔT experiments (Figure 5.7). Initial water flux with T_f of 50 °C was 6.7 L m^{-2} h^{-1}, or 55% of the water flux when operating with deionized water as feed at similar conditions. A gradual decline

in water flux with concentration was observed that became progressively more severe as the concentration factor approached 1.1, and with each additional concentration cycle (Figure 5.7a), although the water flux was restored to its initial rate each time the brine was diluted to its initial concentration. Salt rejection was very high except at the highest concentrations reached, and even at a concentration factor exceeding NaCl saturation it was greater than 99.7%. Thermal efficiency also progressively declined with concentration and with additional concentration cycles, following a similar trend as the water flux (Figure 5.8a).

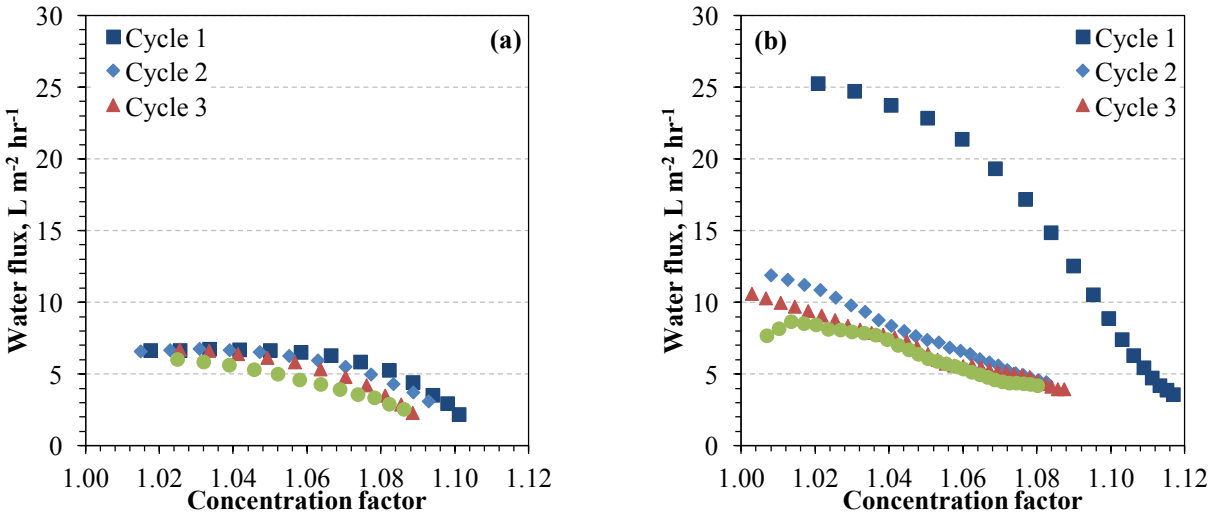

Figure 5.7. Water flux as a function of concentration factor for experiments with GSL brine as feed solution, constant T_d of 30 °C, and constant T_f of (a) 50 °C and (b) 70 °C. Both feed and distillate flow rates were 1.6 L min^{-1} in co-current flow configuration, using Cell 1. Four concentration cycles were performed, during which the GSL water was concentrated until flux declined below 50% of its initial value due to scaling, or the conductivity of distillate exceeded 2000 µS cm^{-1}. After each concentration cycle the solution was diluted to original concentration.

Initial water flux with T_f of 70 °C was 25.3 L m^{-2} h^{-1}, or 65% of the water flux when operating with deionized water as feed at similar conditions. In contrast to the experiments performed with T_f of 50 °C, the water flux declined rapidly with concentration, and was not fully restored when the brine was returned to its initial concentration (Figure 5.7b). Salt rejection declined below 99% at the highest concentration of the first concentration cycle. Although salt rejection recovered when the brine was diluted to its initial concentration, it declined further with additional concentration cycles, and by the final concentration cycle declined below 98%. Thermal efficiency was almost constant for the first concentration cycle up to a concentration

factor of approximately 1.09, but sharply declined as the concentration further increased (Figure 5.8b). As with water flux, thermal efficiency was not fully recovered when the brine was diluted to its initial concentration, and further declined with each additional concentration cycle.

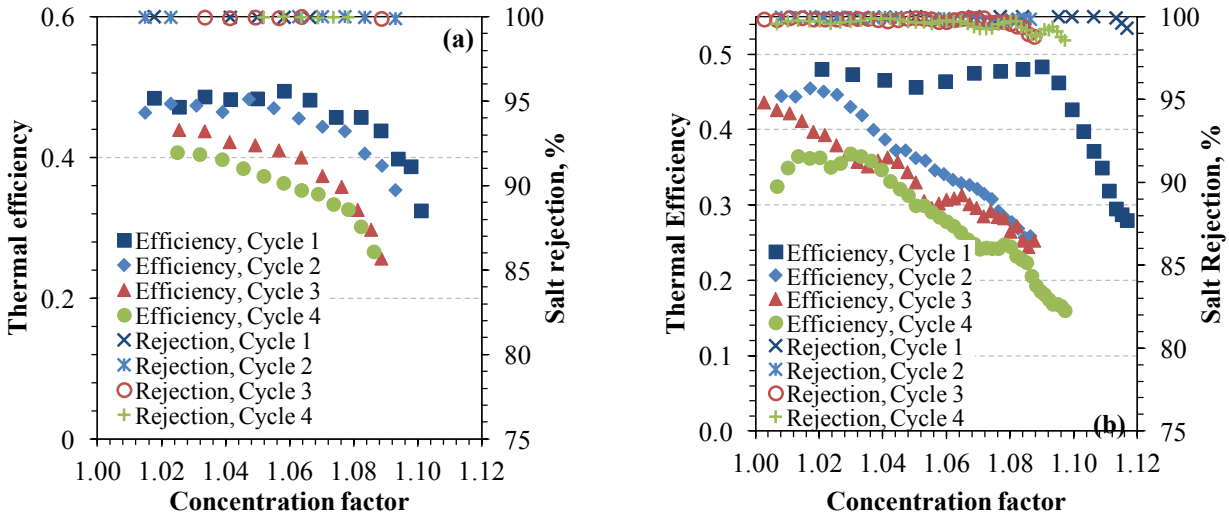

Figure 5.8. Thermal efficiency and salt rejection for experimental data presented in Fig. 5.7. GSL brine was the feed solution with constant T_d of 30 °C and constant T_f of (a) 50 ºC and (b) 70 °C.

The membranes were analyzed using SEM and EDS to investigate scaling morphology and composition. Several distinct crystalline structures formed on the surface of the membrane used for the experiments performed with T_f of 50 °C and are shown in Figure 5.9. EDS analysis found predominantly NaCl layers (Figure 5.9a-1) that also appeared to serve as nucleation sites for crystals containing magnesium and chloride, but also potassium and oxygen in smaller quantities (Figure 5.9a-2). Smaller crystals on the membrane itself were found to contain predominantly magnesium, sulfur, and oxygen, but also chloride (Figure 5.9a-3). Cross-section images of the same membrane showed indications that a crystalline scale layer had penetrated the membrane structure (Figure 5.9b). The extent of penetration varied and was not complete, and had advanced to approximately a quarter of the total thickness of the membrane in some areas. This area of the membrane also showed signs of damage to the membrane structure, as abnormally large pores were noted throughout the area that had experienced scale layer penetration. Isolated crystals where also observed scattered randomly throughout the remainder of the membrane structure.

The surfaces of the membranes used for the experiments performed with T_f of 70 °C were absent of large, distinct crystalline structures. EDS analysis revealed sodium and chloride present on the membrane surface, but the cubic structure typical of NaCl was not observed. The primary large surface structures appeared as an amorphous layer containing predominantly magnesium, chloride, and oxygen (Figure 5.10a), mostly in the areas of the membrane that had been close to the spacer filaments. Cross-section images indicate that scaling had penetrated into the membrane structure and was more homogeneous than the scaling that occurred during experiments with T_f of 50 °C (Figure 5.10b). The internal damage to the membrane structure was more severe than the membranes tested with T_f of 50 °C, and very large pores were found throughout the membrane approximately a quarter to a third of the distance from the feed surface to the distillate surface. These enlarged pores also contained crystals that EDS identified to be composed of NaCl, indicating that liquid water likely penetrated the membrane structure to some extent. Both membranes experienced similar decline in hydrophobicity following the experiments, and contact angles of 52.2° and 58.8° were measured for the membranes used for experiments performed with T_f of 50 °C and 70 °C, respectively.

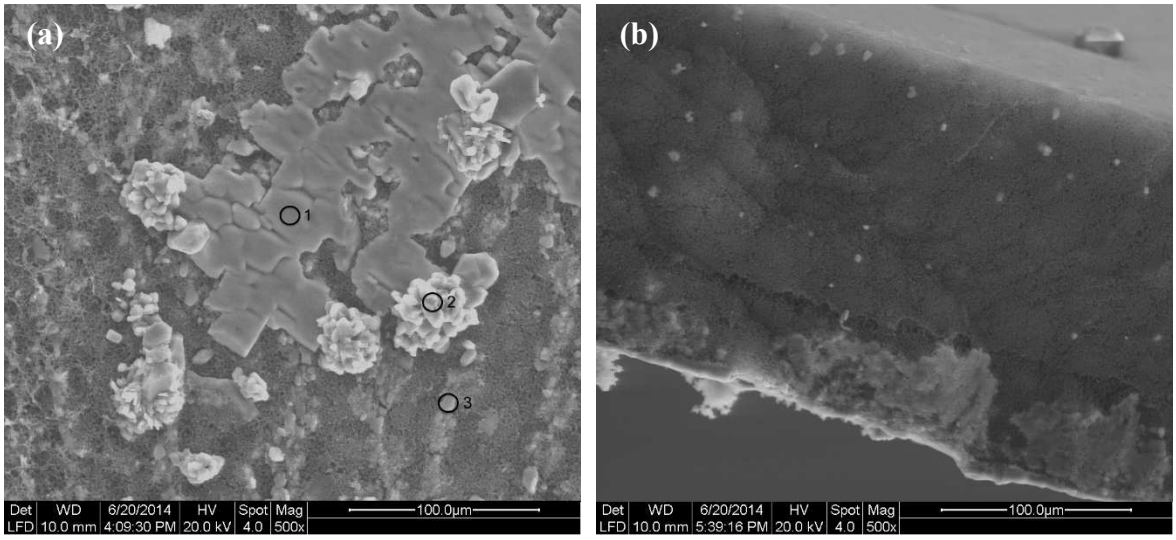

Figure 5.9. (a) Surface and (b) cross-section SEM micrographs of the membrane used with GSL brine as feed, constant T_f of 50 °C, constant T_d of 30 °C, with feed and distillate flow rate of 1.6 L min^{-1} co-current flow using Cell 1. Four concentration cycles were performed. Surface layers included predominantly NaCl (1), (2) crystals containing magnesium, chloride, potassium, and oxygen, and (3) scale containing magnesium, sulfur, oxygen, and chloride. Membrane feed side is towards bottom of image (b), where enlarged pores similar to those seen in membranes scaled with pure NaCl (Fig. 5.5) are visible.

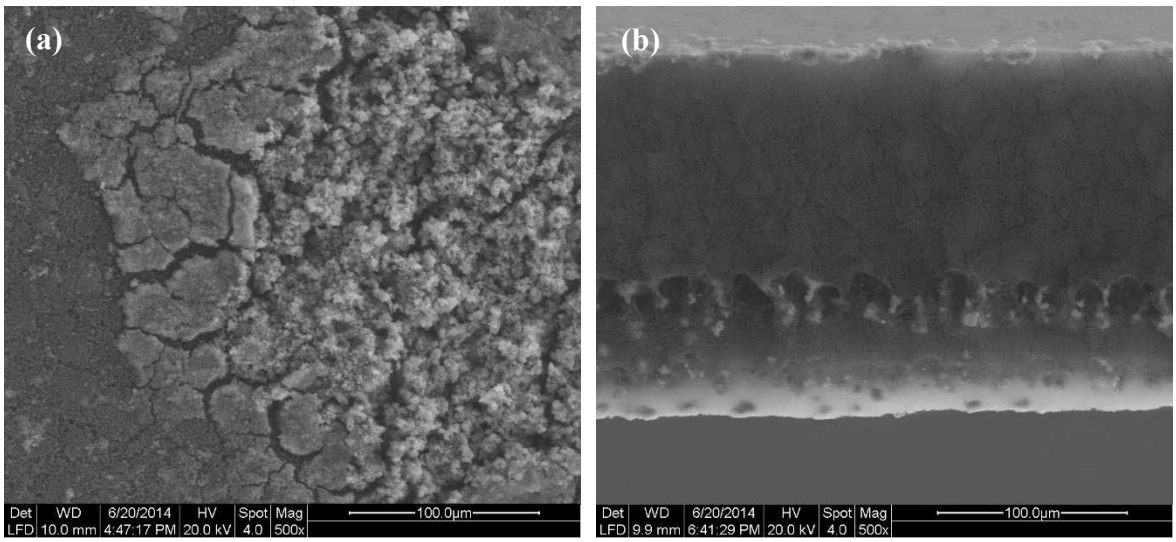

Figure 5.10. (a) Surface and (b) cross-section SEM micrographs of the membrane used with GSL brine as feed, constant T_f of 70 °C, constant T_d of 30 °C, with feed and distillate flow rate of 1.6 L min^{-1} co-current flow using Cell 1. Four concentration cycles were performed. Surface layers were predominantly composed of amorphous structures containing sodium, magnesium, chloride, and oxygen. Membrane feed side is towards bottom of image (b). Damage to the membrane structure was more severe, with pores enlarged to a greater degree than those seen in membranes scaled with pure NaCl (Fig. 5.5).

5.5.4.3 Comparison of scaling and fouling between GSL water and pure NaCl solution

Compared to the effects of scaling with pure NaCl, there appear to be several factors that contribute to a decline in water flux and thermal efficiency for the MD process when used to concentrate the GSL water. These include reversible effects that recover when the concentration is decreased with all other conditions being the same, and irreversible effects that do not recover when the concentration decreases. Moreover, the irreversible effects are much more significant at higher ΔT operation. NaCl crystallization is likely the predominant cause of the reversible decline at high concentrations; the visible scale layer covering the membrane surface disappeared with reduced concentration as the NaCl crystals dissolved. Of all the conditions tested, only the pure NaCl experiments with a T_f of 50 °C did not exhibit significant irreversible decline. Although irreversible decline was observed in the NaCl experiments performed with T_f of 70 °C, this is likely related to pore wetting and the loss of effective surface area due to the rapid dissolution of the NaCl scale layer when the solution was diluted below saturation concentration. Pore wetting is not likely to be the primary cause of irreversible decline in the North Arm GSL experiments, as severe decline in performance was observed in both sets of experiments despite negligible decline in salt rejection.

Unlike the pure NaCl experiments, which saw steady performance decline in the first concentration cycle up until NaCl saturation due to increased concentration, performance decline in the North Arm GSL experiments experienced a progressive decline in flux almost immediately, and was especially rapid in the experiments performed with T_f of 70 °C. SEM and EDS analysis of membranes from both sets of experiments showed evidence of magnesium, chloride, and oxygen on the surface (Figure 5.9 and Figure 5.10) despite the fact that no magnesium salts exceeded saturation at the bulk concentrations experienced during the experiments. However, generally speaking the GSL brine is very high in magnesium and is an economically important source of $MgCl_2$ [53]. Solubility of $MgCl_2$ increases with temperature, and high NaCl concentrations inhibit the diffusion of Mg^{2+} [54]. Therefore, it is plausible that the increase in temperature and concentration polarization at higher ΔT may have created conditions favorable to $MgCl_2$ crystallization at the membrane surface despite below-saturation concentration in the bulk solution.

Another possible explanation for the irreversible effects may be fouling by colloid-sized particles present in the water. Whereas water flux for pure NaCl experiments was mostly independent of total water recovered at both low and high ΔT, a convergence in performance was observed in the North Arm GSL experiments for the different operating temperatures. By the 4th concentration cycle and approximately 1 L of total water recovery, water flux was similar for both T_f = 50 °C and T_f = 70 °C experiments even at reduced concentration, despite the much greater driving force at higher ΔT (Figure 5.11). Similar behavior has also been observed in pressure-driven membrane processes where fouling is primarily a result of the deposition of colloid-size particles [55]. This flux convergence phenomenon is largely due to the interplay between the normal hydraulic drag force that results from the water flux, the barrier force that results from the membrane-colloid interaction, and the shear hydraulic force that results from the bulk flow rate of the feed. The GSL water used in the present study was high in total organic carbon (TOC) and magnesium (Table 5.2). Divalent cations are known to form complexes with carboxyl groups in natural organic matter (NOM) and enhance fouling rates in membrane filtration processes [56, 57]. It is possible that such complexes may have formed in the GSL water during concentration and deposited onto the membrane surface into a fouling layer. The presence of magnesium and oxygen on the membranes used in experiments performed with T_f of 70 °C as well as the amorphous nature of the surface structures observed in the SEM analysis

(Figure 5.10) provide support for the explanation that this fouling may be a result of NOM-Mg^{2+} complexes.

EDS analysis did not indicate presence of calcium in the scaling or fouling layer of any of the membranes tested, despite the fact that calcium is also known to form complexes with NOM, and the OLI simulation predicted high scaling tendency for both $CaCO_3$ and $CaSO_4$. However, the concentration of magnesium in the GSL brine was an order of magnitude greater than the concentration of calcium. Additionally, $CaSO_4$ crystallization has a relatively long induction time and is inhibited by the presence of NaCl [58]. Dissolved organic matter, specifically humid acid, has also been shown to inhibit $CaCO_3$ scaling in the DCMD process [35].

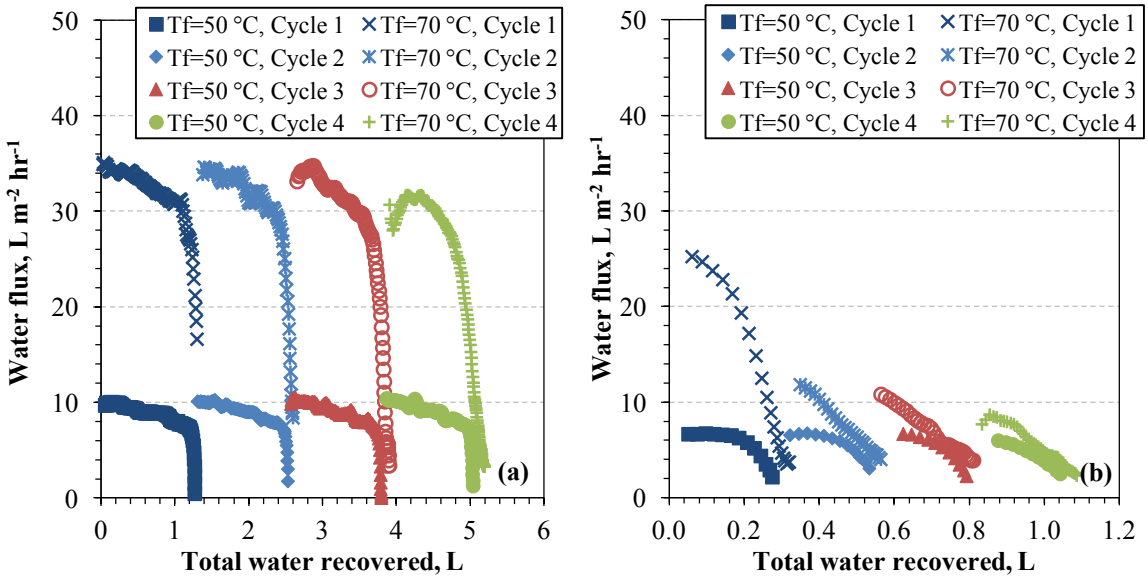

Figure 5.11. Comparison of water flux for T_f of 50 °C and T_f of 70 °C over four concentration and dilution cycles for (a) 200 g L^{-1} NaCl solution and (b) North Arm GSL brine using Cell 1, plotted as a function of total water recovered. Distillate temperature was constant at 30 °C and flow rate for both feed and distillate was 1.6 L min^{-1} in co-current configuration.

5.5.4.4 Repeated concentration at reduced water recovery

To investigate long-term scaling and fouling behavior while limiting potential damage to the membrane caused by NaCl scaling, additional concentration and dilution experiments were performed with the total water recovery limited to 8%. These experiments were performed using T_f of 50 °C and T_d of 30 °C. The initial water flux was close to 9 L m^{-2} h^{-1} and declined to approximately 8.5 L m^{-2} h^{-1} with increased concentration (Figure 5.12). Similar to the

experiments at higher water recovery, water flux declined with each additional concentration cycle, even in the absence of severe flux decline characteristic of NaCl scaling. Also, a decline in salt rejection was observed beginning with the 5th concentration cycle after 25 hours of operation, ultimately falling below 98.5% towards the end of the 7th concentration cycle.

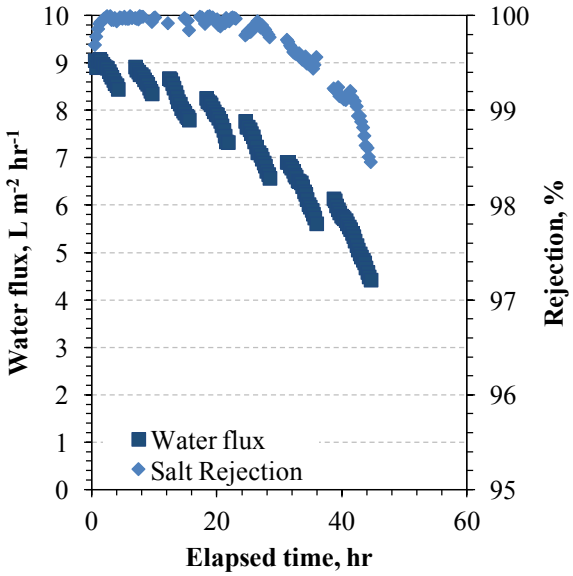

Figure 5.12. Water flux and salt rejection as a function of time for experiments using GSL brine as feed, constant T_f of 50 °C, and constant T_d of 30 °C over seven concentration and dilution cycles using Cell 2. For each concentration cycle the brine was concentrated until 8% recovery before dilution. Both feed and distillate flow rates were constant 1.6 L min^{-1} in co-current configuration.

SEM analysis of the membranes used in these experiments indicated a fouling layer similar to that observed in the concentration experiments with T_f of 70 °C; however, it was much more extensive and covered most of the membrane surface (Figure 5.13a). The lower temperature and concentration polarization, lower overall concentration factor, and longer overall time of these experiments providing further support for the hypothesis that the fouling layer was a result of deposition of NOM-Mg^{2+} over time rather than crystallization of magnesium salts. Cross-section images indicated that this layer formed only on the membrane surface and did not penetrate into the membrane structure itself, and unlike the experiments performed at higher water recovery did not display enlarged pores in the membrane structure (Figure 5.13b). However, loss of hydrophobicity was more severe than the experiments with

higher recovery but shorter duration, and the membrane used in this run of experiments was found to have a contact angle of only 28.2°, which may explain the increased wetting tendency and decline in salt rejection.

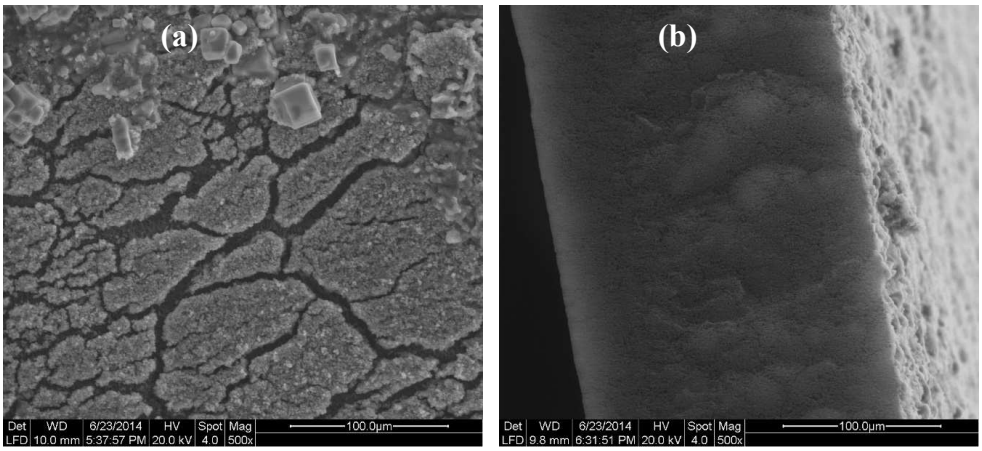

Figure 5.13. (a) Surface and (b) cross-section SEM micrographs of membrane used for 7 concentration cycles using GSL brine as feed, constant T_f of 50 °C, constant T_d of 30 °C over seven concentration and dilution cycles using Cell 2. For each concentration cycle the brine was concentrated until 8% recovery before dilution. Both feed and distillate flow rates were constant 1.6 L min^{-1} in co-current configuration. Feed side of the membrane is on the right in image (b).

5.5.4.5 Scale mitigation

Limiting the extent of concentration to prevent scaling by NaCl was successful at preventing damage to the membrane itself; however, fouling still occurred and resulted in loss of performance and salt rejection. Temporary operation with T_f of 20 °C and T_d of 30 °C between each concentration cycle to reverse the direction of water flux was tested for its effectiveness in preventing scaling and fouling buildup, and to maintain long-term performance and salt rejection.

Repeating the concentration and dilution experiments with 5 minutes of reverse temperature operation between each concentration cycle reduced the extent of performance decline compared to previous experiments performed without temperature reversal (Figure 5.14a), but gradual decline in water flux and salt rejection were both observed. The technique was substantially more effective when reverse temperature operation continued until reverse water flux reached steady state, which generally took 20-40 minutes (Figure 5.14b). SEM micrographs revealed little evidence of scaling or fouling on the membrane surfaces (Figure

5.15a), or in the membrane pores themselves (Figure 5.15b). Contact angle was found to be 89.6°, which is similar to the contact angle of the membrane used in the pure NaCl experiments with feed temperature at 50 ºC.

The efficacy of reversing the temperature gradient to mitigate the performance loss due to scaling/fouling suggests that organic fouling was more substantial than scaling by magnesium salts. Operation in this mode reverses the temperature and concentration polarization, creating conditions that should easily dissolve salts of the composition identified by EDS analysis such as $MgCl_2$, KCl, K_2SO_4. In contrast, organic fouling (e.g. NOM, humic acid) generally requires rinsing with DI water accompanied by acid/base cleaning to fully recover performance in the MD process [59, 60].

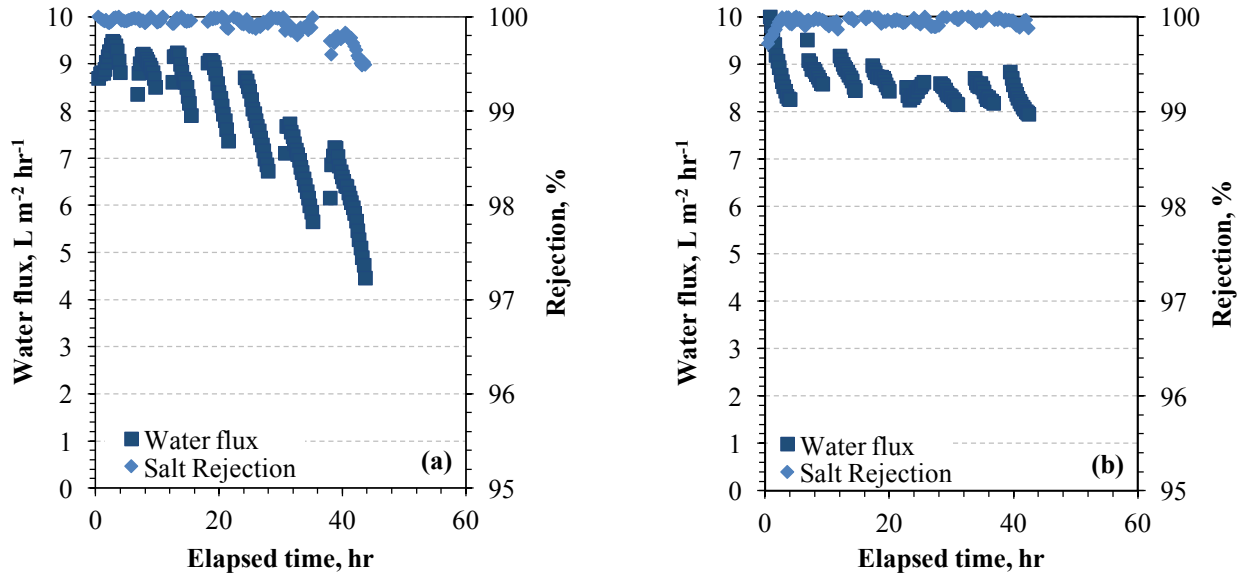

Figure 5.14. Water flux and salt rejection as a function of time for multiple concentration and dilution cycles with temperature reversal using GSL brine as feed, constant T_f of 50 °C, and constant T_d of 30 °C using Cell 2. For each concentration cycle the brine was concentrated until 8% recovery before dilution, followed by temporary operation with GSL brine at constant T_f of 20 °C and constant T_d of 30 °C for (a) 5 minutes or (b) until stable reverse flux was observed before beginning the next concentration cycle. Both feed and distillate flow rates were constant 1.6 L min^{-1} in co-current configuration.

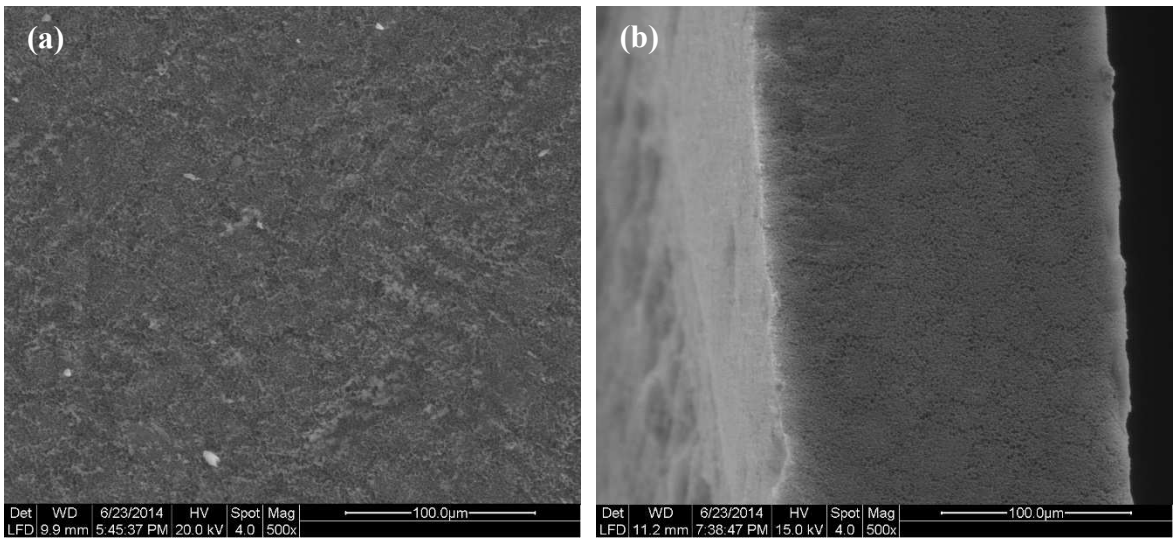

Figure 5.15. (a) Surface and (b) cross-section SEM micrographs of membrane used for multiple concentration cycles with temperature reversal using GSL brine as feed, constant T_f of 50 °C, constant T_d of 30 °C using Cell 2. For each concentration cycle the brine was concentrated until 8% recovery before dilution, followed by 5 minutes of operation with GSL brine at constant T_f of 20 °C and constant T_d of 30 °C before beginning the next concentration cycle. Both feed and distillate flow rates were constant 1.6 L min^{-1} in co-current configuration. Feed side of the membrane is towards the left in image (b).

5.6 Conclusion

This study investigated the effects of scaling and fouling on performance and durability of DCMD for the concentration of a hypersaline brine collected from the North Arm of the Great Salt Lake containing sparingly soluble salts and natural organic matter. Impacts on water flux, thermal efficiency, and salt rejection were observed that resulted from reversible effects occurring only at high concentration factors, and irreversible effects that were independent of concentration.

At the highest concentration factors, NaCl crystallization on the membrane surface caused rapid decline in performance and termination of the process. However, the NaCl crystal layer easily dissolved and performance was fully restored upon dilution when the difference between the feed and distillate temperature (ΔT) was not greater than 20 °C. At higher ΔT operation, NaCl crystallization damaged the internal pore structure of the membranes and progressively increased wetting tendency with each concentration cycle.

Theoretical calculation of the scaling tendencies of various salts present in the GSL brine was an effective method for predicting the concentration limit imposed by NaCl crystallization,

and terminating the process before this concentration was reached, preventing damage to the membrane structure. This approach was ineffective for predicting scaling behavior of sparingly soluble salts, which did not precipitate on the membrane surface in a manner expected based on theoretical solubility in the bulk solution.

The effects of NaCl crystallization on performance and salt rejection were similar for both pure NaCl solutions and the GSL brine. However, additional effects were observed during concentration of the GSL brine that caused a progressive decline in water flux, thermal efficiency, and salt rejection that were not restored upon dilution to the original concentration. These effects were determined to be predominantly a result of fouling by NOM-Mg^{2+} complexation.

Operation at reduced water recovery to keep the NaCl concentration below saturation was effective at preventing NaCl crystallization and damage to internal pore structure during GSL brine concentration. Performance decline and loss of salt rejection resulting from other effects were mitigated by periodic operation with higher distillate temperature than feed temperature, reversing the direction of the driving force of the DCMD process and direction of water flow. However, the approach was time and energy intensive, requiring 20-40 minutes of reverse operation between each concentration cycle to completely prevent performance decline and maintain high salt rejection.

5.7 References

[1] N. Ghaffour, T.M. Missimer, G.L. Amy, Technical review and evaluation of the economics of water desalination: Current and future challenges for better water supply sustainability, Desalination, 309 (2013) 197-207.

[2] A.M.O. Mohamed, M. Maraqa, J. Al Handhaly, Impact of land disposal of reject brine from desalination plants on soil and groundwater, Desalination, 182 (2005) 411-433.

[3] J.A. Epstein, Utilization of the dead sea minerals (a review), Hydrometallurgy, 2 (1976) 1-10.

[4] D.L. Gallup, Geochemistry of geothermal fluids and well scales, and potential for mineral recovery, Ore Geol Rev, 12 (1998) 225-236.

[5] A. Maimoni, Minerals recovery from salton sea geothermal brines: a literature review and proposed cementation process, Geothermics, 11 (1982) 239-258.

[6] H.H. Werner, Contribution to the mineral extraction from supersaturated geothermal brines Salton Sea Area, California, Geothermics, 2, Part 2 (1970) 1651-1655.

[7] M. Ahmed, A. Arakel, D. Hoey, M.R. Thumarukudy, M.F.A. Goosen, M. Al-Haddabi, A. Al-Belushi, Feasibility of salt production from inland RO desalination plant reject brine: A case study, Desalination, 158 (2003) 109-117.

[8] A.H. Hamzaoui, A. M'Nif, H. Hammi, R. Rokbani, Contribution to the lithium recovery from brine, Desalination, 158 (2003) 221-224.

[9] J.A. Epstein, E.M. Feist, J. Zmora, Y. Marcus, Extraction of lithium from the dead sea, Hydrometallurgy, 6 (1981) 269-275.

[10] M. Petersková, C. Valderrama, O. Gibert, J.L. Cortina, Extraction of valuable metal ions (Cs, Rb, Li, U) from reverse osmosis concentrate using selective sorbents, Desalination, 286 (2012) 316-323.

[11] H. Bukowsky, E. Uhlemann, D. Steinborn, The recovery of pure lithium chloride from "brines" containing higher contents of calcium chloride and magnesium chloride, Hydrometallurgy, 27 (1991) 317-325.

[12] O.J. Morin, Design and Operating Comparison of Msf and Med Systems, Desalination, 93 (1993) 69-109.

[13] R. Sheikholeslami, Assessment of the scaling potential for sparingly soluble salts in RO and NF units, Desalination, 167 (2004) 247-256.

[14] T. Koo, Y.J. Lee, R. Sheikholeslami, Silica fouling and cleaning of reverse osmosis membranes, Desalination, 139 (2001) 43-56.

[15] K.W. Lawson, D.R. Lloyd, Membrane distillation, Journal of Membrane Science, 124 (1997) 1-25.

[16] Y.B. Yun, R.Y. Ma, W.Z. Zhang, A.G. Fane, J.D. Li, Direct contact membrane distillation mechanism for high concentration NaCl solutions, Desalination, 188 (2006) 251-262.

[17] F. He, J. Gilron, K.K. Sirkar, High water recovery in direct contact membrane distillation using a series of cascades, Desalination, 323 (2013) 48-54.

[18] M. Safavi, T. Mohammadi, High-salinity water desalination using VMD, Chemical Engineering Journal, 149 (2009) 191-195.

[19] A. Alkhudhiri, N. Darwish, N. Hilal, Treatment of high salinity solutions: Application of air gap membrane distillation, Desalination, 287 (2012) 55-60.

[20] X. Ji, E. Curcio, S. Al Obaidani, G. Di Profio, E. Fontananova, E. Drioli, Membrane distillation-crystallization of seawater reverse osmosis brines, Separation and Purification Technology, 71 (2010) 76-82.

[21] C.R. Martinetti, A.E. Childress, T.Y. Cath, High recovery of concentrated RO brines using forward osmosis and membrane distillation, Journal of Membrane Science, 331 (2009) 31-39.

[22] A. Pérez-González, A.M. Urtiaga, R. Ibáñez, I. Ortiz, State of the art and review on the treatment technologies of water reverse osmosis concentrates, Water Research, 46 (2012) 267-283.

[23] D. Qu, J. Wang, B. Fan, Z.K. Luan, D.Y. Hou, Study on concentrating primary reverse osmosis retentate by direct contact membrane distillation, Desalination, 247 (2009) 540-550.

[24] T.Y. Cath, Osmotically and thermally driven membrane processes for enhancement of water recovery in desalination processes, Desalin Water Treat, 15 (2010) 279-286.

[25] E. Drioli, E. Curcio, A. Criscuoli, G.D. Profio, Integrated system for recovery of CaCO3, NaCl and MgSO4·7H2O from nanofiltration retentate, Journal of Membrane Science, 239 (2004) 27-38.

[26] E. Curcio, X. Ji, A.M. Quazi, S. Barghi, G. Di Profio, E. Fontananova, T. Macleod, E. Drioli, Hybrid nanofiltration–membrane crystallization system for the treatment of sulfate wastes, Journal of Membrane Science, 360 (2010) 493-498.

[27] F. Macedonio, E. Drioli, E. Curcio, G. Di Profio, Experimental and economical evaluation of a membrane crystallizer plant, Desalin Water Treat, 9 (2009) 49-53.

[28] K.L. Hickenbottom, T.Y. Cath, Sustainable operation of membrane distillation for enhancement of mineral recovery from hypersaline solutions, Journal of Membrane Science, 454 (2014) 426-435.

[29] M. Gryta, Concentration of NaCl solution by membrane distillation integrated with crystallization, Separation Science and Technology, 37 (2002) 3535-3558.

[30] M. Gryta, Direct contact membrane distillation with crystallization applied to NaCl solutions, Chem Pap-Chem Zvesti, 56 (2002) 14-19.

[31] F. Edwie, T.-S. Chung, Development of simultaneous membrane distillation–crystallization (SMDC) technology for treatment of saturated brine, Chemical Engineering Science, 98 (2013) 160-172.

[32] C.M. Tun, A.G. Fane, J.T. Matheickal, R. Sheikholeslami, Membrane distillation crystallization of concentrated salts - flux and crystal formation, Journal of Membrane Science, 257 (2005) 144-155.

[33] M. Gryta, Alkaline scaling in the membrane distillation process, Desalination, 228 (2008) 128-134.

[34] M. Gryta, Long-term performance of membrane distillation process, Journal of Membrane Science, 265 (2005) 153-159.

[35] E. Curcio, X.S. Ji, G. Di Profio, A. Sulaiman, E. Fontananova, E. Drioli, Membrane distillation operated at high seawater concentration factors: Role of the membrane on CaCO3 scaling in presence of humic acid, Journal of Membrane Science, 346 (2010) 263-269.

[36] L.D. Nghiem, T. Cath, A scaling mitigation approach during direct contact membrane distillation, Separation and Purification Technology, 80 (2011) 315-322.

[37] F. He, K.K. Sirkar, J. Gilron, Studies on scaling of membranes in desalination by direct contact membrane distillation: CaCO3 and mixed CaCO3/CaSO4 systems, Chemical Engineering Science, 64 (2009) 1844-1859.

[38] J. Gilron, Y. Ladizansky, E. Korin, Silica Fouling in Direct Contact Membrane Distillation, Ind Eng Chem Res, 52 (2013) 10521-10529.

[39] M. Gryta, Fouling in direct contact membrane distillation process, Journal of Membrane Science, 325 (2008) 383-394.

[40] E. Guillen-Burrieza, R. Thomas, B. Mansoor, D. Johnson, N. Hilal, H. Arafat, Effect of Dry-out on the Fouling of PVDF and PTFE Membranes under Conditions Simulating Intermittent Seawater Membrane Distillation (SWMD), Journal of Membrane Science, (2013).

[41] R.W. Schofield, A.G. Fane, C.J.D. Fell, Heat and mass transfer in membrane distillation, Journal of Membrane Science, 33 (1987) 299-313.

[42] S. Al-Obaidani, E. Curcio, F. Macedonia, G. Di Profio, Al-Hinai, E. Drioli, Potential of membrane distillation in seawater desalination: Thermal efficiency sensitivity study and cost estimation, Journal of Membrane Science, 323 (2008) 85-98.

[43] F. Macedonio, E. Curcio, E. Drioli, Integrated membrane systems for seawater desalination: energetic and exergetic analysis, economic evaluation, experimental study, Desalination, 203 (2007) 260-276.

[44] A. Alkhudhiri, N. Darwish, N. Hilal, Membrane distillation: A comprehensive review, Desalination, 287 (2012) 2-18.

[45] A.P.H.A. Andrew D Eaton, American Water Works Association, Water Environment Federation, Standard methods for the examination of water and wastewater, 21st ed., American Public Health Association (APHA), Washington, DC, USA, 2005.

[46] G. Schock, A. Miguel, Mass transfer and pressure loss in spiral wound modules, Desalination, 64 (1987) 339-352.

[47] J.L. Domagalski, W.H. Orem, H.P. Eugster, Organic geochemistry and brine composition in Great Salt, Mono, and Walker Lakes, Geochimica et Cosmochimica Acta, 53 (1989) 2857-2872.

[48] J.W. Gwynn, Great Salt Lake, Utah: Chemical and Physical Variations of the Brine and Effects of the SPRR Causeway, 1966-1996, (1998).

[49] T. Arnow, Water-Level and Water-Quality Changes in Great Salt Lake, Utah 1843-1985, (1985).

[50] R.J. Spencer, H.P. Eugster, B.F. Jones, Geochemistry of great Salt Lake, Utah II: Pleistocene-Holocene evolution, Geochimica et Cosmochimica Acta, 49 (1985) 739-747.

[51] S. Al-Jibbouri, J. Ulrich, The Influence of Impurities on Crystallization Kinetics of Sodium Chloride, Crystal Research and Technology, 36 (2001) 1365-1375.

[52] H. Langer, H. Offermann, On the Solubility of Sodium-Chloride in Water, J Cryst Growth, 60 (1982) 389-392.

[53] T.G. Tripp, Production of Magnesium from Great Salt Lake, Utah, USA, Natural Resources and Environmental Issues, 15 (2009) 55.

[54] J.G. Albright, R. Mathew, D.G. Miller, J.A. Rard, Isothermal diffusion coefficients for sodium chloride-magnesium chloride-water at 25.degree.C. 1. Solute concentration ratio of 3:1, The Journal of Physical Chemistry, 93 (1989) 2176-2180.

[55] Y.-N. Wang, C.Y. Tang, Protein fouling of nanofiltration, reverse osmosis, and ultrafiltration membranes—The role of hydrodynamic conditions, solution chemistry, and membrane properties, Journal of Membrane Science, 376 (2011) 275-282.

[56] S.K. Hong, M. Elimelech, Chemical and physical aspects of natural organic matter (NOM) fouling of nanofiltration membranes, Journal of Membrane Science, 132 (1997) 159-181.

[57] C.Y. Tang, Y.-N. Kwon, J.O. Leckie, The role of foulant–foulant electrostatic interaction on limiting flux for RO and NF membranes during humic acid fouling—Theoretical basis, experimental evidence, and AFM interaction force measurement, Journal of Membrane Science, 326 (2009) 526-532.

[58] R. Sheikholeslami, H.W.K. Ong, Kinetics and thermodynamics of calcium carbonate and calcium sulfate at salinities up to 1.5 M, Desalination, 157 (2003) 217-234.

[59] S. Srisurichan, R. Jiraratananon, A.G. Fane, Humic acid fouling in the membrane distillation process, Desalination, 174 (2005) 63-72.

[60] M. Gryta, M. Tomaszewska, J. Grzechulska, A.W. Morawski, Membrane distillation of NaCL solution containing natural organic matter, Journal of Membrane Science, 181 (2001) 279-287.

CHAPTER 6
CONCLUSION

As demand for water around the world continues to grow and fresh water resources are depleted or threatened, many communities are becoming increasingly reliant on unconventional resources such as desalinated water to meet demand. Although technical advances in pressure-driven membrane desalination processes such as RO have led to an expansion of global seawater desalination capacity in recent decades, significant challenges remain that impede the economic use of inland brackish water resources. To minimize the volume of reject brine produced, inland desalination processes typically require high water recoveries, which is limited in pressure-driven membrane processes due to the increase in osmotic pressure difference with concentration and increased risk of scaling by sparingly soluble salts and silica.

This dissertation provides valuable support to aid in the development MD as a technology capable of sustainable operation at high water recoveries in the desalination of impaired resources and brines with high scaling potential. In particular, effective strategies to minimize silica scaling through the use of chemical pretreatment and optimization of feed temperatures were demonstrated, and new discoveries were made regarding the mechanisms by which silica scaling impacts MD performance. MD was also demonstrated to be capable of sustained operation during treatment of hypersaline brines, and performance could be maintained with the application of process optimization and scale mitigation strategies. The dissertation also provides valuable insight into key challenges and potential directions of future research to support further development of MD as a strategy for enhancing overall water recovery in desalination processes.

Results suggest that scaling behavior and its impacts on MD performance may be more complex than those of pressure-driven processes and are influenced by many factors, including hydrodynamic conditions, solution chemistry, and operating temperatures. For example, while MD was found to be initially more resistant to silica scaling than NF and achieved higher concentration before scaling occurred, performance decline occurred rapidly after the onset of scaling in MD and the long-term impacts of scaling were more severe compared to NF at similar hydrodynamic conditions and temperatures in the bulk flow. However, the scale layer only impacted MD performance when present on the feed side of the membrane where evaporation occurs, and had no effect when the temperature difference across the membrane (and thus the

direction of water flux) was reversed, indicating that the effects of the scale layer on mass and heat transfer resistances were negligible. Rather, performance decline was due to the impacts of silica scale on the effective partial vapor pressure difference and evaporation rates at the interface between the scale layer and the membrane surface, which were found to be strongly influenced by operating temperatures. Therefore, the lack of temperature polarization phenomenon in NF may have effects on the difference in apparent scaling propensity between the two processes in addition to those caused by the influence of temperature on the degree of saturation and reaction kinetics at the membrane surface. Further investigation that replicates the temperature polarization phenomena of MD in pressure-driven membrane processes could potentially eliminate some of these variables and provide more insight into the differences between the impacts of scaling on the driving force and overall energy efficiency of MD compared to pressure-driven membrane processes.

Chemical cleaning using a high-pH solution was only partially effective at removing silica scale and was unable to restore the scale resistant properties of MD membranes. Thus, as with other membrane processes, strategies to prevent the onset of silica scaling are necessary to maintain sustainable operation of MD at silica concentrations exceeding saturation. Adjustment of feed pH using HCl or NaOH was found to be an effective strategy to minimize silica scaling due to its effects on silica solubility and polymerization rates. However, silica scaling behavior in MD was also found to be highly influenced by interactions with other ions, and further investigation of these interactions could lead to the development of other methods to manipulate feed water chemistry that effectively reduce scaling potential. For example, silica scaling was accelerated by the presence of divalent cations, but carbonate alkalinity was found to inhibit silica scaling and mitigate the catalytic effect of calcium ions on silica polymerization. Increasing carbonate alkalinity might reduce silica scaling risk to acceptable levels, and could potentially be accomplished by the injection of waste CO_2 from power plants and industrial processes into mineral-rich feed streams. This might be promising for MD because these facilities also generate waste heat that could be utilized to provide energy for the driving force. Alternatively, chemical pretreatment that provides both pH adjustment and increased alkalinity (e.g., Na_2CO_3) might achieve similar or better silica scale mitigation than NaOH. Also, the presence of valuable minerals intended for recovery in a later stage of treatment could be considered to optimize selection of chemical pretreatment. For example, the Great Salt Lake

water tested in this investigation is utilized commercially for extraction of K_2SO_4, yet also contained high magnesium and silica concentrations. In this case, feed water acidification using H_2SO_4 might reduce silica scaling risk in the MD process while potentially assisting K_2SO_4 recovery due to the addition of SO_4^{2-} ions.

In addition to chemical pretreatment strategies, scaling risk and its impacts on MD processes may be reduced with process optimization and modification. As a thermally-driven membrane separation process, MD is subject to both concentration and temperature polarization, both of which are highly dependent on operating temperature. Accordingly, feed temperature was found to have a major influence on both crystallization and colloidal scaling behaviors in MD. Operation at lower temperature reduced scaling rates and overall impacts of scaling by silica and sodium chloride, even at similar or higher bulk feed concentrations, despite decreased solubility with temperature. Because water flux in MD is highly influenced by the temperature difference between the feed and distillate, this suggests that concentration polarization tends to dominate over temperature effects on solubility as feed temperature increases, which leads to increased supersaturation at the membrane surface. The effect of drag forces associated with increased water flux may also play an important role in colloidal fouling by silica. Thus, optimization of feed temperature may be a useful strategy to minimize scaling and fouling while maintaining desired performance, especially because the thermal efficiency of MD is not strongly affected by temperature. Further investigation on the concept of critical temperature in MD that provides an ideal balance of water flux, efficiency, and scaling risk for different solution chemistries and process configuration could provide valuable guidelines and design parameters for the scaling up of MD for commercial applications.

APPENDIX A

PERMISSIONS RELEASE FOR PUBLISHED ARTICLES

From: **Emmy Gustafson** emily.miner.gustafson@gmail.com
Subject: Re: Permission request to reprint published article for doctoral dissertation
Date: April 6, 2018 at 5:26 PM
To: John Bush jobush@mymail.mines.edu
Cc: Tzahi Cath tcath@mines.edu

EG

Hi John,

You have my permission to include the article “Prevention and management of silica scaling in membrane distillation using pH adjustment”, which was published in *Journal of Membrane Science,* 554 (2018) 366-377, in your doctoral dissertation.

Thanks for the email and Congrats again!!

Emily M. Gustafson

On Apr 6, 2018, at 5:14 PM, John Bush <jobush@mymail.mines.edu> wrote:

> Emily M. Gustafson,
>
> As co-author of the article “Prevention and management of silica scaling in membrane distillation using pH adjustment”, which was published in *Journal of Membrane Science,* 554 (2018) 366-377, I would like to thank you for your contributions to the article.
>
> At your earliest convenience, please respond to a kind request for your permission to include the article in my doctoral dissertation submitted to the Faculty and Board of Trustees of the Colorado School of Mines in partial fulfillment of the requirements for the degree of Doctor of Philosophy (Civil and Environmental Engineering).
>
> Thank you!
> John A. Bush
>
> ~~~~~~~~~~~~~~~~~~~~~~~~~~~~~~~
> John Bush
> PhD Candidate
> Civil and Environmental Engineering
> Colorado School of Mines
> 1500 Illinois St.
> Golden, CO 80401
> jobush@mymail.mines.edu
> (303)503-6193
> ~~~~~~~~~~~~~~~~~~~~~~~~~~~~~~~

From: **Waechter, Christopher** cwaechter@usbr.gov
Subject: Re: [EXTERNAL] Permission request to reprint published article for doctoral dissertation
Date: April 9, 2018 at 9:34 AM
To: John Bush jobush@mymail.mines.edu

CW

You have my permission to include in your dissertation any part of the article "Prevention and management of silica scaling in membrane distillation using pH adjustment", which was published in *Journal of Membrane Science,* 554 (2018) 366-377.

Feel free to send me any sort of documentation you might require for this permission and I will fill it out and return it today if needed. Otherwise, consider this email as permission to use the article in your dissertation.

Chris Waechter, EIT
Environmental Engineer
cwaechter@usbr.gov
(303)445-3893
Dept of the Interior I Bureau of Reclamation
TSC I Civil Engineering Division I Water Treatment Group

On Fri, Apr 6, 2018 at 5:16 PM, John Bush <jobush@mymail.mines.edu> wrote:

> Christopher A. Waechter,
>
> As co-author of the article "Prevention and management of silica scaling in membrane distillation using pH adjustment", which was published in *Journal of Membrane Science,* 554 (2018) 366-377, I would like to thank you for your contributions to the article.
>
> At your earliest convenience, please respond to a kind request for your permission to include the article in my doctoral dissertation submitted to the Faculty and Board of Trustees of the Colorado School of Mines in partial fulfillment of the requirements for the degree of Doctor of Philosophy (Civil and Environmental Engineering).
>
> Thank you!
> John A. Bush
>
> ~~~~~~~~~~~~~~~~~~~~~~~~~~~~~~~
> John Bush
> PhD Candidate
> Civil and Environmental Engineering
> Colorado School of Mines
> 1500 Illinois St.
> Golden, CO 80401
> jobush@mymail.mines.edu
> (303)503-6193
> ~~~~~~~~~~~~~~~~~~~~~~~~~~~~~~~

From: **David Jassby** davidjassby@gmail.com
Subject: Re: Permission request to reprint published article for doctoral dissertation
Date: April 6, 2018 at 5:42 PM
To: John Bush jobush@mymail.mines.edu
Cc: Tzahi Cath tcath@mines.edu

DJ

Hi John,

Thanks for including me on this paper - you have my permission (of course…)!

> On Apr 6, 2018, at 4:19 PM, John Bush <jobush@mymail.mines.edu> wrote:
>
> David Jassby,
>
> As co-author of the article "Prevention and management of silica scaling in membrane distillation using pH adjustment", which was published in *Journal of Membrane Science,* 554 (2018) 366-377, I would like to thank you for your contributions to the article.
>
> At your earliest convenience, please respond to a kind request for your permission to include the article in my doctoral dissertation submitted to the Faculty and Board of Trustees of the Colorado School of Mines in partial fulfillment of the requirements for the degree of Doctor of Philosophy (Civil and Environmental Engineering).
>
> Thank you!
> John A. Bush
>
> ~~~~~~~~~~~~~~~~~~~~~~~~~~~~~~~
> John Bush
> PhD Candidate
> Civil and Environmental Engineering
> Colorado School of Mines
> 1500 Illinois St.
> Golden, CO 80401
> jobush@mymail.mines.edu
> (303)503-6193
> ~~~~~~~~~~~~~~~~~~~~~~~~~~~~~~~

David Jassby, Ph.D.
Associate Professor
Department of Civil and Environmental Engineering
University of California, Los Angeles
310-825-1346
jassby@ucla.edu

From: **Craig Turchi** craig.turchi@gmail.com
Subject: Re: Permission request to reprint published article for doctoral dissertation
Date: April 9, 2018 at 3:34 PM
To: John Bush jobush@mymail.mines.edu
Cc: Craig Turchi craig.turchi@nrel.gov, Tzahi Cath tcath@mines.edu

CT

John,

Sorry for the delay. Yes, I approve of your request to include our article in your dissertation. Thank you for your good work!

Craig

sent from Craig Turchi's phone.

On Mon, Apr 9, 2018, 3:31 PM John Bush <jobush@mymail.mines.edu> wrote:

> Craig S. Turchi,
>
> As co-author of the article “Prevention and management of silica scaling in membrane distillation using pH adjustment”, which was published in *Journal of Membrane Science,* 554 (2018) 366-377, I would like to thank you for your contributions to the article.
>
> At your earliest convenience, please respond to a kind request for your permission to include the article in my doctoral dissertation submitted to the Faculty and Board of Trustees of the Colorado School of Mines in partial fulfillment of the requirements for the degree of Doctor of Philosophy (Civil and Environmental Engineering).
>
> Thank you!
> John A. Bush
>
> ~~~~~~~~~~~~~~~~~~~~~~~~~~~~~~~~
> John Bush
> PhD Candidate
> Civil and Environmental Engineering
> Colorado School of Mines
> 1500 Illinois St.
> Golden, CO 80401
> jobush@mymail.mines.edu
> (303)503-6193
> ~~~~~~~~~~~~~~~~~~~~~~~~~~~~~~~~